COIL CONDENSATION DETECTION FOR HUMIDITY CONTROL

A Thesis

by

CHARLES PECKITT KANEB

Submitted to the Office of Graduate and Professional Studies of
Texas A&M University
in partial fulfillment of the requirements for the degree of

MASTER OF SCIENCE

Chair of Committee,	Charles Culp
Members of Committee,	David Claridge
	Bryan Rasmussen
Head of Department,	Andreas Polycarpou

May 2014

Major Subject: Mechanical Engineering

ABSTRACT

Conditioning the air inside a building requires controlling both primary components of its enthalpy: temperature and humidity. Temperature sensors used in buildings are sufficiently reliable, durable, accurate, and precise that they can be relied on for sophisticated building control systems. Commercial resistive and capacitive humidity sensors become inaccurate near saturation and often fail permanently when exposed to liquid water. Excessive humidity can cause both occupant discomfort and permanent damage to buildings. In American climates dehumidification accounts for the vast majority of the energy used to control humidity. Therefore, a sensor which can survive and accurately measure humidity in hot, wet conditions will allow considerable savings.

Simulations of the energy consumption and savings available from enthalpy economizer control and supply air temperature resets were performed for buildings in Houston, Dallas, and Philadelphia. Temperature economizers were shown to attain between 90% and 95% of the savings of an enthalpy economizer. A spreadsheet simulation of enthalpy economizer use showed that the savings available are heavily dependent on the ability to avoid its use on very hot, humid days.

A newly-designed condensation sensor was developed for this project. It relies on the order-of-magnitude difference in AC reactance between humid air and liquid water. When installed on an AHU, it detects water condensing off the cooling coil as the temperature of the air drops below the dew point. Electronics were designed to provide the 0.25 V, 131 kHz current required and to obtain a 0 V output when dry and a 5 V output when wet.

A field reliability test was successfully performed with the sensor passively monitoring the transitions from wet to dry at Langford Building A and the Jack E. Brown Building at Texas A&M University, College Station, TX. The sensor was shown to be able to provide the reliable state change detection needed to control an economizer. The main limitation of this sensor is slow response on dry-to-wet and wet-to-dry transitions. Most measured dry-to-wet response times were between 5 and 10 minutes, which were driven by the time required to saturate the cooling coil.

DEDICATION

To my uncle, Guy Peckitt, for encouraging my interest in scientific and technical matters, and helping me explore them for the past twenty years.

ACKNOWLEDGEMENTS

This project was made possible by the support of the Energy Systems Laboratory at Texas A&M University. Thanks go to Dr. Charles Culp for advising me and supporting me as I navigated past its problems and pitfalls. Kevin Christman, Jim Watt, Joseph Martinez, and Dr. Lei Wang contributed to my knowledge of building science and asked questions that helped drive development.

Steve Payne and Erwin Thomas of the Texas A&M Physics Electronics Shop helped me work out electronics and instrumentation problems; without the Physics Electronics Shop it would be virtually impossible to develop electronics in College Station. Layne Wylie generously gave me access to the Mechanical Engineering Student Machine Shop's equipment. Mathew Wiederstein and Michael Martine provided invaluable help with measurements and building access.

TABLE OF CONTENTS

LIST OF FIGURES

Page

LIST OF TABLES

Page

NOMENCLATURE

Variable	Definition
T_{OA}	Dry bulb temperature of the outside air, °F
T_{RA}	Dry bulb temperature of the return air, °F
T_{MA}	Dry bulb temperature of the mixed air, °F
T_{SA}	Dry bulb temperature of the supply air, °F
h_{OA}	Total enthalpy of the outside air, $\frac{Btu}{lb}$
h_{RA}	Total enthalpy of the return air, $\frac{Btu}{lb}$
h_{MA}	Total enthalpy of the mixed air, $\frac{Btu}{lb}$
has	Total enthalpy of the supply air, $\frac{Btu}{lb}$
DP_{OA}	Dew point temperature of the outside air, °F
DP_{RA}	Dew point temperature of the return air, °F
DP_{MA}	Dew point temperature of the mixed air, °F
DP_{SA}	Dew point temperature of the supply air, °F
$\dot{Q}_{Sensible}$	Sensible heat flow provided by the AHU's cooling or heating coil to the mixed air, $\frac{Btu}{min}$
$\dot{Q}_{Latent}$	Latent heat flow provided by the AHU's cooling or heating coil to the mixed air, $\frac{Btu}{min}$
$\dot{V}$	Supply air volumetric flow rate, $\frac{ft^3}{min}$
ρ_{air}	Density of supply air, $\frac{lb}{ft^3}$

(Maximum of [ΔT, 0])	Temperature difference across the cooling coil used to calculate energy consumption for sensible cooling
(Maximum of [Δw, 0])	Humidity ratio difference across the cooling coil used to calculate energy consumption for latent cooling
x_{OA}	Mass fraction of outside air in the mixed air
w_{OA}	Outside air humidity ratio, $\frac{lbs\ water}{lbs\ dry\ air}$
w_{RA}	Return air humidity ratio, $\frac{lbs\ water}{lbs\ dry\ air}$
w_{SA}	Supply air humidity ratio, $\frac{lbs\ water}{lbs\ dry\ air}$
$\dot{m}_{AIR}$	Mass flow rate of supply air to a space, $\frac{lbs}{min*ft^2}$
Δh	Difference in enthalpy between using 100% outside air and mixed air using the minimum outside air fraction, $\frac{Btu}{lb}$
Δcost	Difference in cost between using 100% outside air and mixed air using the minimum outside air fraction, $\frac{\$}{1000\ ft^2*year}$
η_{econ}	$\frac{Annual\ energy\ savings\ of\ an\ economizer\ with\ specified\ high\ limits, Btu}{Annual\ energy\ savings\ of\ a\ psychrometrically\ ideal\ economizer, Btu}$
t_{check}	Time required to determine whether the cooling coil is wet or dry at a given supply air temperature, minutes
τ_{coil}	Time constant of the coil with regards to changes in temperature when the CHWV setting is changed, minutes
T_{sensor}	Time required for the sensor to change state once the cooling coil leaving temperature has decreased below the dew point, minutes

$T_{measurement}$	Time required to measure a mixed-air dew point temperature by stepped reductions in cooling coil leaving temperature, minutes
$R_{operating}$	Ratio of the time spent with the AHU operating normally to the time spent at alternate supply temperatures while measuring dew points
Z_R	Resistive component of the total sensor impedance, Ω
Z_C	Capacitive component of the total sensor impedance, Ω
Z_L	Inductive component of the total sensor impedance, Ω
Z_{sensor}	Total impedance of the sensor, Ω
F	Oscillation frequency of the relaxation oscillator in Section 7.1, hz
V_{out}	Output voltage from a stage of a circuit, V
V_{in}	Input voltage to a stage of a circuit, V
P	Power dissipated by the voltage divider, W
DP_{OA}, DP_{RA}, DP_{MA}, DP_{SA}	Dew point temperatures of outside air, return air, mixed air, and supply air, °F
$\dot{V}_{MA}$	Volumetric flow rate of mixed air, ft^3/min
$\dot{m}_{MA}$	Mass flow rate of mixed air, lbs/min
$\vec{V}$	Component of air velocity perpendicular to coil, ft/min
$\dot{m}_{w,MA}$	Mass flow rate of water contained in the mixed air, lb/min
$\dot{m}_{w,SA}$	Mass flow rate of water contained in the supply air, lb/min
$\dot{m}_{removed}$	Mass flow rate of water removed from the mixed air by the cooling coil, lb/min

$\dot{m}_{w,actual}$	Measured mass flow rate of water removed from the mixed air by the cooling coil, lb/min
$m_{trapped}$	Mass of water trapped in the boundary layer near the fins of the cooling coil, lbs
$\rho_{trapped}$	Ratio of $m_{trapped}$ to the total internal volume of the coil, $\frac{lbs}{ft^3}$
P_{SAT}	Saturation vapor pressure of water in air at a given temperature, kPa
T_{CCL}	Cooling coil leaving temperature at any given time, °F
$T_{initial}$	Original cooling coil leaving temperature before a change in CHWV position, °F
T_{final}	Final cooling coil leaving temperature, °F
$\bar{x}$	Mean of the measured coil water capacities, lbs
S_x	Sample deviation of the measured coil water capacities, lbs
$t_{a/2,\ v}$	T-statistic for a given confidence level a and number of degrees of freedom v that the sample mean of the coil water capacities is within the interval given for its value

1. INTRODUCTION

Cooling and space heating of American commercial buildings consumed 650 TBtu of electrical energy in 2003, according to the U.S. Energy Information Administration [1]. This accounted for 19% of the 3.5 quadrillion Btu total electricity consumption of commercial buildings, at a cost of approximately $10 billion. Controlling indoor humidity and temperature requires this energy expenditure for occupant comfort and building protection.

Humidity and temperature are usually controlled in commercial buildings by the heating and cooling coils in air-handling units (AHUs). Dehumidification is traditionally provided by cooling the mixed air to 55°F, which is the dew point traditionally needed to make the indoor air comfortable. Overcooling can result if the space loads are less than the cooling capacity of the air discharged into the space. When this occurs, reheating the air is often done to offset overcooling. Energy will then be consumed to reheat the air to maintain a comfortable space temperature.

In hot and humid climates, humidity control makes up a significant portion of building energy consumption. According to TIAX [2], sensible heat ratios vary from 0.5 to 0.8 depending on weather conditions, meaning 20% to 50% of the total cooling energy is used for dehumidification. An Energy Management and Control System (EMCS) is normally used to control the HVAC systems. For the EMCS to be able to control the humidity in the spaces supplied by the AHU, it must have reliable data about the mixed air humidity, or adopt a control strategy that ensures that the design latent

load can be met with any mixed air humidity level. This can cause unnecessary reheat usage as shown on the psychrometric diagram in Figure (1.1).

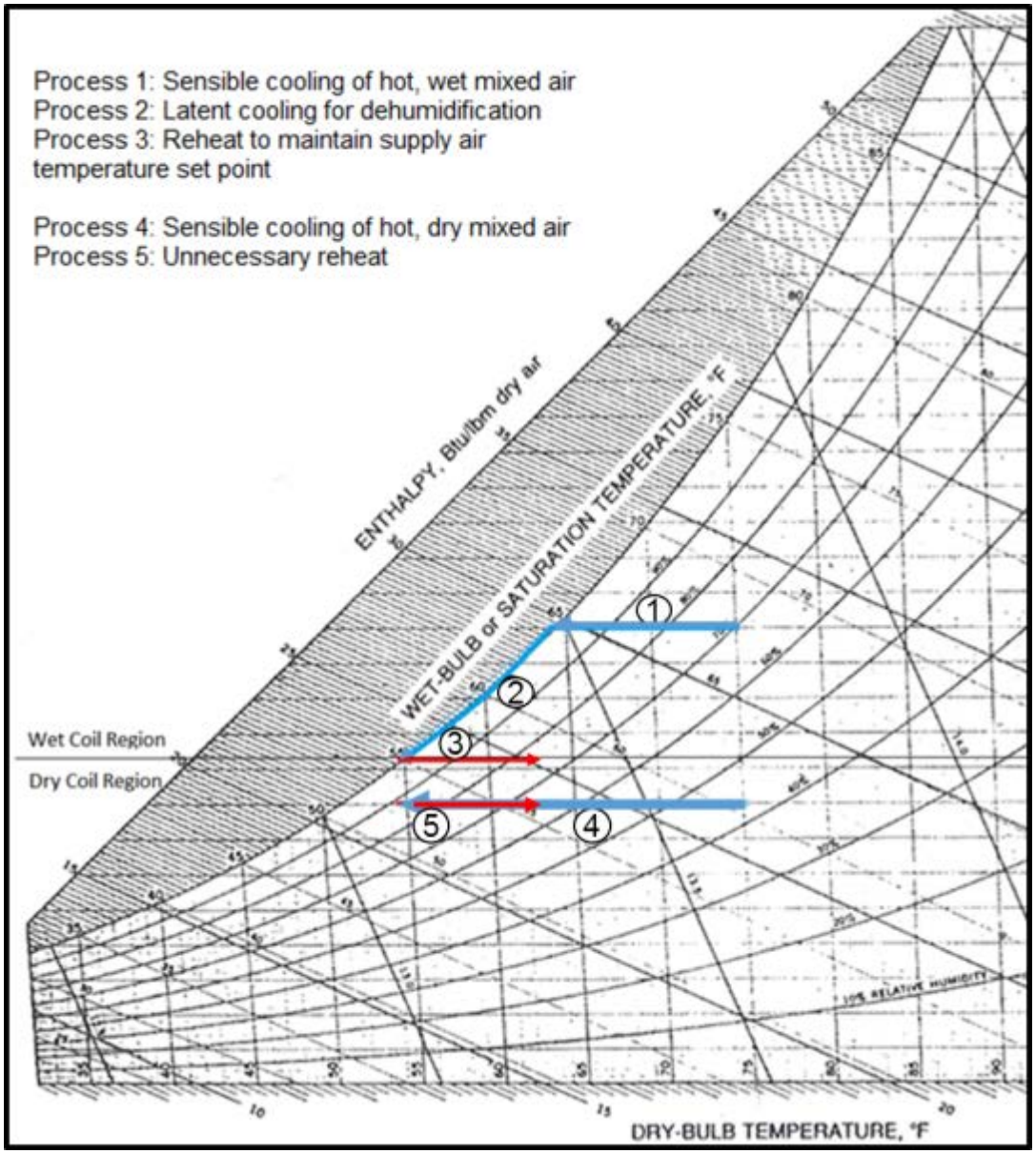

Figure (1.1) Psychrometric Chart Shows Benefits of Enthalpy Sensors

The literature shows that humidity sensors currently used in commercial buildings become inaccurate and suffer short life spans in the very humid conditions encountered in the southern United States. Several manufacturers' data sheets [3-8], indicate that they should not be used in saturated or condensing environments. Griesel et al. [9] state that "Continuous high humidity conditions are representing [sic] a great challenge for capacitive humidity sensors causing increased errors and calibration drift. During longer episodes of saturation some sensors tend to give readings well above 100% RH and beyond tolerance. Although in some cases manufacturers cut off these values to limit the output range at 100% RH the sensor internally is in a critical state which can lead to calibration drift or damage." In this study, tests were performed on several commercial resistive and capacitive sensors. The results, described in the "Existing Humidity Sensors" section, showed that commercial sensors are not suitable for use where condensing environments can occur. For example, the Measurement Specialties HS1101LF gave a capacitance value two orders of magnitude greater than the expected value at saturation when exposed to water.

The purpose and objective of this study was to find a method that would allow for reliable mixed air humidity measurements, then prototype a design that performs this task, and finally test it in a building environment. Secondary objectives included evaluating the potential for energy savings with this sensor using WinAM simulations and economizer models, and testing commercially available humidity and dew point temperature sensors.

2. LITERATURE REVIEW

The literature review for this thesis was comprised of sections on psychrometrics and humidity control, economizers and outside air control, present commercial humidity sensors, electrochemical and physical properties of water, and analog electronics. The first three sections established the state of equipment used in buildings for humidity and air control, while the last two aided the design of the new sensor.

Many different types of air humidity sensors exist, with different conditions where they will provide accurate results [10]. These sensors use the changes in the electrical, mechanical, and physical properties of materials to detect changes in humidity. Most building humidity sensors use the change of capacitance or resistance in a porous medium due to water absorption, or the change of reflectivity when water begins to condense on a chilled mirror [10]. Infrared sensors that detect water vapor directly recently became available [11]. Metal oxide, absorbent salt, soil conductivity, human hair and direct capacitance sensors are the current technologies used to detect or measure the presence of water vapor [10]. Wilson and Fontes, in the “Sensor Technology Handbook” [10] stated that sensors drift under conditions of high humidity and are damaged by liquid water.

Outside air is used to displace and dilute contaminants inside a building, and to maintain positive pressure to prevent infiltration of unconditioned, unfiltered air. Occupants, furnishings, cooking, and industrial processes produce building air contamination, so the minimum quantity of outside air needed to maintain acceptable indoor air quality will depend on the sizes of these sources. ASHRAE Standard 62.1-2010 [12] provides procedures to “specify minimum ventilation rates and other

measures intended to provide indoor air quality that is acceptable to human occupants and that minimizes adverse health effects."

Since conditioning incoming outside air usually involves heating, cooling, or dehumidifying the air, the outside airflow rate is often kept near this minimum to save energy [13]. Both Harriman et al. [13] and Henderson [14] point out that an additional energy cost will be incurred when controlling humidity. Under wet coil conditions both sensible and latent heat is removed from the supply air.

However, when the enthalpy or temperature of the outside air is less than that of the return air, and the internal gains of the building would otherwise require cooling, replacing more return air with outside air can reduce the energy consumption. This is known as an "economizer" cycle and if correctly controlled can reduce or eliminate cooling energy consumption when the outside air enthalpy is below that of the return air.

2.1 Psychrometrics, Humidity, Humidity Control (Sections 1, 3, and 4)

Harriman et al. [13] define *humidity moderation* as "…the HVAC system helps the building avoid extremes of humidity, but that humidity can still swing, uncontrolled, throughout a broad range over 24 hours" [13, p4] and *humidity control* as "…the indoor humidity is held within a defined range at all times. That range may be wide or narrow, and it may only have a high or low limit rather than both. But when a building is said to require humidity control, we assume the system must not allow the indoor humidity to rise or fall beyond the limits specified by the owner" [13, p4]. Sections 5 - 9 from this reference describe the problems which can occur with poor humidity control. Insufficient humidity causes static charge buildup and promotes viral growth; excessive humidity allows mold and bacteria to grow.

Rose [15] points out that any surface that offers resistance to water vapor passing through will have condensation on it whenever its temperature drops below the dew point of the air next to it. Such surfaces include walls, windows, doors, or vapor barriers. This causes problems when insulation or paneling is installed on the “wet side” of any water retarder, which argues against the recommendations of Harriman et al. [13] that demand a very watertight and airtight building envelope for several types of commercial buildings. Rose gives recommendations that are determined by the climate, recommending: “For hot humid climates such as Houston, Miami, or Charleston, no interior vapor retarder and no low-permeance finishes such as vinyl wall covering on interior surfaces” [15, p182]. The wet side of a vapor retarder changes with the weather – an exterior window may have condensation on the inside surface on a cold day and on the outside surface on a hot, humid day.

Preventing condensation on surfaces and maintaining comfort over a fairly broad range of room temperatures lead to the recommendations in a paper by Schell [16] of measuring and controlling the dew point. The dew point is a function of the water concentration – for any given air temperature, there is a maximum amount of water vapor that can be dissolved in it. Thermal comfort depends on the occupants’ ability to shed heat to the surrounding air, which is heavily affected by the water concentration. Schell [16] points out that a 10°F span of dew point temperatures (55°F to 65°F) corresponds to a fairly narrow span of relative humidity at 75°F (50% to 70% RH). Therefore, if the dew point can be measured accurately, very tight control of humidity in a given airstream can be maintained. Shah et al., in a 1993 U.S. patent [17] described a control system dependent on dew point control which used a chilled mirror dew point sensor to measure it.

2.2 Economizers and Outside Air Control (Section 3)

Outside air temperature or outside air enthalpy is measured in order to control an economizer. In Taylor and Cheng's paper, "Economizer High Limit Controls and Why Enthalpy Economizers Don't Work" [18], the energy required to condition the mixed air depends on the difference between the mixed and supply temperature if the cooling coil is dry, and on enthalpy if the cooling coil is wet. Taylor and Cheng then describe the need for accurate humidity measurement when running an "enthalpy economizer" and recommends against their use given the inaccuracy of commercial humidity sensors. Their results, from San Francisco, Atlanta, and Albuquerque, show that differential enthalpy control cannot be accurately maintained when using a capacitive humidity sensor.

Wang and Song [19], show that over 70% of the energy used by a normal air-side system can be saved by running a strictly temperature controlled economizer when only sensible loads need to be met. With high-temperature cutoffs at close to 75°F and large supply volumes, it was possible to avoid cooling whenever the outside air temperature was below the room set point. Their simulation charted the possible savings or costs over a range of possible weather conditions. However, this paper makes no mention of humidity control, their temperature economizer use allowed outside air at up to 75 °F to be used as supply air regardless of outside air humidity. The Oklahoma climate that they simulated contains a large number of hours with high outside air humidity. Harriman et al. describe [13] many situations where economizer operation would be harmful, including when the outside air dew point is above the desired value for the space.

Feng et. al. [20], describe a test and an hour-by-hour simulation of a building in Lincoln, Nebraska, first with no economizer, then with a temperature economizer, then with an enthalpy economizer. Their results showed a 15% energy consumption reduction for a properly working enthalpy economizer when compared to a temperature economizer. Compensating for a ± 10% error in the mixed air relative humidity measurement gave a 0.8% to 1.2% increase in energy consumption. Therefore, tight accuracy in measurement wasn't necessary for good results. However, Feng et al. suffered repeated failures of humidity sensors when trying to test long-term accuracy over a few months. All-Weather Inc. [21] and Supco [22] recommend against the use of capacitive humidity sensors in saturated conditions, and Feng et al. explicitly note failures of these sensors.

Papers by Mumma [23] and Shank and Mumma [24] describe the design of control systems for dedicated outside air systems. They demonstrate that knowledge of outside air humidity is necessary for control of dampers and energy recovery devices. An energy recovery ventilator can only outperform a sensible heat recovery ventilator if it is operated when the outside air is humid. These conditions cause transfer of water from the incoming outside air to the exhaust air, reducing latent loads.

In a 1993 U.S. patent, Shah, Krueger, and Strand [17] designed a control system that took signals from both a dew point sensor and a relative humidity sensor and combined them into one controlling variable. They had previously encountered difficulty when trying to operate near the boundary between wet and dry coils. When the space was cooled by a dry coil, the temperature would decrease, causing the relative humidity to rise, which would force the control to reduce the discharge air temperature to condense water out of the mixed air. Incorporating a dew point check allowed compensation for this by keeping the system in the dehumidification mode only if the

dew point was too high for comfort.

2.3 Present Commercial Humidity Sensors (Section 4)

Many different types of air humidity sensors exist, with different conditions where they will provide accurate results. Electrical, mechanical, and physical properties of materials change when exposed to wetter or drier air. Many types of sensors have been used industrially to measure humidity or detect water, and these are described below.

Wilson and Fontes [10] give a general overview of the porous medium and chilled mirror sensors. Porous medium sensors work by having water absorbed into one side of an electrical component, changing its electrical properties. Since water has a high dielectric constant compared to air, the capacitance of an element with a porous electrode will increase when exposed to a more humid atmosphere. Since water has a lower resistance than air, allowing an element to be saturated will allow more current flow. Wilson states that this allows for both capacitive and resistive humidity sensors to be built.

Capacitive porous medium sensors are in broad use in buildings due to their 2% - 5% accuracy over the 10% - 90% range of relative humidity and their low cost [10, 25]. However, their response was slower than resistive porous medium sensors; Wilson and Fontes state “Response time is from 30 to 60 seconds for a 63% RH step change” [10, p 271] for the capacitive sensors, while Wilson and Fontes [10] cite 10 to 30 seconds for a resistive sensor. The chilled mirror type is suitable for measuring the dew point over a broad range of water concentrations, limited mainly by the built-in junction chiller/heater’s ability to reach that temperature. In service, its main limitation is cleanliness. The mirror must be kept clean to reflect light adequately. Roveti [25]

concentrates on the electrical outputs of these sensors. The capacitive and thermal conductivity sensors were found to have a nearly linear output over their working range, while the resistive sensor had a 10:1 difference between 90% and 100% relative humidity. This indicates its suitability as a “wet-dry” sensor if its durability is adequate.

Problems encountered with capacitive sensors included failure in condensing and saturated environments. A “saturated” environment is one where the relative humidity reaches the maximum value that can be maintained. A “condensing” environment occurs when air is cooled below its dew point and liquid water is separated from the air. Consense Corp. points out [26] that “The onset of condensation is a binary event” – liquid water is either present or absent. Griesel et al. state in their paper [9] that “Continuous high humidity conditions are representing [sic] a great challenge for capacitive humidity sensors causing increased errors and calibration drift. During longer episodes of saturation some sensors tend to give readings well above 100% RH and beyond tolerance. Although in some cases manufacturers cut off these values to limit the output range at 100% RH the sensor internally is in a critical state which can lead to calibration drift or damage.”

Feng et al. [20] has several examples of sensor failure preventing enthalpy economizer use, and shows poor results from previously saturated sensors. Kang and Wise [27] describe the construction of a porous medium polyimide sensor, the working principle, and the difficulty in returning the porous layer to a dry state before the dielectric material is damaged by the water when saturated. Their test sensors included a heater to reduce the RH whenever it rose above 80% - as warmer air can contain more water, a heated sensor can avoid condensation and extend the measurement range. Vaisala Inc. claims in an advertisement [28] that their “Humicap” sensors are capable of full recovery from saturation, but do not indicate what sort of technology is

used to allow this.

Several other papers and sales documents recommend against using the porous medium resistive and capacitive sensors in wet environments. Chen and Lu [29] provide several microscope photographs and drawings showing absorption in the porous layer of humidity sensors and damage caused to metal oxide and polyimide humidity sensors due to condensation. Most of their tests, both static and transient, were performed at low (< 10% RH) humidity to avoid damage. All-Weather Inc. [21], and Supco [24], both issue recommendations to avoid saturated and condensing environments with their porous medium sensors. Stokes [30] describes an air handling unit with a capacitive humidity sensor following the cooling coil, where the sensor indicated an apparent 100.6% RH continuously.

Chilled mirror sensors work on a different principle. Air passes through a tube containing a light, a mirror, and a photocell. Behind the mirror is a Peltier junction device, capable of rapidly cooling the mirror, and a temperature sensor. The light reflects off of the mirror and is detected by the photocell when dry. When the mirror is chilled to below the dew point water condenses on it and prevents reflection to the photocell. Charles Francisco's 1963 U.S. patent for this cycling chilled mirror system is given as reference [31].

Able Instruments and Controls [32] compared several types of sensors to determine which work best over several ranges of humidity. They found that "Accuracies of ± 0.2°C are possible with chilled mirror hygrometry. Multi-stages of Peltier cooling supplemented in some cases with either additional air or water cooling can provide an overall measurement range of - 85°C to almost 100°C dew point. Response times are fast and operation is relatively drift free. Inert construction and minimal maintenance requirements (the two features are intrinsically linked) also considered [sic], the chilled

mirror hygrometer is an excellent choice of sensor for demanding applications where the cost can be justified."

Heinonen's paper [33] describes operating a chilled mirror sensor as a dew point sensor between 0°C and - 40°C in a measurements and standards facility. Cooper's patent [34] is for a sapphire mirror coating that improves reflectivity of IR at the frequencies that water absorbs, allowing for increased precision and detection of a contaminated sensor.

Disadvantages of chilled mirror sensors include their cost, with current prices ranging from $2570 [35] to $5190 [36]. Another problem is keeping them clean. General Eastern describes a sophisticated "PACER" system to reduce contamination on the mirror in reference [37]. Able Instruments' guide [11] gives the reduced time that condensate is in contact with the mirror as an advantage of a cycling chilled mirror sensor over a sensor that continuously tries to maintain itself near the dew point.

Difficulties with the porous medium and chilled mirror building humidity sensors have led to investigation of several other types. Ueno and Straube were able to get accurate long-term results at high humidity levels using a block of wood as a capacitive sensor in their paper [38], but the response times were slow (36 - 48 hours for a step change). Consense Corp. in Maine sells what they claim to be a highly sensitive condensation sensor, but their website [26] does not give any information about how the sensor works. Human hair based humidity sensors were used for many years before the development of electronic sensors, but availability of suitable hair is limited. Nguyen Thi Thu Ha et al. [39] developed a hair sensor that rotated a mirror to direct light to different locations in order to improve sensitivity. Their results were consistent for individual sensors, but large sample-to-sample variations impeded calibration. General Electric [11] has developed and is selling a sensor based on IR absorption of specific

wavelengths by water vapor in the supply air. The data sheet for the GE Telaire Vaporstat 9002 provides expected values up to 95% RH.

Other types of water sensors are used in agriculture to detect the water content of the soil and in the oil and gas fields to detect liquid water in a pipe. A similar, thin gap sensor appears to be a viable water detector for this project. Soil water content is measured by several methods, and “holdup meters” are used to determine when a water injection into a well should end. Operation and characteristics of a capacitive, fluid contact holdup meter are described in Liu et al.’s paper [40]. Both holdup and soil sensors are capable of measuring the concentration of liquid water in a mixture and therefore must survive in a wet environment.

In a 1970 paper [41] Davis and Hughes describe a water contact resistance sensor using a pair of conductive grids with a small (50 μm) gap between them to allow measurements of small quantities of water. The response from the sensor was not measured as it was significantly shorter than the time it took for the soil water concentration to change. They reported that the sensors lasted for the length of their study. Blad et al. measured the capacitance of a similar sensor in their paper [42]. They found that they could measure the water content in unsaturated soil as well due to the difference in the dielectric properties between water and air.

Seyfried and Murdock [43] describe an alternating current “reflectometry” soil sensor. AC is provided to a soil sample via a pair of steel rods. As the water content of the soil increases, so does its capacitance. The bistable multivibrator circuit they use is set up to change frequency with a change in capacitance. The frequency is recorded and the instrument is calibrated against ethanol, water, and dry soil to allow it to measure the water content of various soil samples. It was able to measure the quantity of water within 2% for a given soil type, but output varied between different soils. Hanek

et al. [44] give the results of a multiyear test of similar sensors, all of which survived.

Other types of sensors have been tested for soil moisture measurement. A porous, needle type capacitive sensor similar to those used in air handlers was tested by Iwashita and Katayangi [45]. They were able to calibrate it and get accurate results for the soil water content, but no long-term testing was done. Malazian et al. [46] tested a vapor pressure measurement sensor using a porous block that absorbed water and was constrained against a load cell. It gave accurate measurements over an 18-month test but large device-to-device variations.

A broad variety of methods to measure humidity have been tested and commercially sold. These devices all have their own advantages and limitations. No device that detects water condensing off the coil in order to measure humidity has been found in the literature. A sensor which uses coil condensate in direct contact with electrodes in order to change the properties of an electrical circuit component will be original work.

2.4 Properties of Water, Electrochemistry of Materials (Sections 5 and 6)

In this project, water condensing off the cooling coil is to be used to complete a circuit in the sensor. Therefore, the electrical properties of the water determine the design of the sensor. The sensor's output must change significantly between wet and dry. Air's electrical resistance is in excess of $1*10^{11}\Omega$/cm, while the resistivity of pure water is 18 MΩ/cm, as given by [47, 48, and 49].

Mealy and Bowman describe in their paper [47] how any salt or metallic impurity in water rapidly reduces resistance – 100 ppb of sodium chloride reduces resistance to approximately 2 MΩ/cm. The New Mexico Department of the Environment paper [49]

details how various purification processes remove ions and how high the resistance rises. Above 10MΩ/cm, an ion exchange resin is needed to remove impurities. Information was not found in the literature about the electrical conductivity of coil condensate; testing several samples from different buildings will be part of this project.

In order to make a sensor self-cleaning, the surface will have to be at an angle to the water flow. According to Rame-Hart [50] if the contact angle between the water and the surface is larger than the slope of the surface, the water will roll off by gravity alone. This is shown in Figure (2.1). Sumner et al. [51] gave results showing that clean laboratory glass's water contact angle was approximately 10°, with progressively dirtier glass going up as high as 32°. Oiled or greased surfaces were hydrophobic, giving contact angles past 90°, and this allows drops to run off nearly horizontal surfaces.

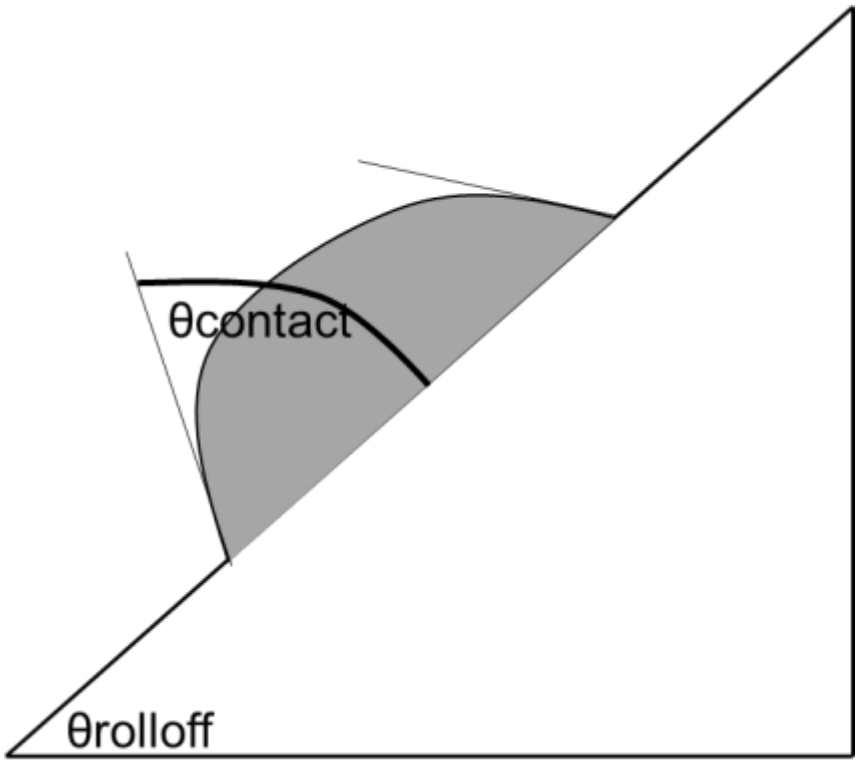

Figure (2.1) Water Runoff On Tilted Plate (Redrawn from Rame-Hart [50])

These electrical and mechanical properties of water will be used to design the coil enthalpy sensor. Differences in resistance will cause differences in electrical output if resistance is the measured property. Water must be able to run off sensing surfaces in order to make the sensor “self-cleaning.”

2.5 Analog Electronics and Test Equipment (Sections 7 and 8)

Analog electronics are used in this project to provide the desired distinct wet and dry states from the sensor. The AC frequencies used are typical of audio electronics, allowing use of common circuit elements. The output from the sensor electronics was monitored by an Onset Electronics Hobo U12-012 Logger, with inputs to the logger specified in its data sheet [52].

Storr, on the “electronicstutorials.ws” website [53] describes several circuits that can produce AC signals. Storr states that “Schmitt Waveform Generators can also be made using standard CMOS Logic NAND gates connected to produce an inverter circuit. Here, two NAND gates are connected together to produce another type of RC relaxation oscillator circuit that will generate a square wave shaped output waveform.” The circuit described by [53] was used for the 10 V, 1 kHz oscillator. Fairchild Semiconductor’s datasheet [54] for the Schmitt triggers used described their operating conditions. Later circuits used a Maxim 1099DS integrated circuit as a square wave oscillator. In its datasheet [55], Maxim Semiconductor describes the circuit, which “consists of a fixed-frequency 1.048 MHz master oscillator followed by two independent factory-programmable dividers.”

Filtering and amplification were required to get the desired output from the sensor. Shrader, in “Electronic Communication” [56], describes a filter as a “combination of capacitors, coils, and resistance that will allow certain frequencies to pass through or be impeded.” The average DC level of the sensor’s output had to be separated from the AC signal, and Shrader states that a filter is appropriate here: “Low-pass filters are used in electronic power supplies to pass DC but not variations of current or voltage…They can be employed between a transmitter and an antenna to prevent frequencies higher than the desired frequencies (such as harmonics) from appearing in the antenna.”

Sinclair and Dunton, in their “Practical Electronics Handbook” [57] describe the use of operational amplifiers to amplify signals in inverting and noninverting configurations and gives the equations necessary for design. Sinclair and Dunton claim that “The frequency range of an op-amp depends on two factors, the gain-bandwidth product for small signals, and the slew rate for large signals.” The required gain-bandwidth product for this application was calculated to be 5 MHz, which was satisfied by the Texas Instruments LME49710 amplifier, whose data sheet [58] claims a 45 MHz minimum gain-bandwidth product.

2.6 Literature Summary

The literature shows that the savings available from enthalpy economizers are heavily dependent on climate and on the accuracy of the humidity measurement provided to the Energy Management and Control System (EMCS). Existing humidity sensors have limitations that prevent their being used to determine a coil wet/dry state. The only sources found in the literature for a sensor that detects water in contact with

electrodes used it for soil moisture measurement. A sensor operating on a similar principle for building control has not been investigated. A reliable “coil enthalpy” sensor will significantly increase the operating range of an economizer in climates where outside air humidity varies widely.

3. ECONOMIZERS

An economizer is a system that allows an AHU to select a mixture of return and outside air so as to require the least energy for conditioning. Dampers and ducts have to be large enough to allow the mixed air to be composed of nearly all outside air (OA) or nearly all return air (RA). The Energy Management and Control System (EMCS) selects the air source based on the data it receives from its sensors. “Temperature” and “enthalpy” based controls are common. Figures (3.1) and (3.2) show an AHU featuring an economizer control.

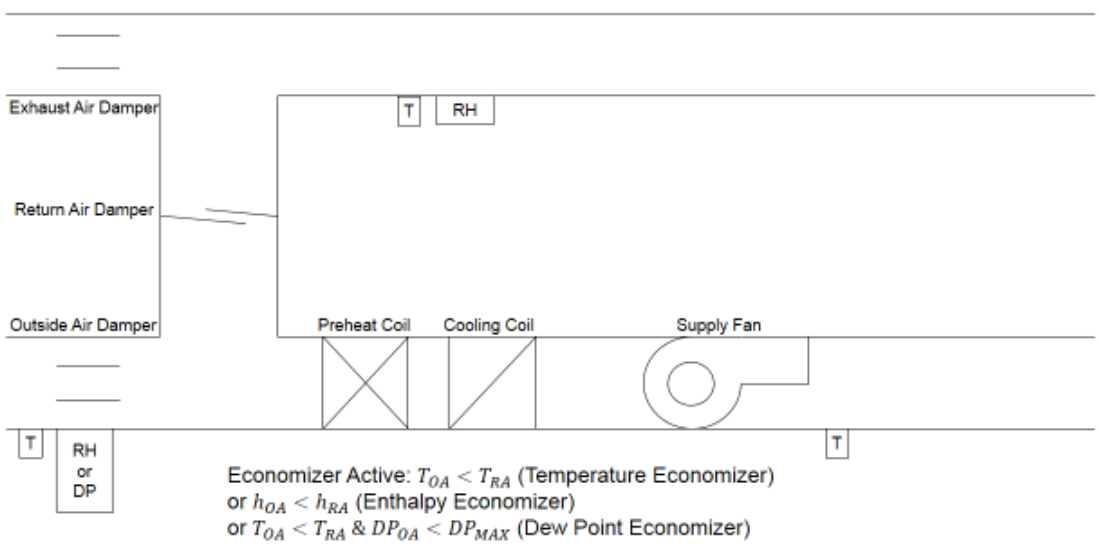

Figure (3.1) AHU with Economizer Active (Redrawn from Lee et al. [59])

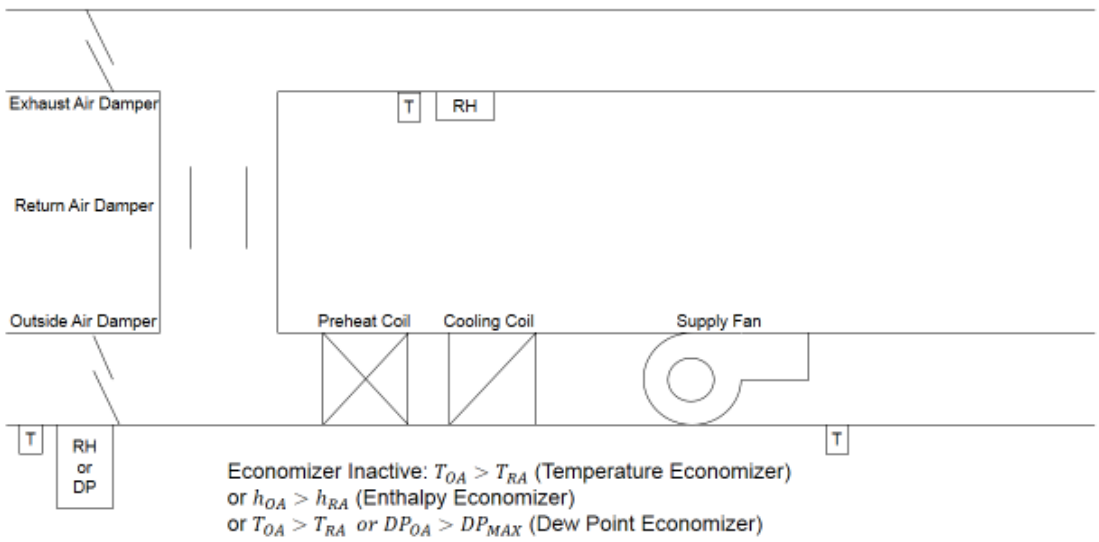

Figure (3.2) AHU Drawing With Economizer Inactive (Redrawn from Lee et al. [59])

Two savings estimates for a working "coil enthalpy" sensor were made. WinAM 4.3.35, a quasi-static simulator from the Texas A&M Energy Systems Laboratory, was used to simulate various economizer limit controls in Section 3.3. A cooling coil energy consumption model was also created in Microsoft Excel. The energy required to condition air to the desired supply air temperature depends on its temperature and humidity. For a workable simulation over 172 bins of dry bulb and dew point temperature, constant density was assumed, and this gives the following equations for the energy required for cooling in Btu:

$$\dot{Q}_{Sensible} = \dot{V} * \rho_{air} * \Delta T = 1.08 * \dot{V}_{cfm} * \Delta T_{°F} \qquad \text{Equation (3.1)}$$

$$\dot{Q}_{latent} = \dot{V} * \rho_{air} * \Delta W = 4840 * \dot{V}_{cfm} * \Delta W_{\frac{lbw}{lbda}} \qquad \text{Equation (3.2)}$$

A “dry” cooling coil needs to remove only sensible heat from the mixed air, as the water concentration of the air is less than or equal to the saturation limit at the supply temperature. If the mixed air temperature is already below the desired supply temperature, the chilled water valve is closed and no energy is consumed by the coil. A “wet” cooling coil removes sensible heat from the air until the saturation limit is reached, and then removes both sensible and latent heat until the saturated design condition is reached. The energy consumption of the coil is then given by Equation (3.3).

$$\dot{Q}_{Total} = \dot{V} * \rho_{air} * (Maximum\ of\ [\Delta T, 0] + Maximum\ of\ [\Delta W, 0]) \qquad \text{Equation (3.3)}$$

3.1 Spreadsheet Simulations

The energy savings for the economizer are then given by the difference between the energy requirement for conditioning the return air/outside air mix and the energy requirement for conditioning only the outside air. Tables of the energy savings, or energy losses, from running an economizer during various weather conditions were then generated.

An enthalpy table with a suggested control sequence is given in Figure (3.3). RA conditions of 75°F dry bulb and 55°F dew point gave an enthalpy of 29 Btu/lb. Each region of the chart had a different recommended operating sequence.

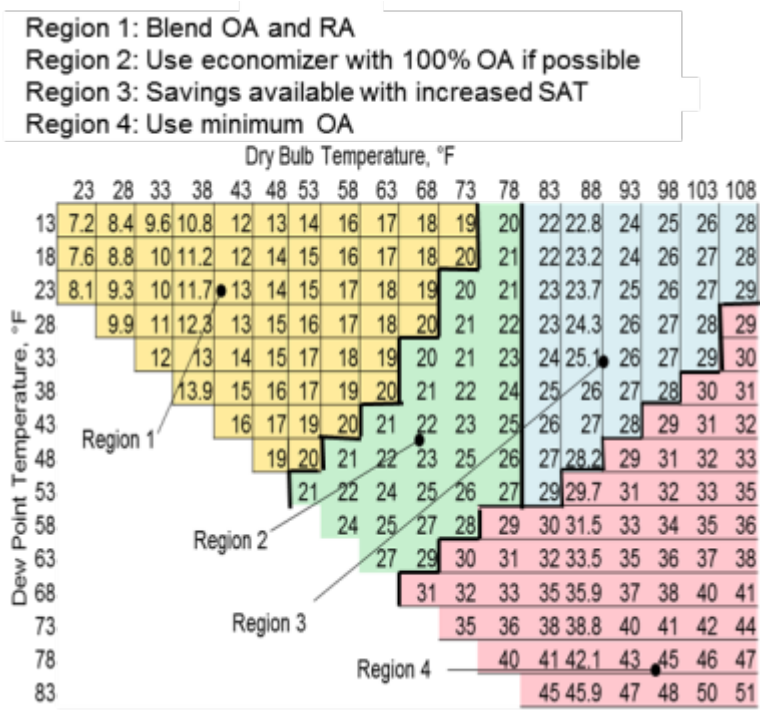

Figure (3.3) Enthalpy Versus Temperature and Dew Point

In Region 1 (boxed values), the outside air was dry and cool enough that its enthalpy was below that of the 55°F saturated supply air, requiring either only sensible cooling or satisfying the loads by itself. Region 1 can be referred to as the “free cooling” region, where the optimal OA/RA was not 100% OA. To avoid coil freezing, the economizer may have to be disabled below 34°F - 38°F dry bulb OAT.

In Region 2 (unlined), 100% OA requires less total cooling than RA, and is the lower cost option. In Region 3 (vertically lined), OA has lower enthalpy than RA, but requires much more sensible cooling than RA. An enthalpy economizer would only be effective here if the supply air temperature could be increased to take advantage of the

free latent cooling. In Region 4 (horizontally lined) of Figure (3.3), OA use should be minimized, as its enthalpy is greater than that of the RA.

An alternate method of using this information to determine an efficient control sequence is to calculate the cost of conditioning this air in Btu/lb using Equation (3.4). The results are shown in Figure (3.4). This chart suggests two possibly advantageous control strategies: one featuring a dry bulb temperature cutoff at 75°F and a dew point cutoff at 60°F, and one with a dry bulb temperature cutoff at 70°F. Figures (3.4) and (3.5) use Equation (3.4), derived from Equation (3.3). In Equation (3.4), the outside air mass fraction when the economizer is disabled is x_{OA}, with the return air fraction represented by $1 - x_{OA}$. An x_{OA} of 0.2 is used for the remainder of the spreadsheet analysis.

$$\frac{Q_{saved}}{\dot{m}_{supplied}} = (x_{OA} * 0.24 \frac{Btu}{lb * °\mathrm{F}} * (T_{OA} - T_{SA}) + \big((1 - x_{OA}) * 0.24 * (T_{RA} - T_{SA})\big) - \left(0.24 \frac{Btu}{lb * °\mathrm{F}} * (T_{OA} - T_{SA})\right) + \left(970 \frac{Btu}{lbm} * \left(MAX\big(0, x_{OA} * (w_{OA} - w_{sa}) + (1 - x_{OA}) * (w_{RA} - w_{SA})\big)\right)\right) - (970 \frac{Btu}{lbm} * (MAX(0, w_{OA} - w_{SA}) \qquad \text{Equation (3.4)}$$

Equation (3.4) can be considered descriptive for any economizer when using U.S. Customary System units. Figures (3.4) and (3.5) apply at elevations below 500'.

Economizer savings/loss versus 20% OA, Btu/lb

RA conditions 75° F 0.011 lbw/lbda

SA conditions 55° F 0.009 lbw/lbda

Outside Air Dew Point, °F	Outside Air Humidity Ratio, lbw/lbda	OAT °F 23	28	33	38	43	48	53	58	63	68	73	78	83	88	93	98	103	108
13	0.002	10	9.2	8.2	7.24	6.3	5.3	4.4	3.4	2.4	1.5	0.5	-0.4	-1.4	-2.4	-3.3	-4.3	-5	-6.2
18	0.002	10	9.2	8.3	7.32	6.4	5.4	4.4	3.5	2.5	1.6	0.6	-0.4	-1.3	-2.3	-3.2	-4.2	-5	-6.1
23	0.003	10	9.3	8.4	7.41	6.5	5.5	4.5	3.6	2.6	1.7	0.7	-0.3	-1.2	-2.2	-3.1	-4.1	-5	-6
28	0.003		9.5	8.5	7.53	6.6	5.6	4.7	3.7	2.7	1.8	0.8	-0.1	-1.1	-2.1	-3	-4	-5	-5.9
33	0.004			8.6	7.67	6.7	5.8	4.8	3.8	2.9	1.9	1	-0	-1	-1.9	-2.9	-3.8	-5	-5.8
38	0.005				7.84	6.9	5.9	5	4	3	2.1	1.1	0.2	-0.8	-1.8	-2.7	-3.7	-5	-5.6
43	0.006					7.1	6.1	5.2	4.2	3.2	2.3	1.3	0.4	-0.6	-1.6	-2.5	-3.5	-4	-5.4
48	0.007						6.4	5.4	4.4	3.5	2.5	1.6	0.6	-0.4	-1.3	-2.3	-3.2	-4	-5.2
53	0.009							5.7	4.7	3.8	2.8	1.8	0.9	-0.1	-1	-2	-3	-4	-4.9
58	0.01								3.8	2.9	1.9	1	0	-1	-1.9	-2.9	-3.8	-5	-5.8
63	0.012									1.3	0.3	-0.6	-1.6	-2.5	-3.5	-4.5	-5.4	-6	-7.3
68	0.015										-1.5	-2.5	-3.4	-4.4	-5.4	-6.3	-7.3	-8	-9.2
73	0.017											-4.6	-5.6	-6.6	-7.5	-8.5	-9.4	-10	-11
78	0.021												-8.1	-9.1	-10	-11	-12	-13	-14
83	0.025													-12	-13	-14	-15	-16	-17

Region 1
Region 2
Region 4

Figure (3.4) Economizer Savings and Losses versus Temperature and Dew Point

Economizer savings/loss versus 20% OA, Btu/lb

RA Conditions 75° F 0.011 lbw/lbda

SA Conditions 55° F 0.009 lbw/lbda

Dry Bulb Temperature, °F

Dew Point Temperature, °F	62	63	64	65	66	67	68	69	70	71	72	73	74	75	76	77	78	79
45	3.5	3.3	3.1	2.95	2.8	2.6	2.4	2.2	2	1.8	1.6	1.4	1.2	1.03	0.8	0.6	0.5	0.3
47.5	3.6	3.5	3.3	3.07	2.9	2.7	2.5	2.3	2.1	1.9	1.7	1.5	1.3	1.15	1	0.8	0.6	0.4
50	3.8	3.6	3.4	3.2	3	2.8	2.6	2.4	2.2	2.1	1.9	1.7	1.5	1.28	1.1	0.9	0.7	0.5
52.5	3.9	3.7	3.5	3.35	3.2	3	2.8	2.6	2.4	2.2	2	1.8	1.6	1.43	1.2	1	0.9	0.7
55	3.9	3.7	3.5	3.33	3.1	2.9	2.8	2.6	2.4	2.2	2	1.8	1.6	1.41	1.2	1	0.8	0.6
57.5	3.2	3	2.8	2.64	2.4	2.3	2.1	1.9	1.7	1.5	1.3	1.1	0.9	0.72	0.5	0.3	0.1	-0
60	2.5	2.3	2.1	1.9	1.7	1.5	1.3	1.1	0.9	0.7	0.6	0.4	0.2	-0	-0.2	-0.4	-1	-0.8
62.5	1.7	1.5	1.3	1.09	0.9	0.7	0.5	0.3	0.1	-0.1	-0.3	-0.4	-0.6	-0.8	-1	-1.2	-1	-1.6
65				0.21	0	-0	-0	-0.6	-0.7	-0.9	-1.1	-1.3	-1.5	-1.7	-1.9	-2.1	-2	-2.5
67.5							-1	-1.5	-1.7	-1.9	-2.1	-2.3	-2.5	-2.7	-2.8	-3	-3	-3.4
70										-2.9	-3.1	-3.3	-3.5	-3.7	-3.9	-4.1	-4	-4.5
72.5												-4.4	-4.6	-4.8	-5	-5.2	-5	-5.6
75															-6.2	-6.4	-7	-6.8
77.5																	-8	-8.1

Region 1
Region 2
Region 3

Figure (3.5) Economizer Savings or Losses versus Temperature and Dew Point: Concentrated Region

The main task for economizer control is to avoid operation in the horizontally lined area in the far right corners of Figures (3.4) and (3.5), where the outside air requires far more conditioning than the return air. A scheme with the dry bulb temperature sensor and the dew point sensor has two redundant ways to avoid operation “in the red”; it will shut off the economizer if either sensor is malfunctioning. Its value over a simple temperature cutoff at 65°F is the ability to operate in dry conditions between 65°F and 75°F and to shut down the economizer in very warm, wet conditions in the unlikely event that the outside air temperature sensor fails.

The energy savings available from an economizer depend on the climate and on the control system. Climates such as Denver or Albany allow for considerable “free cooling” from the outside air in the summer. Between 34°F and the supply air temperature set point, energy for heating the outside air to the desired supply temperature is available from the 75°F - 80°F return air, eliminating the need for either heating or cooling when the outside air volume can balance the internal load. Figure (3.6) is the “joint weather bin data” for Houston – the number of hours where the dew point and outside air temperature fall into a given bin. This allows bin-by-bin savings estimates.

Var1\Var2		Var2 - Dry Bulb Temp (F)															
		27.5	32.5	38	43	48	52.5	58	63	68	73	78	83	88	93	98	103
DPT																	
	13	0	0	0	2	2	0	0	0	0	0	0	0	0	0	0	0
	18	0	2	9	11	9	9	2	1	0	0	0	0	0	0	0	0
	23	0	16	7	18	12	6	18	11	1	0	0	0	0	0	0	0
	28	3	14	11	24	21	22	24	25	16	6	0	0	0	0	0	0
	33	0	0	22	41	44	46	30	30	20	0	0	4	0	0	0	0
	38	0	0	17	106	94	78	63	48	9	15	11	4	0	0	0	0
	43	0	0	0	32	107	108	55	52	28	20	7	3	0	2	0	0
	48	0	0	0	0	26	187	83	55	15	10	14	12	6	3	0	0
	53	0	0	0	0	0	53	216	93	53	45	24	37	15	0	0	0
	58	0	0	0	0	0	0	94	318	130	75	81	122	25	0	0	0
	63	0	0	0	0	0	0	0	198	392	214	181	162	68	37	13	3
	68	0	0	0	0	0	0	0	0	285	622	391	261	233	128	63	7
	73	0	0	0	0	0	0	0	0	0	236	686	476	310	197	32	0
	78	0	0	0	0	0	0	0	0	0	0	106	223	43	6	0	0
	83	0	0	0	0	0	0	0	0	0	0	0	0	0	0	1	0
	##	0	0	0	0	0	0	0	0	0	0	3	7	0	0	0	

Figure (3.6) Houston Annual Occurrence For Dry Bulb and Dew Point Bins Using TMY Hourly Data

Figure (3.7) provides an estimate of the savings from economizer operation in Houston by bin. “Joint-Frequency” bins were generated using eBin from the Texas A&M Energy Systems Laboratory. The dry bulb and dew point temperatures on these bins correspond to the midpoint of the bin; a 73˚F bin includes temperatures between 70˚F and 74.9˚F. Assuming a supply airflow per square foot of $\dot{V} = 0.7\ \frac{ft^3}{ft^2\ min}$, and an air density of $\rho = 0.075\ \frac{lbda}{ft^3}$, the hourly mass flow of supply air is given by Equation (3.5).

$$\dot{m}_{air} = \rho\dot{V} = 0.075\ \frac{lbda}{ft^3} * 0.7\ \frac{ft^3}{ft^2\ min} * 60\frac{min}{hr} = 3.15\frac{lbm}{ft^2\ hr} \qquad \text{Equation (3.5)}$$

The efficiency of the cooling system (chiller, distribution system, AHU cooling coil) was assumed to be constant: $\eta_{system} = \frac{1\ kW\ electricity}{12000\ Btu/hr} = \frac{1\ kWh}{12000\ Btu}$, and a constant

electricity cost of $\frac{\$0.10}{kWh}$ was used. This allowed calculation of savings by bin by using Equations (3.6), (3.7), and (3.8). Equation (3.6) calculates $\Delta\dot{Q}$, the change in total cooling required when the economizer is active, with Δh for each temperature and dew point bin given in Figure (3.5). Return air conditions were assumed to be 75°F with a 55° dew point. A sensible energy balance was performed on the building used for the WinAM analysis, and this gave a balance point temperature of approximately 30°F. Equation (3.7) calculates the difference in cooling use per bin by multiplying the number of annual hours in the temperature/dew point joint bin by $\Delta\dot{Q}$, and then determining the cost of that cooling by using η_{system} and the electrical cost. Equation (3.8) is a sample calculation showing the 48°F temperature and 38°F dew point bin in Houston.

$$\Delta\dot{Q} = \dot{m}\Delta h = \rho\dot{V}\Delta h \qquad \text{Equation (3.6)}$$

$$\Delta Cost\ (\frac{\$}{year * ft^2}) = \Delta\dot{Q}\left(\frac{Btu}{hr * ft^2}\right) * n_{hours/year} * \eta_{system}\left(\frac{kWh}{12000\ Btu}\right) * Cost\ (\frac{\$}{kWh})$$

Equation (3.7)

$$\Delta Cost = 5.9\ \frac{Btu}{lbm} * 3.15\ \frac{lbm}{ft^2 * hr} * 94\frac{hr}{year} * 1\left(\frac{kWh}{12000\ Btu}\right) * \frac{\$0.10}{kWh} = \frac{\$0.0145}{ft^2 * yr} = \frac{\$14.50}{ft^2 * yr}$$

Equation (3.8)

Houston savings/cost per year by using economizer rather than 20% OA, by bin

Data are in $\frac{\$}{1000\,ft^2*year}$

Dry Bulb Temperature, °F

Dew Point Temperature, °F	28	33	38	43	48	53	58	63	68	73	78	83	88	93	98	103	108
13	0	0	0	0.3	0.3	0	0	0									
18	0	0.4	1.73	1.8	1.3	1	0.2	0.1									
23	0	3.5	1.36	3	1.7	0.7	1.7	0.8									
28	0.7	3.1	2.17	4.1	3.1	2.7	2.3	1.8	0.7	0.1							
33			4.43	7.2	6.6	5.8	3	2.3	1	0	0	-0.1					
38			3.5	19	15	10	6.6	3.8	0.5	0.4	0	-0.1					
43				5.9	17	15	6.1	4.4	1.7	0.7	0.1	-0	0	-0.1			
48					4.3	27	9.7	5	1	0.4	0.2	-0.1	-0.2	-0.2			
53						7.9	27	9.2	3.9	2.2	0.6	-0.1	-0.4	0			
58							9.5	24	6.6	1.9	0	-3.1	-1.3	0			
63								6.8	3.5	-3.5	-7.5	-11	-6.2	-4.3	-1.8	-1	
68									-11	-40	-35	-30	-33	-21	-12	-2	0
73										-29	-101	-82	-61	-44	-7.9	0	0
78											-23	-53	-11	-1.7	0		
83														0	-0.4		

Figure (3.7) Houston Bin Results

Figure (3.7) clearly shows the benefits of a dew point economizer high limit cutoff control. Note that inadvertent operation of the economizer when the dew point is between 70°F and 74.9°F could eliminate all savings from the economizer operation throughout the year! The losses in the 73°F dew point bin add up to $\frac{\$325}{1000\,ft^2*yr}$ versus total savings over the year of $\frac{\$277}{1000\,ft^2*yr}$. Zhou et al. [60] defined "persistent savings" as "the savings (or waste if negative) that can be achieved if economizer [sic] is enabled all year-round" and the "P-ratio" as "the ratio of the persistent savings over the maximum savings, and can be used as a gauge for potential penalty for running the economizer

all year-round. The penalties range from “minor” for Denver to “devastating” for Houston and Miami.” Zhou et al. give P-ratio values of 88% for Denver, - 427% for Houston, and - 2936% for Miami. The results from Figure (3.7) confirm that losses for year-round operation in Houston would be 4 times the available savings from correct operation.

Dallas and Philadelphia weather were also simulated, with Dallas showing a P-ratio of 19% and Philadelphia showing a P-ratio of 72%. Boxed cells in Figures (3.8) and (3.9) represent bins with savings in excess of $\frac{\$5}{1000\ ft^2 * year}$ and horizontally-lined cells feature losses in excess of $\frac{\$5}{1000\ ft^2 * year}$. These also pointed to the importance of working high limit cutoffs in all climates. In both cities, a dry bulb high limit cutoff either avoids operating the economizer in regions with savings available or operates the economizer in regions where it causes a loss.

Dallas savings/cost per year by using the economizer instead of 20% OA, by bin

Data are in $\frac{\$}{1000\ ft^2 * year}$

Dry Bulb Temperature, °F

Dew Point Temperature, °F	28	33	38	43	48	53	58	63	68	73	78	83	88	93	98	103	108
13	0.6	1	0.58	0.3	0	0	0	0	0	0	0	0	0	0	0	0	0
18	0.3	1.1	0.37	0.3	0.6	0.5	0.5	0.2	0	0	0	0	0	0	0	0	0
23	0.6	2.8	1.41	1.4	1.8	1.6	1.1	0.6	0	0.1	-0	0	0	0	0	0	0
28	0	1.4	3.31	4.9	3.5	2.4	1.3	0.8	0.3	0.1	-0	0	0	0	0	0	0
33	0	0.3	10.9	13	7.4	5.1	1.8	0.9	0.3	0.1	-0	-0	0	0	0	0	0
38	0	0	1.33	9.4	8.3	6.7	3.3	2.1	0.7	0.3	0	-0	0	0	0	0	0
43	0	0	0	3.7	7.9	4.1	3.4	1.8	0.8	0.4	0	-0.1	-0.3	-0.2	-0	0	0
48	0	0	0	0	2.5	6.9	3.9	2.7	1.3	0.7	0.3	-0.2	-0.2	-0.3	-0.3	-0	0
53	0	0	0	0	0	3.5	5.4	6.4	2.9	1.8	0.9	-0	-0.5	-0.5	-0.2	-0	-0
58	0	0	0	0	0	0	1.2	4.5	3.8	1.6	0	-0.8	-1.5	-1.3	-1.4	-2	-0.6
63	0	0	0	0	0	0	0	1	1.3	-2	-3.7	-4	-6.2	-7.1	-8.5	-5	-0.2
68	0	0	0	0	0	0	0	0	-1.1	-5.5	-14	-20	-19	-15	-5.2	0	0
73	0	0	0	0	0	0	0	0	0	0	-7	-7.3	-2.4	-1.9	-0.4	0	0
78	0	0	0	0	0	0	0	0	0	0	0	-0.1	0	0	0	0	0

Figure (3.8) Dallas Bin Results

Philadelphia savings/cost per year by using economizer instead of 20% OA, by bin.

Data are in $\frac{\$}{1000\ ft^2 * year}$

Dry Bulb Temperature, °F

Dew Point Temperature, °F	23	28	33	38	43	48	53	58	63	68	73	78	83	88	93	98	103	108
13	12	14	9.3	5.27	0.7	1.1	0.5	0.3	0.1	0	0	0	0	0	0	0	0	0
18	7.3	17	26	21.2	6.1	2.7	1	0.6	0.2	0	0	0	0	0	0	0	0	0
23	12	22	44	25.1	13	4	1.9	1.9	0.3	0	0	0	0	0	0	0	0	0
28	0.5	16	34	26.7	20	10	6.8	1.8	0.4	0.1	-0	0	0	0	0	0	0	0
33	0	5.7	25	24.1	22	11	5	1.6	1	0.3	-0	0	0	0	0	0	0	0
38	0	0	5.8	32.5	26	19	8	4.1	1.4	0.2	0	0	0	0	0	0	0	0
43	0	0	0	19.3	21	19	8.2	4.3	3.1	1.5	0.1	0	0	-0.1	0	0	0	0
48	0	0	0	0	15	25	15	7.9	4.9	3	0.5	-0.3	-0.1	-0.2	-0.1	0	0	0
53	0	0	0	0	0	9.7	21	17	6.8	3.2	1.6	-0.1	-0.8	-0.4	0	0	0	0
58	0	0	0	0	0	0	10	21	7.5	2.7	0	-2	-3.5	-1.4	-0.2	0	0	0
63	0	0	0	0	0	0	0	3.1	2	-3.1	-5.8	-7	-3.9	-2.5	-2.6	0	0	0
68	0	0	0	0	0	0	0	0	-3.3	-19	-15	-17	-13	-10	-4.2	-0.4	0	0
73	0	0	0	0	0	0	0	0	0	-10	-32	-20	-9.1	-2.9	-1	0	0	0
78	0	0	0	0	0	0	0	0	0	0	-2.6	-1.4	-0.8	0	0	0	0	0

Figure (3.9) Philadelphia Bin Results

Taylor [18] and Zhou et al. [60] compared economizers using hourly building simulations. Taylor's method modeled sensor error in DOE 2.2 for several different types of high limit cutoff and manufacturer specified errors: fixed dry bulb temperature, differential dry bulb temperature, fixed enthalpy, differential enthalpy, differential enthalpy with fixed dry bulb, fixed enthalpy with fixed dry bulb, and fixed dry bulb and fixed dew point. Zhou et al. compared economizer high limit cutoff temperatures per pound of air provided.

3.2 Economizer Index

A single “Economizer Index” can be used to compare economizer control strategies. A theoretical “ideal” economizer control would operate the economizer whenever the energy required to condition the outside air was less than the energy needed to condition the return air, and would reduce to a minimum outside air condition at all other times. This ideal economizer would require perfect (zero-error) temperature and humidity sensors on both outside and return air streams. Any other control scheme will achieve a lower level of savings than this, allowing the “Economizer Index” to be defined as:

$$\eta_{ECON} = \frac{\sum Savings}{\sum Savings,Ideal} \qquad \text{Equation (3.9)}$$

This index varies heavily with climate, as with any calculation involving economizers. The bin method used for the analysis of 100% outside air economizers allows rapid comparison of different economizer limit cutoffs and provides estimates for the losses that can occur when sensors fail. Several different economizer schemes were compared for each climate:

1) 100% OA at all times, which should provide identical results to the “Persistence Index” in Zhou et al. [60]
2) Temperature high-limit cutoff at 58°F
3) Temperature high-limit cutoff at 63°F
4) Temperature high-limit cutoff at 68°F
5) Temperature high-limit cutoff at 73°F
6) Temperature high-limit cutoff at 78°F
7) Temperature high-limit cutoff at 78°F with enthalpy cutoff at 27 Btu/lb
8) Temperature high-limit cutoff at 78°F with enthalpy cutoff at 29 Btu/lb
9) Temperature high-limit cutoff at 78°F with dew point cutoff at 53°F
10) Temperature high-limit cutoff at 78°F with dew point cutoff at 58°F

An example chart is shown in Figure (3.10) for Philadelphia with a high limit temperature cutoff at 78°F and a dew point cutoff at 58°F. The broad bordered area represents the region the economizer is able to operate in. This particular set of cutoffs achieves an economizer index of 0.991.

Philadelphia savings/cost per year by using economizer rather than 20% OA, by bin

Data are in $\frac{\$}{1000\,ft^2 * year}$

Dew Point Temperature, °F \ Dry Bulb Temperature, °F	28	33	38	43	48	53	58	63	68	73	78	83	88	93	98	103	108
13	14	9.3	5.27	0.7	1.1	0.5	0.3	0.1									
18	17	26	21.2	6.1	2.7	1	0.6	0.2									
23	22	44	25.1	13	4	1.9	1.9	0.3									
28	16	34	26.7	20	10	6.8	1.8	0.4	0.1	-0							
33	5.7	25	24.1	22	11	5	1.6	1	0.3	-0							
38		5.8	32.5	26	19	8	4.1	1.4	0.2	0							
43			19.3	21	19	8.2	4.3	3.1	1.5	0.1	0	0	-0.1				
48				15	25	15	7.9	4.9	3	0.5	-0.3	-0.1	-0.2	-0.1			
53					9.7	21	17	6.8	3.2	1.6	-0.1	-0.8	-0.4	0			
58						10	21	7.5	2.7	0	-2	-3.5	-1.4	-0.2			
63							3.1	2	-3.1	-5.8	-7	-3.9	-2.5	-2.6			
68								-3.3	-19	-15	-17	-13	-10	-4.2	-0.4		
73									-10	-32	-20	-9.1	-2.9	-1	0		
78										-2.6	-1.4	-0.8	0				

Region with economizer active

Region to use minimum OA

Figure (3.10) Economizer With High-Limit Cutoffs At 78°F Dry Bulb and 58°F Dew Point, Philadelphia

Values for this index based on the control scheme chosen are listed in Table (3.1). One assumption made is that the economizer operates down to 33°F outside dry bulb temperature; operating down to only 38°F in Philadelphia results in an economizer

index of 0.711 rather than 0.987. This is a larger loss than any of the high limit cutoffs against an ideal economizer, including total failure of the high limit cutoff, which resulted in an economizer index of 0.72. The main conclusions are that the vast majority of savings can be attained by simple temperature cutoff control and that dew point cutoff control can give identical performance to conventional enthalpy cutoff control. For example, in Dallas an economizer with cutoffs at 78°F dry bulb and 29 Btu/lb had an index of 0.978, while an economizer with cutoffs at 78°F dry bulb and 58°F dew point had an index of 0.986.

Economizer High Limits	**Houston**	**Dallas**	**Philadelphia**
100% OA	-0.936	0.194	0.72
Tdb < 58°F	0.746	0.784	0.942
Tdb < 63°F	0.922	0.901	0.976
Tdb < 68°F	0.945	0.958	0.946
Tdb < 73°F	0.743	0.945	0.87
Tdb < 78°F	0.241	0.816	0.8
Tdb < 78°F & H < 27 Btu/lb	0.963	0.941	0.971
Tdb < 78°F & H < 29 Btu/lb	0.989	0.978	0.991
Tdb < 78°F & Tdp < 53°F	0.841	0.925	0.933
Tdb < 78°F & Tdp < 58°F	0.969	0.986	0.989

Table (3.1) Table of Results From Economizer Simulation

3.3 WinAM Simulations

WinAM 4.3.35, a simulator from the Texas A&M Energy Systems Laboratory, was then used to generate year-round savings. WinAM calculated the energy consumption of the AHU each hour for one year (8760 hours) to evaluate the effects of temperature and enthalpy economizers. The WinAM simulation used a hypothetical 80,000 ft^2 commercial building with a single SDVAV AHU. The building's parameters are given in Table (3.2) and are meant to be typical for an office building.

Temperature, enthalpy, and inactive economizers were simulated using 2012 weather data from Houston, Dallas, and Philadelphia. Temperature economizer high-limit control parameters for minimum energy consumption were optimized by trial and error. Enthalpy economizer control parameters were set to exclude air above 78°F and 29 Btu/lb; above those values return air requires less cooling. WinAM does not feature dew point high-limit cutoffs; 78°F and 29 Btu/lb give a 55°F dew point.

Parameter	Value	Unit
System Type	SDVAV with Reheat	
Cooling Energy Source	Plant Electric Chillers	
Reheat Energy Source	Plant Gas Boilers	
Conditioned Floor Area	80000	sq. ft.
Interior Zone Percentage	66	%
Exterior Window and Wall Area	25000	sq. ft.
Window Percentage	20	%
Roof Area	40000	sq. ft.
Exterior Wall U-Value	0.15	Btu/ft^2*hr*°F
Exterior Window U-Value	1.2	Btu/ft^2*hr*°F
Roof U-Value	0.1	Btu/ft^2*hr*°F .
Weekday AHU Start Time	2	a.m.
Weekday AHU Stop Time	11	p.m.
Weekend AHU Start Time	2	a.m.
Weekend AHU Stop Time	11	p.m.
Minimum Primary Airflow	0.2	cfm/sq. ft.
Maximum Primary Airflow	1.6	cfm/sq. ft.
Interior Temperature Set Point	75	°F
Perimeter Temperature Set Point	76	°F
Minimum Outside Airflow	15	% of total flow
Economizer Properties	Variable	
Cooling Supply Air Temperature	55	°F
Peak Lighting Load	1.5	W/sq. ft.
Peak Plug Load	1.5	W/sq. ft.
Peak Occupancy	200	sq. ft./person
Sensible Heat Per Person	250	Btu/hr
Latent Heat Per Person	250	Btu/hr
Supply Fan Peak Power	0.781	hp/kcfm
Supply Fan Control Type	VFD	
Off-Peak Load Ratio	0.5	
Peak Hours Start Time	6	a.m.
Peak Hours End Time	6	p.m.

Table (3.2) Test Building Parameters for WinAM Model

Annual savings spreadsheets were then generated from the simulation outputs. The chilled water savings for an enthalpy economizer, relative to a temperature economizer, ranged from 1.9% in Houston to 5.2% in Philadelphia. These results are shown in Figure (3.11).

Chilled Water Savings		
City	Temperature Economizer Vs. No Economizer	Additional Savings For Enthalpy Economizer
Houston	10.7%	1.9%
Dallas	15.9%	3.3%
Philadelphia	32.7%	5.2%

Figure (3.11) Overall Savings From Enthalpy Economizers

The difference in monthly chilled water consumption between the temperature and the enthalpy economizer use is shown in Figures (3.12), (3.13), and (3.14). The only time an enthalpy economizer would be active, and the temperature economizer would be disabled, is when the outside air temperature is between 63°F and 78°F and the outside air is dry enough for the enthalpy to be below 29 Btu/lb. However, some months still showed chilled water savings of over 10%. The data series shown in Figures (3.12), (3.13), and (3.14) is the chilled water savings for each month.

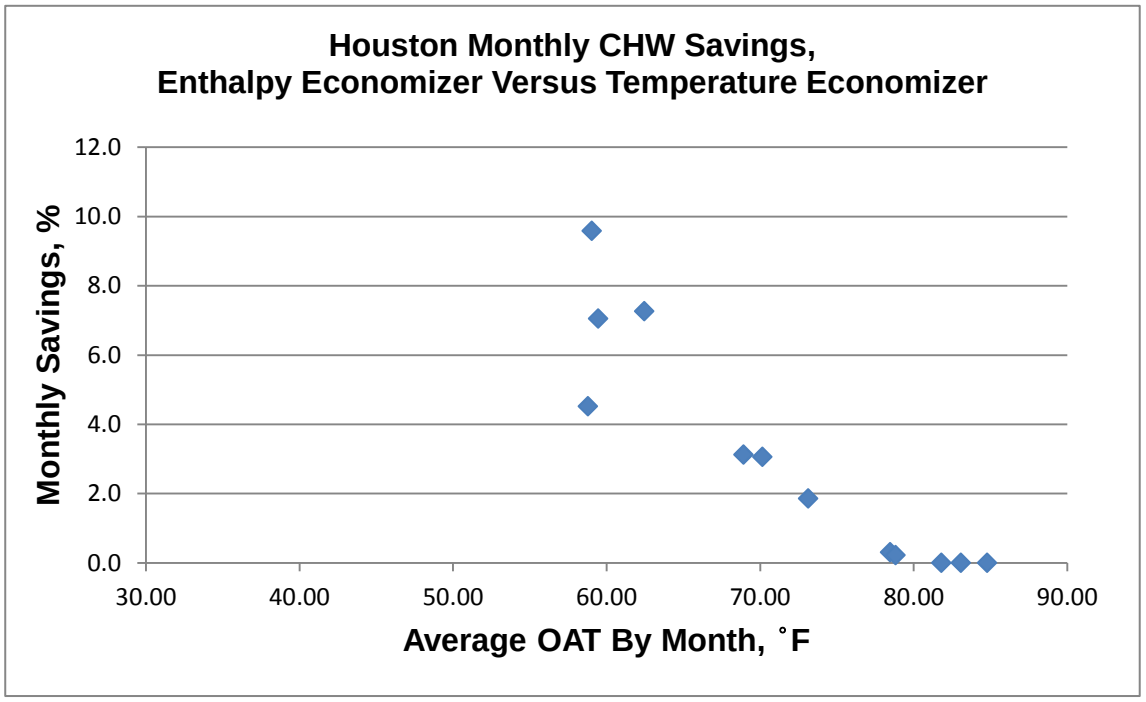

Figure (3.12) Houston Enthalpy Economizer Savings Beyond Temperature Economizer

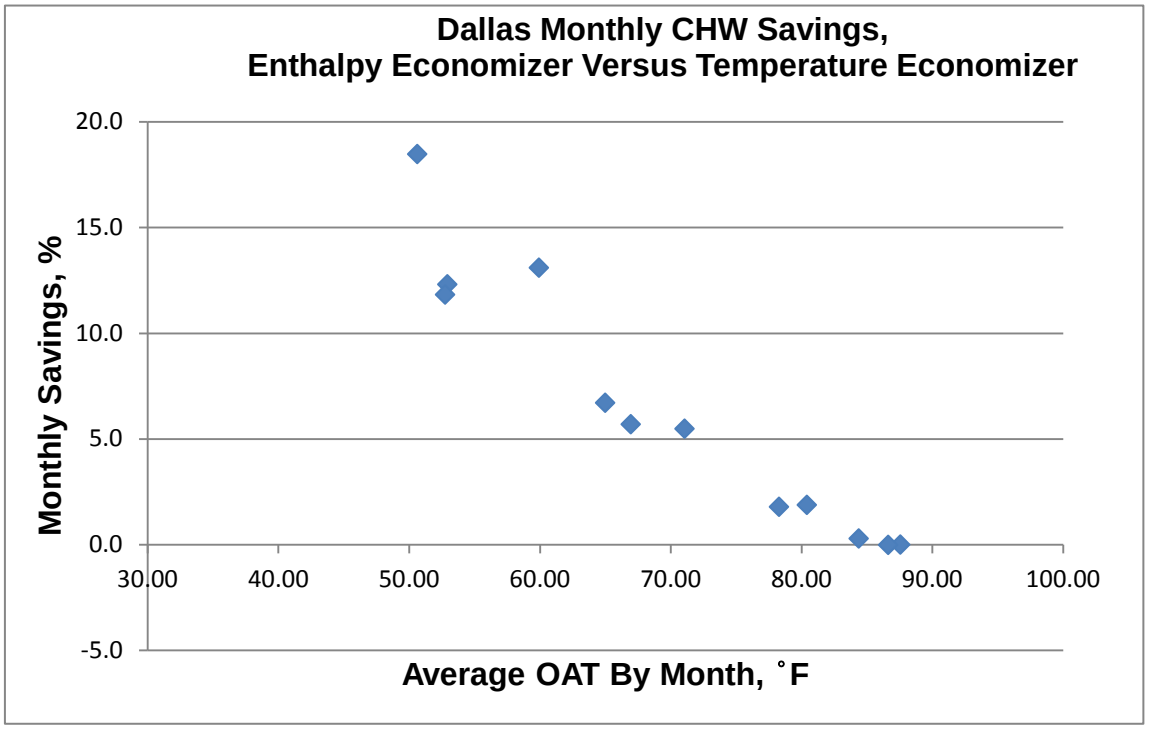

Figure (3.13) Dallas Enthalpy Economizer Savings Beyond Temperature Economizer

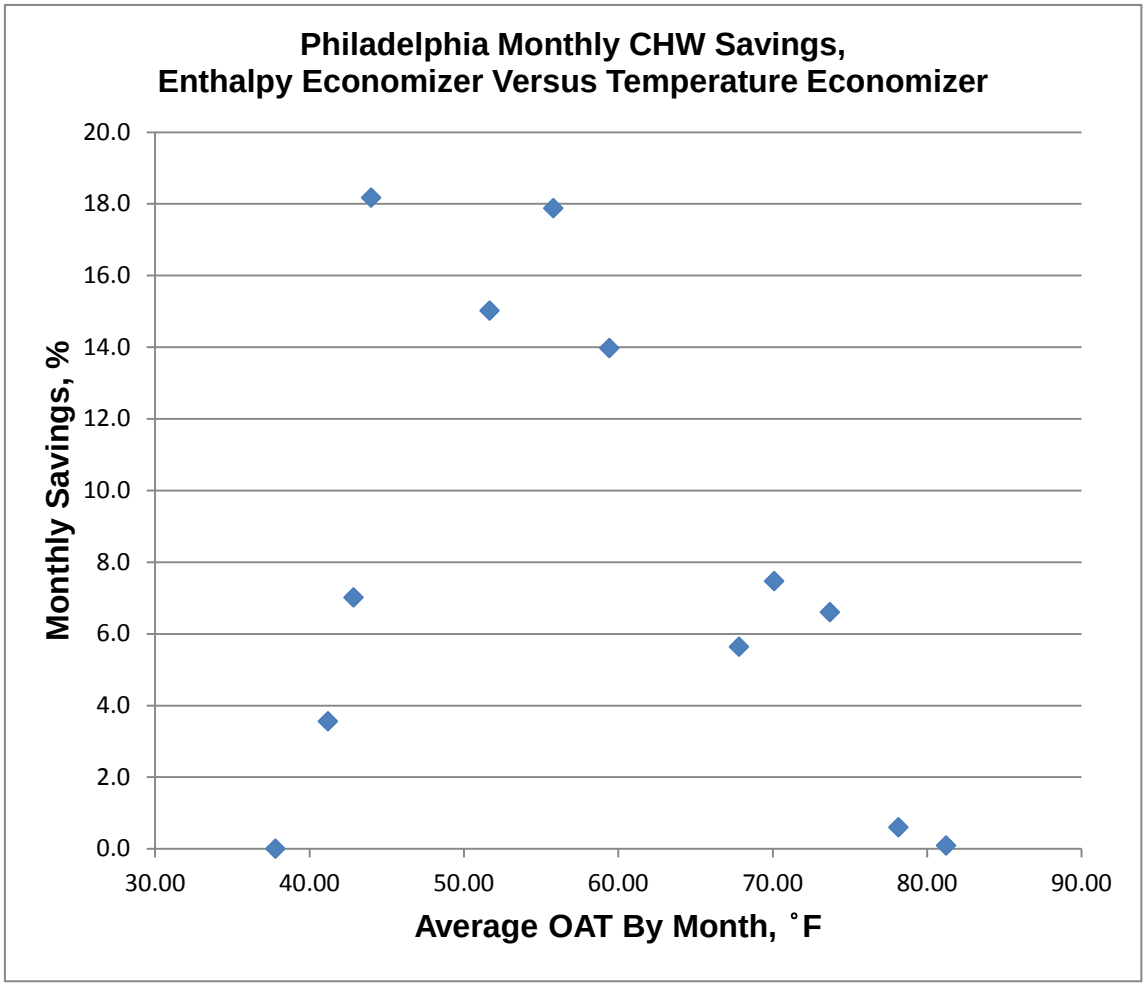

Figure (3.14) Philadelphia Enthalpy Economizer Savings Beyond Temperature Economizer

Both the WinAM analysis and the Economizer Index calculations indicate that a marginal savings of 2% - 5% of chilled water is possible with an economizer controlled using temperature and enthalpy high limits compared to one with a temperature high limit. This represents $1000-2000 per year for a 100,000 ft^2 building. The economizer index calculations show that performance of properly operating high-limit controls will be

similar between enthalpy and dew point cutoffs, and that the “freeze stat” low limit set point is also important. One additional benefit of a dew point or humidity sensor in an economizer application is that it provides an independent high-limit cutoff that will avoid operating the economizer in conditions that destroy savings. Either a 58°F maximum dew point or a 73°F maximum dry bulb temperature will avoid these conditions in any climate analyzed.

4. COMMERCIAL HUMIDITY SENSOR TESTS

A sensor was required to detect if water is condensing on the coil. The minimum requirements for this sensor were to provide a clear difference between the “wet” and “dry” states and to survive for several years in an AHU. If a commercially available sensor were able to achieve these, it would save a considerable amount of time in design, fabrication, testing, and electronics for a new sensor design.

Humidity sensors of the resistive, capacitive, and chilled mirror types are widely available commercially. In the literature review, several sources [9, 20, 27] pointed to possible problems when using capacitive or resistive sensors to detect the difference between condensing and noncondensing states. Six different resistive or capacitive sensors were purchased from Digikey (http://www.digikey.com/). Their data sheets are in references [3-8]. Their cost ranged from $5 to $10.

The sensors were installed in a solderless breadboard and connected to power, ground, and the signal as specified in the pin-out diagrams in their datasheets. The TDK CHS-MSS and TDK CHS-CSC-20 were connected to a National Instruments analog input board with an analog-to-digital converter. A National Instruments LabView Virtual Instrument was then used to record the voltage while the sensor was under test. The Parallax HS1101, Measurement Specialties HS1101LF, and Honeywell HIH-1000 were simple two-terminal components whose capacitance varied with humidity. They were connected to a multimeter capable of measuring capacitance. The multimeter used a 10 kHz, 0.5 V triangle waveform to perform capacitance measurements. The Honeywell HIH-5030 was connected to 5 V power and ground, with the voltage output displayed on an oscilloscope.

Once connected, several tests were performed to determine the suitability of these sensors for the task of determining the state of the coil. Their response to changes in relative humidity was tested by using a portable electric heater to raise the temperature without adding water to the air, thus decreasing the relative humidity. The Honeywell HIH-1000 failed to show any difference in capacitance and was removed from further tests. This may have been caused by shipping or handling damage, or a sample defect.

The other five sensors were then subjected to the “dunk” test to determine how quickly and completely they could recover from total inundation. These sensors have a top surface area of less than 5 cm^2, so a single, large, 1 cm^3 drop of water falling from the cooling coil directly onto the sensor can cover it completely to a depth of 2 mm. With power, signal, and ground connected and data being recorded, the sensor was briefly placed in a jar of tap water and then removed.

The results are shown in Table (4.1) and Figure (4.1). The TDK CHS-MSS, shown in Figure (4.2) failed completely, registering a constant high output after the dunk. The TDK CHS-CSC-20, shown in Figure (4.3) failed completely, giving an apparently completely random output regardless of conditions, varying between 0 V and 0.75 V. The Parallax HS1101, shown in Figure (4.4) also failed, with its capacitance dropping by three orders of magnitude.

Sensor	Value (low) before dunk	Value (high) before dunk	Value (low) after dunk	Value (high) after dunk	Result
TDK CHS-MSS	0.4 V	2 V	2.6 V	2.6 V	FAILED
TDK CHS-CSC-20	0.6 V	1.8 V	0 V	0.75 V	FAILED
Parallax HS1101	0.68 µF	1.83 µF	5 nF	5 nF	FAILED
Measurement Specialties HS1101LF	130 pF	190 pF	16 nF	140 pF	FAILED
Honeywell HIH-5030	0 V	4 V	0 V	0 V	FAILED

Table (4.1) Results of Commercial Humidity Sensor Test

The behavior of the other two sensors was more complicated. The Measurement Specialties HS1101LF, shown in Figure (4.5), generated out-of-range outputs of 9.45 nF - 16.5 nF after being submerged; the data sheet gives 190 pF as the maximum value when saturated. However, after being dried at 140°F for fifteen minutes, the sensor returned to its normal output range. This was repeated twice with similar results. Leaving the sensor overnight in a building also returned it to the normal range; this process took in excess of two hours. The Honeywell HIH-5030, shown in Figure (4.6) was able to restore itself to normal operation after the first three dunk test cycles, but failed permanently on the fourth, giving an output of 0 V. The results from these tests are shown in Figure (4.1).

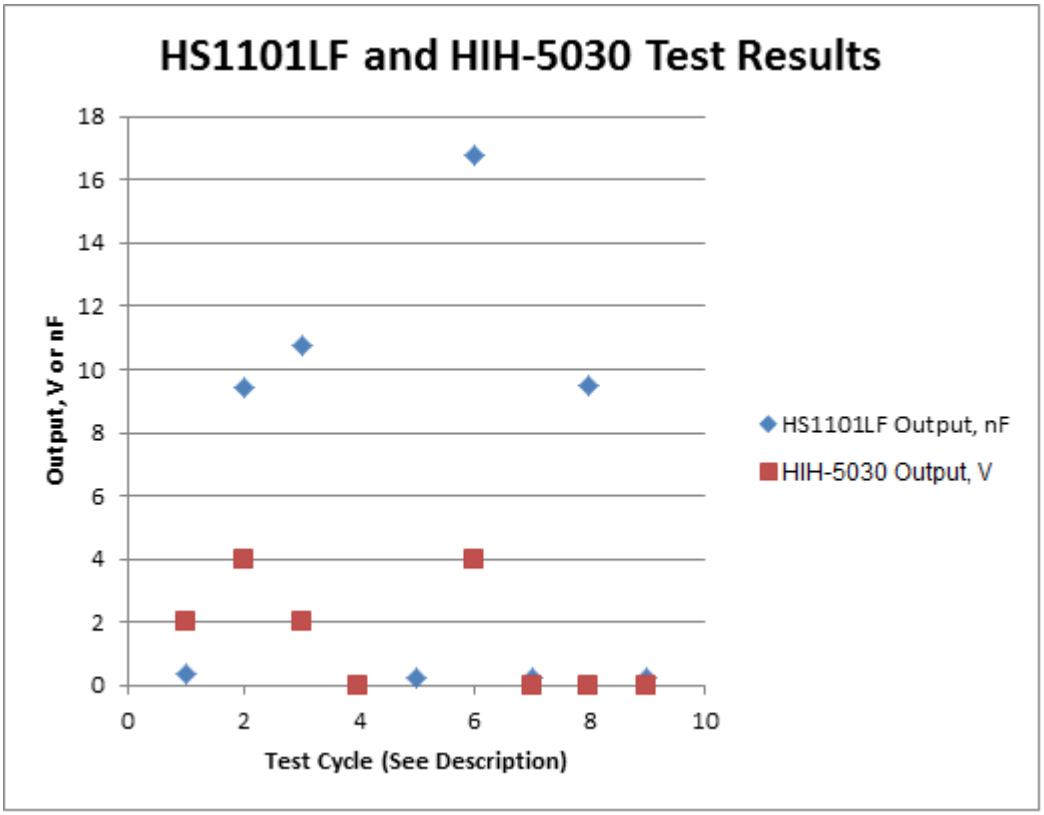

Figure (4.1) HIH-5030 and HS1101LF Test Results

None of these sensors passed the bench tests. None of the sensors could be installed in an AHU to detect water coming off of the coil. The conclusion from these tests is that a sensor used for this application would have to operate on a different principle than the porous medium sensors tested in this section.

Figure (4.2) TDK CHS-MSS Resistive Humidity Sensor With Built-In Electronics To Deliver Voltage Output (Digikey Image)

Figure (4.3) TDK CHS-CSC-20 Capacitive Humidity Sensor With Built-In Electronics to Deliver Voltage Output (Digikey Image)

Figure (4.4) Parallax HS1101 Capacitive Humidity Sensor

Figure (4.5) Measurement Specialties HS1101LF Capacitive Humidity Sensor

Figure (4.6) Honeywell HIH-5030 Capacitive Humidity Sensor
With Built-In Electronics to Deliver Voltage Output (Allied Electronics Image)

5. INITIAL TESTING AND DEVELOPMENT

Test results showed that commercial capacitive and resistive humidity sensors failed to meet the requirements identified for enthalpy measurement at the AHU cooling coil. Sources from the literature survey identified that these failures are likely due to the inherent properties of these sensors. Griesel et al. [9] listed several failure behaviors due to condensation during testing, including out-of-range readings, continued high-limit readings, and total cutoff and failure.

Since a successful “coil enthalpy” sensor would have to operate in a condensing environment whenever the coil was wet, a sensor operating under a different principle was necessary. In order to test whether a sensor could simply detect the onset of condensation by having water complete a circuit between two electrodes, a prototype was quickly fabricated from a test tube with two aluminum foil electrodes attached by cyanoacrylate glue and a hole in the bottom to allow water to drain.

Preliminary testing was conducted using the DC resistance measurement function on a Sears Craftsman 82139 multimeter. When dry, the resistance was in excess of 40 MΩ and beyond the meter’s upper limit. When the sensor was immersed in water, its resistance dropped into the 5-15 MΩ range. This large difference was promising and indicated that this was a valid means of detection. This prototype is shown in Figure (5.1)

Figure (5.1) Test Tube Test “Sensor”

Several limitations of this sensor were immediately apparent and further testing used different designs. The hole in the bottom had a diameter of approximately 1 cm, preventing the contacts from being bridged by small quantities of water. The electrodes were vulnerable to mechanical damage and tearing. Permanent attachment of the electrodes would require a different adhesive. A new sensor would have to be able to operate on as little as one drop of water, with a volume of roughly 1 cm^3, and would have to respond within five to ten minutes. This time requirement is analyzed in Section 5.1.

5.1 Response To State Changes

A fast response from the sensor was desired for control purposes and measurement accuracy. If frequent measurements of the dew point are to be taken as part of a building control sequence, the time required to take the measurements can be a significant portion of the time the AHU is operating. Several sensor “wet or dry” checks must be performed for each dew point temperature measurement. To perform one of these checks, the coil must first reach the steady state target temperature after approximately 5 coil time constants, and then the sensor must be monitored for its characteristic response time. The total time for a dew point measurement is given by Equations (5.1) and (5.2).

$$t_{check} = 5 * \tau_{coil} + t_{sensor} \qquad \text{Equation (5.1)}$$

$$t_{measurement} = t_{check} * \left(\frac{ABS(T_{initial} - T_{dew\ point})}{T_{step}} + 1\right) \qquad \text{Equation (5.2)}$$

where $t_{measurement}$ is the total time needed to take a dew point measurement, $ABS(T_{initial} - T_{dew\ point})$ is the difference between the supply air temperature at the start of the measurement and the dew point, and T_{step} is the amount the temperature is changed between each attempt to detect water. A sample control sequence to measure the dew point when the supply air temperature can be controlled is shown in Figure (5.2).

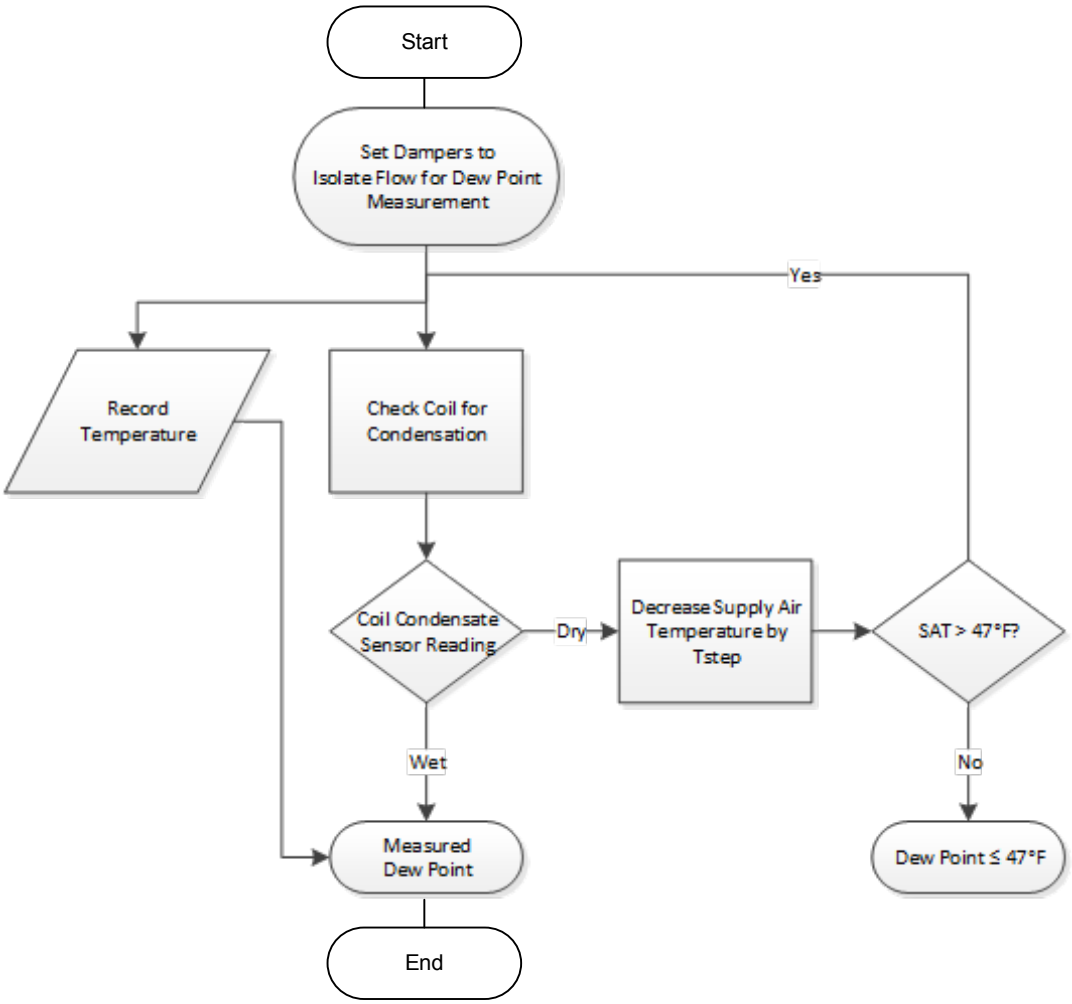

Figure (5.2) Control Sequence For Dew Point Measurement

An upper limit on the time allowed is provided by occupant comfort concerns. If the supply temperature used in the measurement is above the temperature needed to satisfy the sensible load, the room temperature will rise unless the mass of supply airflow is increased. Another limitation is the ratio of time spent testing to the time in normal operation. If three dew point measurements are taken per day, then this ratio is given by Equation (5.3).

$$R_{operating} = \frac{t_{AHUon}}{t_{meas} * n_{meas}} = \frac{t_{AHUon}}{3 * t_{meas}} \quad \text{Equation (5.3)}$$

For testing purposes, it was estimated that the maximum acceptable t_{meas} would be 15 minutes, and in order to measure mixed air dew points between 50 °F and 60 °F, up to 5 measurements would be required, meaning that the maximum acceptable t_{check} would be 3 minutes.

Factors influencing the delay between the supply air temperature falling below the dew point and water being detected at a given sensor location include the mass airflow, the humidity ratio difference between the actual dew point and the new supply temperature, the height and width of the cooling coil, the spacing between fins on the cooling coil, the design of the internal drains of the cooling coil, and the distance between the drip rail and the coil drain. The complexity of these calculations and the possibility of any one factor introducing a significant error meant that experimentally determining these delays appeared to be a more reliable method.

Timed testing of the delays involved was performed in Section 8.2, using SDVAV AHUs with coils featuring 12 fins/inch with external dimensions of 8’ x 4’ x 12”. Dry-to-wet time delays ranged from 45 seconds to 21 minutes. Wet-to-dry time delays were between 30 minutes and 45 minutes. Two applications were developed where this dry-to-wet response time was acceptable. In Section 8.6.1 a procedure was found to confirm a dew point provided by a weather station by testing the coil state with the coil leaving temperature above and below the dew point. In Section 8.6.2, economizer control using this sensor was determined to be practical.

5.2 Clip-On Sensor and Testing

The results of this test supported locating the sensor directly on the coil. The large glass sensor was unsuitable for this application. A very small (2.5 cm x 1 cm) and lightweight (< 10 g) new sensor was designed to be supported by press fits between its edges and fins on the cooling coil without damage. The electrodes would have a very small gap between them so that a small quantity of water would immediately trip it. A drawing of this sensor is shown in Figure (5.3)

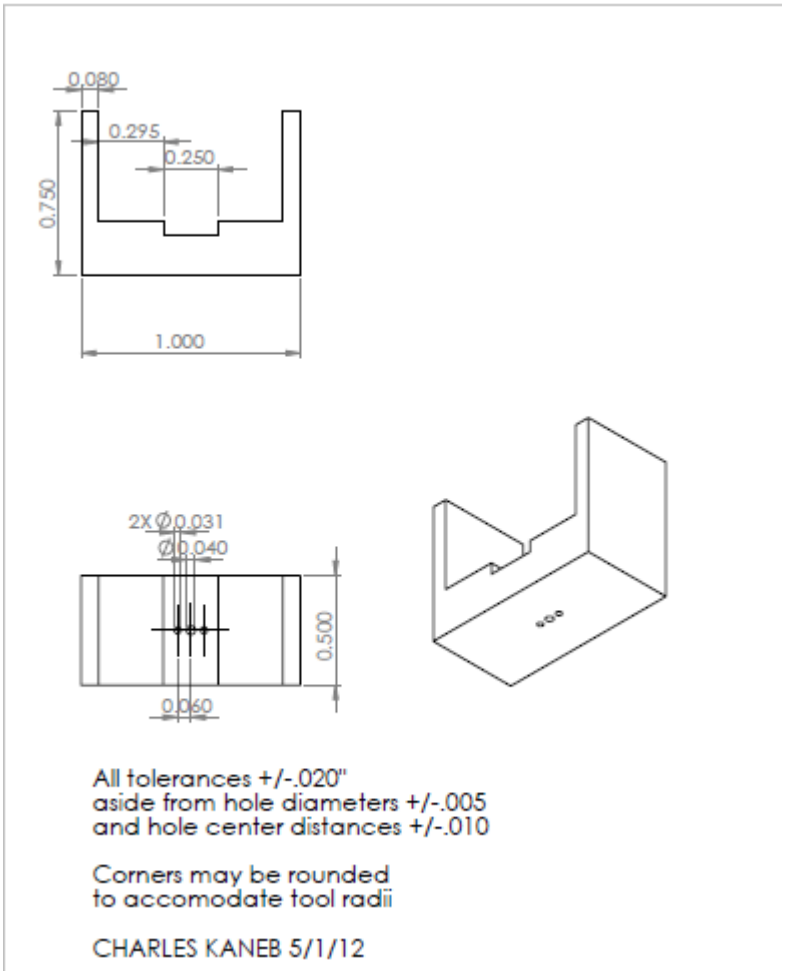

Figure (5.3) Drawing of Clip-On Sensor

These sensors were manufactured at the Texas A&M University Mechanical Engineering Student Machine Shop. Several difficulties were encountered during fabrication. Drill bits with a diameter of less than 0.060” broke frequently, requiring extraction. Electrodes with a length of 0.500” or smaller had bend start and finish length tolerances of over ±0.060” on the sheet metal brake; most sheet metal parts manufactured on that equipment have several inches between bends.

A 0.005” hole location tolerance and a 0.002” clearance between hole and screw required precision machining. On a 0.040” diameter hole this 0.007” allowable misalignment was 1/6 of the dimension and varied between sensors. A photograph of this type of sensor is shown in Figure (5.4).

Figure (5.4) Clip-On Sensor

Preliminary measurements of the electrical properties were then measured using a multimeter to guide the initial design of the sensor electronics. The glass sensors had wet resistances of 1 MΩ - 10 MΩ, resulting in currents of a few hundred nA when connected to a 5 V circuit. Circuit design to differentiate between a resistance this large and an open circuit proved difficult. The small currents involved also made them vulnerable to electromagnetic interference. Similar results were observed for the DC resistance of the clip-on sensors. These problems meant that more precise measurements were necessary.

A Fluke PM6303A LCR (Inductance (L), Capacitance (C), and Resistance (R)) meter was then used to evaluate the AC properties of these sensors. It was set to operate at 1 kHz, passing current through the sensor and measuring its impedance and phase angle. From these the meter was able to calculate the resistance and inductance or capacitance of the device connected to its terminals. The tests were performed on July 12, 2012 using 316 stainless steel electrodes on the sensor. The results are shown in Table (5.1)

1 kHz LCR Meter	kΩ	pF	Degrees	kΩ
Condition	Resistance	Capacitance	Phase Angle	Reactance
Bare Leads		0.5	88.4	318.6
Sensor, dry		0.7		
Wet with RO Water	185		17.5	176.4
Submerged, RO water	14		12	13.7
Wet with condensate	48		18	45.7
Submerged, condensate	3.9		16.4	3.7

Table (5.1) LCR Meter Results

Several different measurements were taken. Water was collected from the condensate drain at Langford AHU A-1, a 20,000 cfm SDVAV AHU featuring a 12 fins/inch, 4' x 8' x 1' coil, at Texas A&M University, College Station, TX. Its resistivity varied between approximately $1x10^3$ Ω*cm and $1x10^6$ Ω*cm sample to sample. Purer water has a higher resistivity. Completely pure water has a resistivity of 18 MΩ*cm [48] but absorbs atmospheric and surface impurities readily causing its resistivity to drop. It

was thought that water with a higher resistivity would be more difficult to detect, so reverse osmosis water was obtained for testing. This water had resistivity in excess of 1 MΩ*cm. Results from these tests are shown in Table (5.1).

These properties showed clear differences in reactance between the dry and wet states. Schmitt trigger oscillators giving a 1 kHz square wave output were then built, and a PCB was iteratively developed with an oscillator, terminals for the sensor, an averaging capacitor, and DC output terminals. The oscillator gave a square wave with a peak of +10 V. Since the voltage needed to electrolyze water is 1.23 V, and electrolytic cells for water operate on 1.8 - 2.2 V, electrolytic breakdown occurred between the terminals, shown by bubbles of hydrogen and oxygen at the terminals when submerged. This was sufficient to detect small quantities (< 1 cm^3) of water and give a DC output when the electrodes were bridged.

Many different combinations of electrodes were tested. Since these sensors were expected to last several years in an air handling unit without service, the electrodes needed to be capable of withstanding continuously wet conditions while connected to power. Electrodes and electronics were tested by submerging the sensor in a container of water while connected to power. Any continued visible corrosion, or loss of electrical continuity, was considered a failure. Sheet metal electrodes were secured to the sensor body and wiring with self-tapping screws. Stainless steel (316 austenitic alloy) and aluminum electrodes were fabricated from 22-gauge sheets and tested. The 10 V difference across the sensor was enough to cause electrolytic corrosion of at least one metallic component of the system. Since the standard electrode potential of every metal is well below 5 V, conductors will be oxidized if they operate in this application.

Difficulties were encountered with both the sensor electrodes and the wiring to the anode. Stainless steel and aluminum form protective oxides, so these materials were used for both electrodes and wiring, but continuous exposure to large electric currents and water allowed continued corrosion. This allowed thick oxide layers to continue to form, corroding the electrodes and forming a very effective electrical insulation. Copper wires failed rapidly when submerged and exposed to current. All combinations failed to give an acceptable life span in submerged tests. Corrosion was visible within 72 hours on electrodes, fasteners, or wires.

The final attempt to operate this sensor featured an all-aluminum anode and an all-316 stainless steel cathode, with the electrode, screw, and wire all made from the same material. All submerged tests showed corrosion within one week, showing that a completely new sensor design was necessary. This initial testing and development identified the requirements and highlighted practical issues to be solved with a new sensor design. The new sensor design is described in Section 6.

6. SENSOR DESIGN

A new “Coil Enthalpy Limit” sensor was designed and built based on the results of testing prototypes and observations of operating conditions. The requirements are summarized in the following “need statement”: A reliable, inexpensive, durable, and low maintenance device is needed to detect the transition between the dry and wet cooling coil states. To satisfy that description, the sensor had to satisfy the following list of requirements:

1. It must have a life span of several years in a condensing environment.
2. It must be self-cleaning and operate autonomously without maintenance.
3. It must provide a 0 – 5 V DC output with a clear difference between wet and dry states.
4. It must collect water from enough area on the coil to register a wet condition when the dew point is reached. It must activate with less than 2 cm^3 of water.
5. For active measurement of the mixed air dew point by incremental adjustment of cooling coil leaving temperature, the coil state must change and the sensor must respond within 3 minutes of the air crossing the dew point. For operation as a high-limit economizer control, shutting off the economizer when the coil becomes wet, the sensor and coil system must respond within 10 minutes.
6. It must operate at a low voltage, below the voltage needed to harm occupants or technicians.
7. It must operate at a low enough voltage to avoid corrosion.

Several operating principles for the new sensor were considered. Liquid water has several physical properties whose values differ by an order of magnitude from those of humid air, and the differences are shown in Table (6.1).

Property	**Unit**	**Water**	**Air**
Density	kg/m^3	1000	1.2
Surface Tension	$mN*m/m^2$	72.3	0
Thermal Conductivity	W/m^2*K	0.58	0.024
Electrolytic/Breakdown Voltage	V or V/cm	1.23 to 1.8 V	30 kV/cm
DC Resistance	Ω/cm	10^4 to $1.8*10^7$	$1.3*10^{18}$ to $3.3*10^{18}$
Impedance, 1 mm gap, 9 V AC 1 kHz	Ω	3500 to 300,000	$>50*10^6$
Dielectric Constant		80	1.0006
Refractive Index		1.33	1.0002

Table (6.1) Properties of Air and Water

Each of these properties provided at least an order of magnitude difference between dry and wet states. This would allow a binary output, satisfying requirement 3. The other requirements for the sensor, and testing described in Section 5, determined the properties to be used for the prototype sensors. The sensor was then designed to measure the impedance of the air and water between two electrodes.

All of these properties are measured in experimental and commercial environments. Density is measured by weighing a known volume of a substance. Surface tension is determined by measuring the force required to insert a probe of known area into a fluid. Thermal conductivity is measured by measuring the electricity needed to heat a wire to maintain it at a constant temperature difference above the

temperature of the flow. The impedance or dielectric constant can be measured by determining the current produced by a known input voltage. Agilent Technologies [61] states that “The unknown impedance (Zx) can be calculated from measured voltage and current values. Current is calculated by using the voltage measurement across an accurately known low value resistor (R).”

The difficulty of measuring density, surface tension, thermal conductivity, or electrolytic breakdown voltage using a device capable of lasting several years in a condensing environment removed these properties from consideration. Measurement of thermal conductivity is used in hot wire anemometry, and Lomas [62] stated that “It has been said that one remains a novice in hot wire anemometry until the first probe has been broken, and whether or not this is true, probe breakage is so common that a quick and easy method of repair is desirable.” Measuring the breakdown voltage required a potential difference between submerged electrodes greater than the 1.23 V needed to break down water, causing corrosion of the electrodes as discussed in Section 5. The change in the refractive index was used by the existing chilled mirror sensors, with prices of $2570 [35] or more.

Resistivity and the dielectric constant could be measured by the use of stationary electrodes with potential differences of 0.25 V. One sensor was then designed that could measure either the dielectric constant or the resistivity of the water or air in the gap between electrodes, depending on whether the plates were insulated. The resistivity of impure water, including the coil condensate detected by this sensor, is several orders of magnitude smaller than that of pure water, as dissolved metallic salts conduct electricity by motion of ions. The dielectric constant of water is 80, while that of air is 1.005.

The design of this “Coil Enthalpy Limit” sensor was dependent on the electrochemical properties of available conductors and the flow rate of condensate available to be collected on the electrodes. The quantity of condensate that could be collected from the cooling coil was then calculated and used to determine the size and position of electrodes that would meet the response and reliability requirements. With the size, properties, and spacing of the electrodes known, the electrical properties of the sensor were then calculated. The body of the sensor was then designed to hold the electrodes at the separation and angle required by the desired electrical properties and to meet the need for the sensor to be self-cleaning.

6.1 Electrical and Chemical Design

6.1.1 Corrosion Avoidance

The electrodes used for the impedance sensor were expected to pass between 1 μA and 100 μA of current through water in the gap. In order to meet the durability requirements, the corrosion at the anode that was experienced (see Section 5.2 for details) had to be avoided. Connections from the electronics to the sensor would have to be completely sealed to avoid galvanic corrosion at junctions between the copper wires and the electrodes. Crimp-on terminals were welded to the sensing plates and the junction with the wire was then sealed.

Sensor failure from corrosion can occur by creation of an oxide layer with insufficient conductivity, creation of an oxide layer which flakes off, or electrochemical corrosion. Stainless steel sheet electrodes, 316 alloy, with a 0.25 V potential difference

across the gap avoid all three types of failure and allow the sensor to meet requirement 1, lasting a three-month test in a building as a prototype.

Stainless steel electrodes provide adequate conductivity when corroded to allow a sensor to continue to operate. The resistivity of iron oxides at 300° K ranges from 6.07 * 10^{-3} Ω*cm for Fe_3O_4 to 2.5 * 10^{-1} Ω*cm for Fe_2O_3 [63], while the resistivity of aluminum oxide is 1 * 10^{14} Ω*cm [64]. An additional resistance of 100 kΩ on a sensing area of 1 cm^2 of aluminum only requires a 100 nm thick layer of aluminum oxide, while an iron oxide layer with the same thickness would have a resistance of 0.25 μΩ. Therefore, if oxidation could be stopped after a protective layer, steel or 316 stainless steel would be suitable for the electrodes.

The metal used for the sensor plate needed to form a passive oxide layer to avoid further corrosion. The main criterion for this is the Pilling-Bedworth ratio *R*, the ratio of the volume of a metal oxide to the volume of the metal that was used to create the oxide layer. According to McCafferty [65] "Metals which are normally passive have values of *R* between 1 and 2." Aluminum has a Pilling-Bedworth ratio of 1.28, allowing it to form a protective oxide layer, while carbon steel has a ratio of 2.1 - 2.14, causing rust to flake off. The chromium in 316 stainless steel gives it a Pilling-Bedworth ratio of 2.00 and a protective oxide layer that prevents further corrosion. Austenitic 316 stainless steel was chosen to meet the longevity requirement.

Electrochemical corrosion occurs when the potential difference across a pair of electrodes submerged in water is larger than the standard electrode potential of the reaction between the anode material and its oxide. "Corrosion involves the destructive attack of metal by chemical or electrochemical reaction with its environment. Usually corrosion consists of a set of redox reactions that are electrochemical in nature. The metal is oxidized to corrosion products [66] at anodic sites: $M \Leftrightarrow M^{+2} + 2\ e^-$." The

standard electrode potential between iron and the iron (II) ion is 0.44 V, and a sensing voltage lower than this will avoid ionization and electrochemical corrosion. Once the voltage needed to cause corrosion is exceeded, the rate of corrosion is dependent on the current passing through the electrode into the electrolyte. A potential difference of 0.25 V between the 316 stainless steel electrodes was selected to avoid electrochemical corrosion.

In order to register a “wet” state only when water was condensing on the coil, water on the sensor plates had to be cleared off by gravity. Rame-Hart Instrument Corp. [50] describes the angle necessary to have drops roll off a plate: “The tilting plate method captures the contact angles measurements on both the left and right sides of a sessile drop while the solid surface is being inclined typically from 0° to 90°. As the surface is inclined, gravity causes the contact angle on the downhill side to increase while the contact angle on the uphill side decreases. Respectively, these contact angles are referred to as advancing and receding angles. The difference between them is the contact angle hysteresis. In some cases, the drop will roll off the solid as wetting occurs at the roll-off angle. The last valid readings are captured and normally represent the advancing and receding contact angles. In some cases, the solid can tilt all the way to 90° without the drop releasing. The final left and right contact angles are used.”

A drawing of the angle necessary to allow runoff, given by Rame-Hart, is shown in Figure (6.1). The contact angles for water on stainless steels were between 37° and 43° [67], and a 60° plate angle from horizontal was chosen in order to ensure runoff from the surfaces. Drops between 0.1 ml and 2 ml ran off when water was dripped on a sheet of 316 stainless steel held at this angle. In order to meet requirements 1, 2, and 3, the sensor body had to hold stainless steel plates at a 60° angle, and the electronics had to supply 0.25 V.

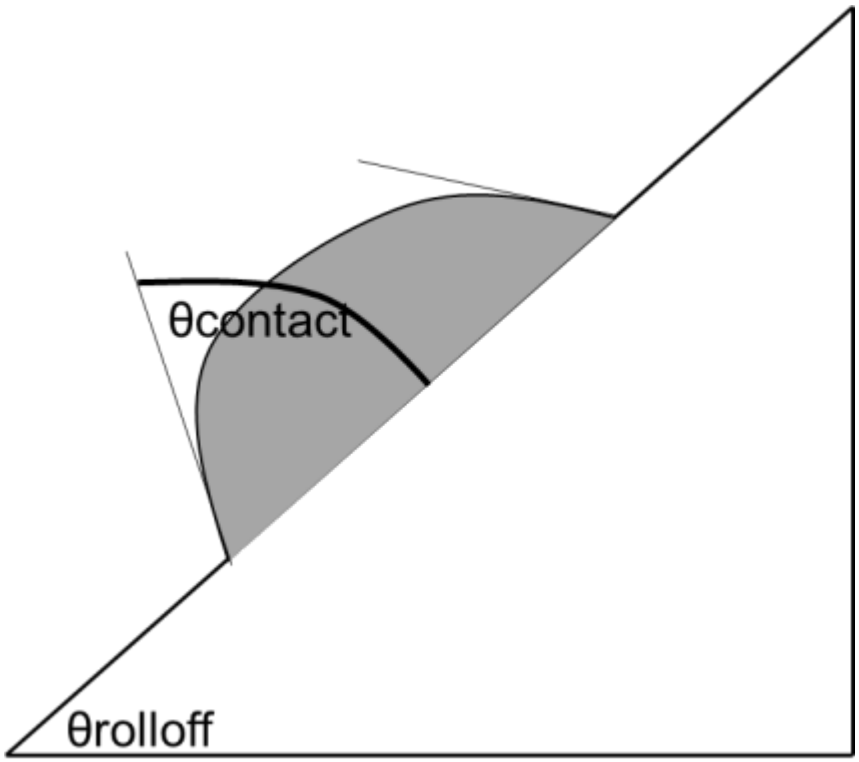

Figure (6.1) Angle Necessary For Runoff (Redrawn from Rame-Hart [50])

6.1.2 Condensate Quantity Calculation

The location and size of the sensor were determined by requirements 4 and 5, shown below. These requirements are:

4) It must collect water from enough area on the coil to register a wet condition when the dew point is reached. It must not require more than 2 cm^3 to activate.

5) For active measurements of the mixed air dew point, it must respond within 3 minutes of crossing the dew point. For passive operation as a high-limit economizer control, it must respond within 10 minutes.

The quantity of water condensed on the coil that is available to the sensor was dependent on the mass airflow and the difference in water concentration between the mixed air and the supply air.

$$\dot{m}_{air} = \dot{V}_{air} * \rho_{air} \qquad \text{Equation (6.1)}$$

$$\dot{m}_{condensate} = \dot{m}_{air} * \Delta w_{air} \qquad \text{Equation (6.2)}$$

Δw_{air} is a function of how far below the dew point temperature the air was cooled. It was linearized in the region of interest as follows:

$$w_{sat}(57.5\ ℉) = 0.010\ \frac{lb(w)}{lb(da)} \qquad \text{Equation (6.3)}$$

$$w_{sat}(51.5\ ℉) = 0.008\ \frac{lb(w)}{lb(da)} \qquad \text{Equation (6.4)}$$

$$\frac{\Delta w}{\Delta T} = \frac{.002\ \frac{lbw}{lbda}}{6\ ℉} = 3.3 * 10^{-4}\ \frac{lb(w)}{lb(da) * ℉} \qquad \text{Equation (6.5)}$$

The total mass flow of condensate for a given temperature decrement between the air and the dew point is given by Equation (6.6).

$$\dot{m}_{condensate} = \dot{V}_{air}\rho_{air} * \left(T_{air} - T_{dew\ point}\right) * 3.3 * 10^{-4}\ \frac{lb(w)}{lb(da) * °\mathrm{F}} \qquad \text{Equation (6.6)}$$

If a collector was to be placed on the fins to collect the “carryover” water, the mass of water that could be collected this way had to be determined. The mass of condensate per unit of collector area was assumed to be constant. The $\frac{m_{carryover}}{m_{total}}$ term varied between coils and was minimized by AHU coil designers in order to avoid condensate being carried down the supply duct. The total collected mass expected is given by Equation (6.7)

$$\dot{m}_{collected} = \dot{m}_{condensate} * \frac{A_{collector}}{2 * A_{coil} * n_{rows}} * \frac{m_{carryover}}{m_{total}} \qquad \text{Equation (6.7)}$$

A test to obtain a value for $\frac{m_{carryover}}{m_{total}}$ was done. With 10,000 cfm of airflow, a supply air temperature 2°F below the dew point of 55°F, and a four-row coil with 40 ft^2 of

area, the total quantity of condensate expected per ft^2 of collector area was 0.0014 $\frac{lbs}{min}$ multiplied by the carryover ratio. The test used a 5” diameter funnel as a collector. The test found that the carryover ratio was well under 0.05 and that 0.1 cc of water was collected in 90 seconds. These calculations indicated that directly collecting water from the coil was impractical.

One (1) cc/min was collected from a 3 cm wide location on the drip rail at Langford AHU A-1. This was assumed to be an adequate quantity of water to operate a sensor. The assumption was then confirmed in the calculations of Section 6.2. Therefore, the sensor would be located on the drip rail instead, as shown in Figure (6.2).

Figure (6.2) Sensor Clamped to Drip Rail

6.2 Resistance Calculations

The electrical properties for this sensor were calculated for measurement of both impedance and dielectric constant. Measuring impedance required the 316 stainless steel sensing plates to be exposed to the air and water, while dielectric constant measurements were made by encapsulating the plates with a varnish that had a dielectric strength of 1700 V/mil. Bench tests showed that the varnished sensor failed to return to its dry capacitance in ambient (75°F, 50% RH) conditions, and only the resistive impedance sensor was used for further testing. To pass currents of more than 1 μA and avoid noise with a 0.25 V input, the plates and the area in contact with water had to be large enough to give an impedance of less than 250 kΩ when wet.

Electrical properties of an impedance sensor depended on the size and shape of the gap between conductors and the resistivity of the substance filling the gap. The resistivity of the relevant materials is given in Table (6.2).

Material	**Resistivity (Ω*cm)**
Copper	0.00000168
316 Stainless Steel	0.000069
Water (Condensate)	1000-100,000
Water (Pure)	18,000,000
Air	$3*10^{18}$

Table (6.2) Resistivity of Materials

This allowed several assumptions to be made about the impedance of the resulting sensor. First, the resistance of the copper wires could be neglected. Second, the resistance of the 316 stainless steel sensor plate was several orders of magnitude smaller than that of the air or water in the gap. Third, the resistivity of the water was assumed to be uniform. Finally, the water droplet was assumed to form a trapezoidal shape between the two plates. With a known voltage between the two sides of the sensor, the impedance could be theoretically determined by integrating the resistivity between the two plates. The region of interest is shown in Figure (6.3).

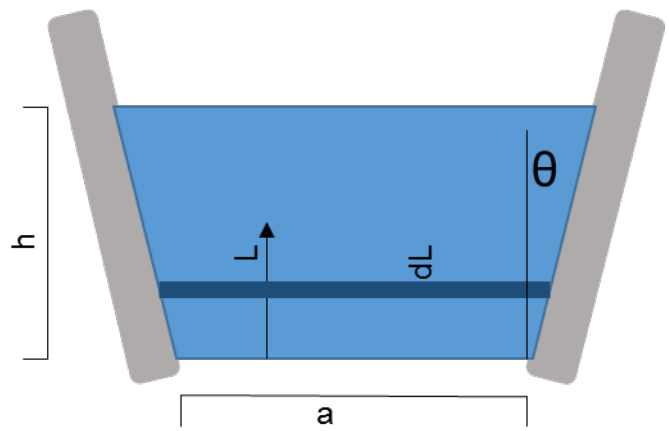

Figure (6.3) Drawing of Plates and Gaps

Given uniformly resistive material between the plates, the equation for resistance between two equipotential surfaces is given by the following equations. The terms in the following equations are given in Table (6.3).

Variable	Description
R	Resistance of the sensor
G	Conductance of the sensor
P	Resistivity of the water
Z	Depth of water drop into the paper
Y	Non-dimensional height above bottom of drop
Y	Height above the bottom of the drop
dy, dY	Differential element of height
H	Total height of drop
A	Gap across bottom of electrodes
Θ	Angle from vertical of electrodes
W	Width between electrodes at a given height

Table (6.3) Variables in Resistance Calculations

Equation (6.8) was obtained from Halladay's "Fundamentals of Physics" [68]. Figure (6.4) shows a rectangular conductor for which this holds true. This can be integrated over the length to find the resistance of part of the conductor with Equation (6.9).

$$R = \frac{\rho L}{A} = \frac{\rho L}{hz} \qquad \text{Equation (6.8)}$$

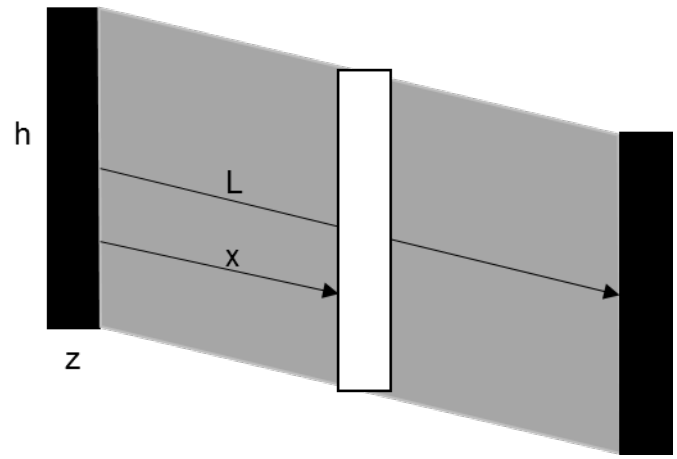

Figure (6.4) Uniform Resistivity and Cross Section.

$$R = \int_0^{x_1} \frac{\rho dx}{hz} = \frac{\rho x}{hz}\Big|_0^{x_1} = \frac{\rho x_1}{hz}$$ Equation (6.9)

If a horizontal slice is taken, as in Figure (6.5) and Equation (6.11), the integral diverges as the height of the slice goes to zero. The natural log of 0 is undefined.

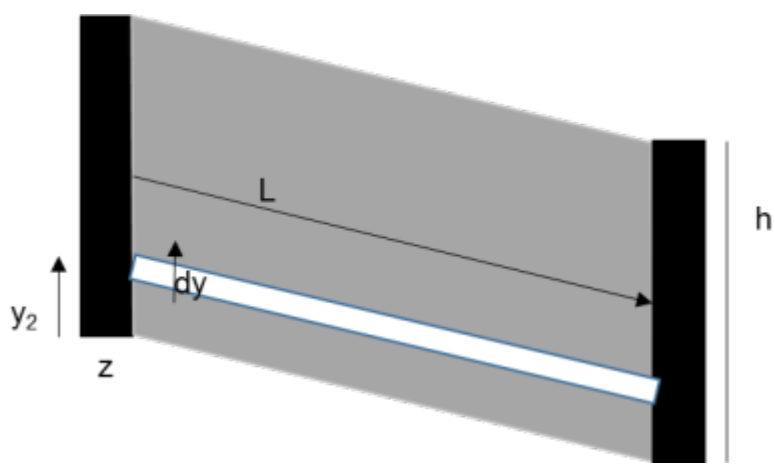

Figure (6.5) Horizontal Slice

$$Y = \frac{y}{h}$$ Equation (6.10)

$$R_2 = \int_0^{y_2} \frac{\rho L}{z dy} = \int_0^{y_2} \frac{\rho L}{z dY h} = \frac{\rho L \ \ln Y}{hz} \Big|_0^{y_2}$$ Equation (6.11)

Therefore, to integrate over a quantity that varies with height, as in Figure (6.3), the conductance G must be used instead. The length of the conductive path varies with height above the bottom of the droplet, and is given by Equation (6.13). The height is then nondimensionalized by dividing by the distance across the bottom of the droplet in Equation (6.14). Conductance G_{sensor} is then found by Equation (6.15). The resistance is then found from the inverse of the conductance.

$$G = \frac{1}{R}$$ Equation (6.12)

$$L(y) = a + y * (2 * \sin(\theta)) = a + y * (2 * \sin(30°)) = a + y$$ Equation (6.13)

$$Y = \frac{y}{a} \quad H = \frac{h}{a}$$ Equation (6.14)

$$G_s = \int_0^h \frac{dy * z}{\rho * L(y)} = \int_0^h \frac{dy * z}{\rho * (a + y(2 \sin \theta))} = \int_0^h \frac{dy * z}{\rho * (a + y)} =$$

$$\int_0^H \frac{dYz}{\rho(1+Y)} = \frac{z * \ln(|y+1|)}{\rho} \Big|_0^H = \frac{z \ln(|H+1|)}{\rho} - \frac{z \ln(|1|)}{\rho} = \frac{z\ (cm) \ln(|H+1|)}{\rho(\Omega * cm)}$$

Equation (6.15)

The units cancel out to a conductance in mhos (1/Ω). The resistance is then found using Equations (6.12) and (6.16). This is only valid for sensors with plate angles of 60° from horizontal; terms in the second equality of Equation 6.16 cancel since 2*sin(30)=1.

$$R_s = \frac{\rho(\Omega * cm)}{z(cm) * \ln(\frac{h}{a} + 1)}$$ Equation (6.16)

The impedance was experimentally determined once the sensor was built; the results are in Table (6.3) in section 6.5. With a resistive component of the impedance of 1.3 kΩ, using a single large drop with z = 3 mm, h = 3 mm, and a = 1 mm, Equation

(6.16) gives a resistivity of the water of 540 Ω*cm. R_s goes to ∞ when h or z goes to 0, indicating an absence of water in contact with both plates, and depends on ρ, z, h, and a. Note that the resistivity of condensate water varied by two orders of magnitude between samples. The current and voltage outputs for this sensor in series with a sensing resistor were then given by Equations (6.17) and (6.18).

$$I = \frac{V_{in}}{R_{sensor}+R_{measurement}} \text{ (Ohm's Law)} \qquad \text{Equation (6.17)}$$

$$V_{output} = V_{in} * \frac{R_{measurement}}{R_{sensor}+R_{Measurement}} = I * R_{measurement} \qquad \text{Equation (6.18)}$$

Stainless steel plates, 316 austenitic alloy, were used. They were 50 mm x 25 mm wide and 0.065" thick, with a 0.25 mm minimum gap (0.010"). A drawing of the plates is included as Figure (6.6).

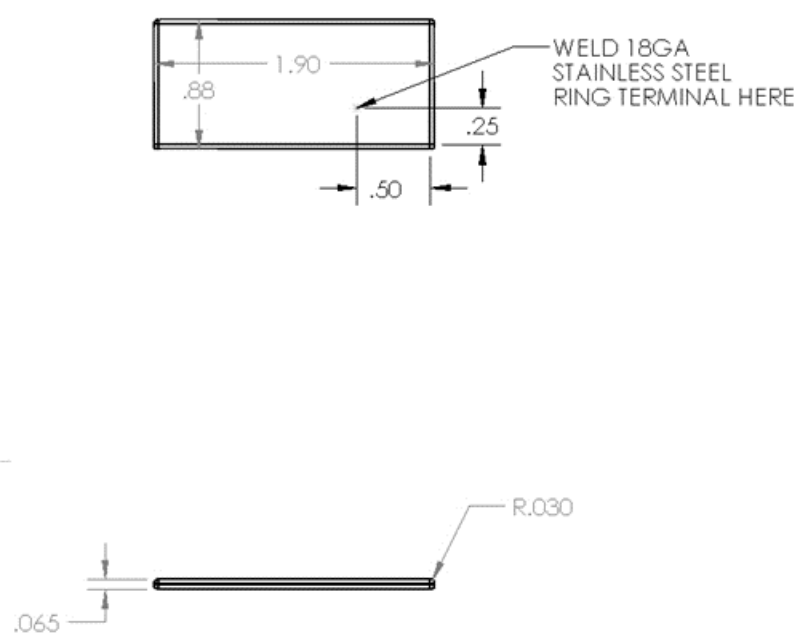

Figure (6.6) Stainless Steel Sheet Electrodes

6.3 Mechanical and Assembly Design

A clamping system was required to secure the plates in a location where water could be gathered from the coil. The plates needed to be secured to the sensor body while maintaining a constant gap at the bottom. The sensor needed to be drained by either gravity or by the airflow coming through the sensor body. Finally, the sensor needed to be clamped to the cooling coil drip rail.

After an unsuccessful attempt to build sensors with a “straight-grooved” clamp at the top of the body, the clamps were redesigned to provide flat, angled clamping faces. High-density polypropylene was chosen for the sensor body due to its resistance to polar solvents such as condensate water, compressive strength of 6000 psi, and tensile strength of 4800 psi.

In order to prevent movement of the plates, at least 10 lbs of friction force was required between the plates and the body of the sensor. This is shown in the free body diagram of the plate, Figure (6.7).

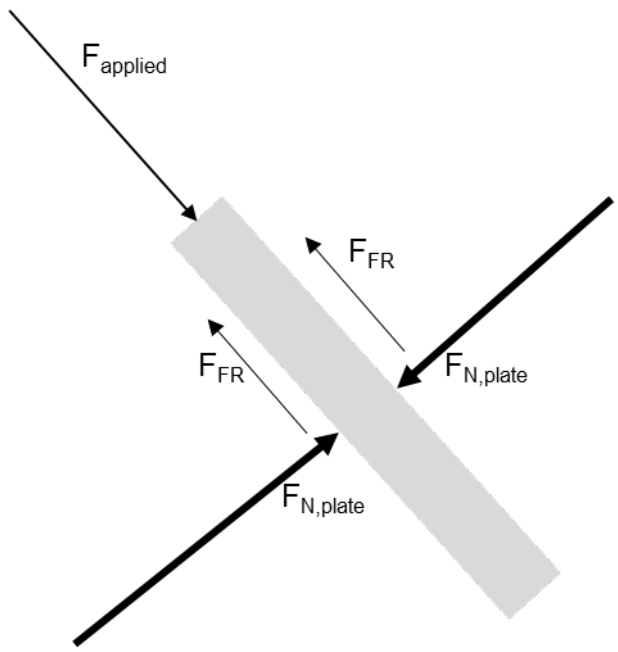

Figure (6.7) Free Body Diagram of Sensor Electrode

With a coefficient of friction μ = 0.1, Equation (6.21) gives the normal force needed to get the required friction force.

$$F_N = \frac{F_{FR}}{\mu} = \frac{F_{applied}}{2\mu} = \frac{10\ lbs}{0.2} = 50\ lbs \qquad \text{Equation (6.21)}$$

The forces on the sensor cap are then resolved by Equations (6.22) and (6.23). Equation (6.24) confirms that the compressive stress on the side of the sensor cap provided by the screw does not exceed 6000 psi, with a screw diameter D_{screw} of 0.132 inches and a height of the sensor cap h_{cap} of 0.5 inches. The free body diagram of the sensor cap is given as Figure (6.8).

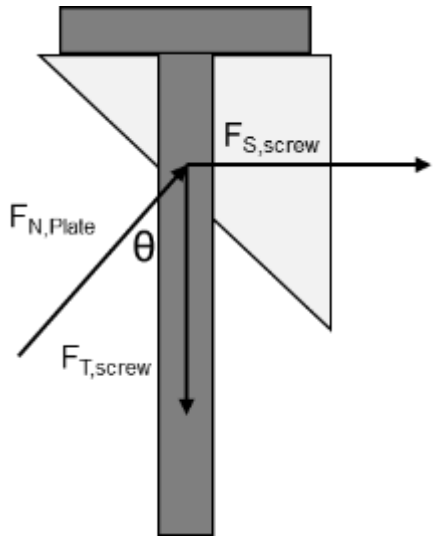

Figure (6.8) Free Body Diagram of Sensor Cap

$$\sum F_y = 0 = F_{N,Plate} * cos\theta - F_{T,screw} = 50\ lbs * \cos 30° - F_{T,screw} = 43.3\ lbs - F_{T,screw}$$

Equation (6.22)

$$\sum F_x = 0 = F_{N,Plate} * sin\theta - F_{S,screw} = 50\ lbs * \sin 30° - F_{S,screw} = 25\ lbs - F_{S,screw}$$

Equation (6.23)

$$\sigma_{Comp} = \frac{F_{S,screw}}{A_{comp}} = \frac{F_{S,screw}}{D_{screw} * h_{cap}} = \frac{25\ lbs}{0.132\ in * 0.5\ in} = 380\ \frac{lb}{in^2}$$

Equation (6.24)

The tensile stresses on the sensor body were calculated in Equations (6.25) and (6.26) by assuming 70% thread depth in the holes for the screws and then applying a stress concentration factor k = 2. The height h is 0.75 in, minor diameter d_{minor} is 0.095 in, and major diameter d_{major} is 0.132 in. The free body diagram is shown in Figure (6.9).

$$A_{screw} = \pi\left(d_{major} - d_{minor}\right) * h = 0.081\ in^2$$

Equation (6.25)

$$\sigma_T = \frac{F_{T,screw}}{A_{screw}} * k = \frac{50\ lbs}{0.081\ in^2} * 2 = 1250\ \frac{lb}{in^2}$$

Equation (6.26)

From these calculations, the sensor body was shown to be able to hold the clamping plates in place against a force of 10 lbs. Since the plates weigh 0.2 lbs, a 50 g vibration or acceleration would not cause the plates to move. A drawing of the sensor assembly is given as Figure (6.10).

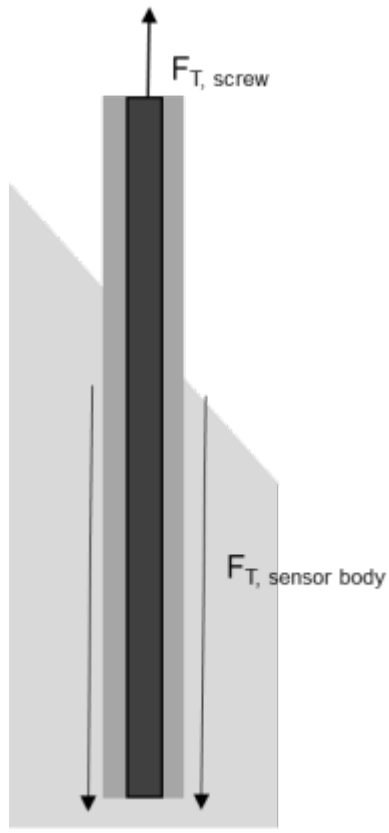

Figure (6.9) FBD of Screw Engagement in Sensor Body

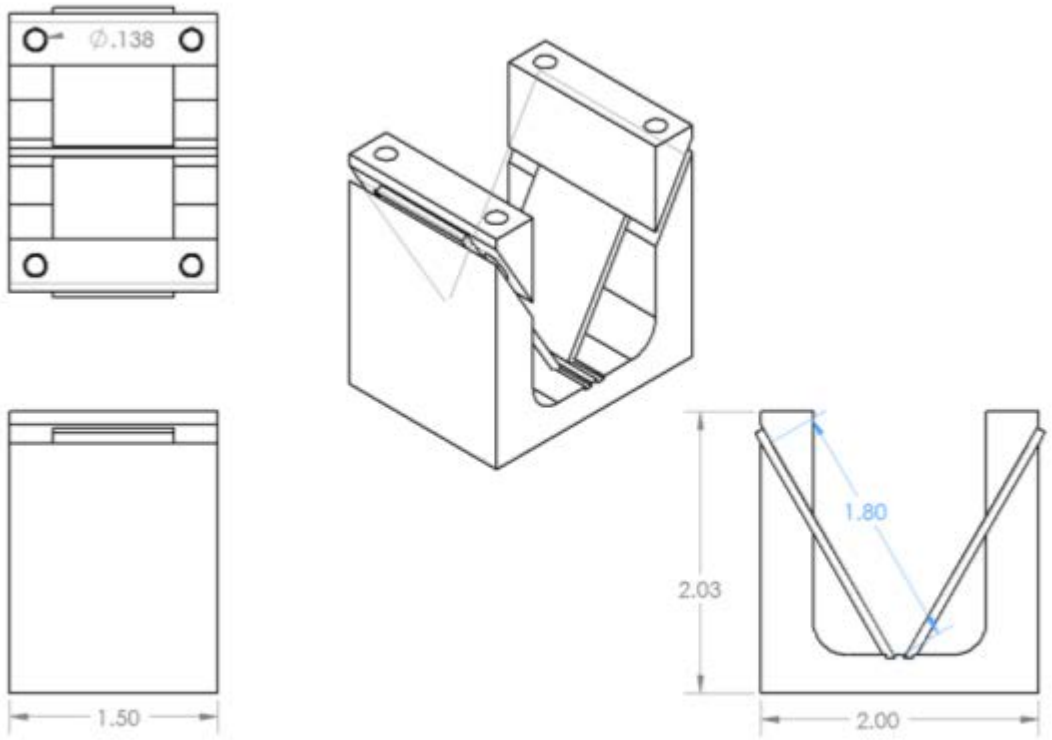

Figure (6.10) Sensor Assembly Cross-Section Showing Plate Attachment

6.4 Sensor Manufacturing

Three sensor assemblies were then fabricated at Texas A&M University's Mechanical Engineering Student Machine Shop. The manufacturing plan used follows:

1) Saw off 2.5 ± 0.125" x 2.1 ± 0.125" blocks from the 1.5" thick sheet using a band saw.
2) Clamp blocks on the 1.5" thick face in the mill vice with the 2.1" edge facing upwards. Face 2.1" thick edge to 2.00 ± 0.005". The vertical bulging caused by the lateral compression of the vice will not affect final dimensions of the part, as the center portion of the sensor body is milled away in Step 5.
3) Rotate blocks 90° with the 2.5" edge facing upwards. Face 2.5" thick edge, then flip to reduce to 2.40 ± 0.005". This yields a rectangular prism with faces perpendicular within ± 0.2°.
4) Clamp the blocks with the 2.40" faces pointing upwards. Using a 3.5" long, #29 drill bit, drill 0.136" diameter (# 29) holes (# 8-32 tap size) 0.188 ± 0.005" from the edges of the blocks. Drill the # 29 holes out to # 17 for 0.75 ± 0.03" depth to provide the clearance holes through the sensor caps.
5) Clamp the blocks on the 2.00" thick faces with the 2.40" faces pointing upwards. Using a 2.5" long, ½" ball endmill to provide a ¼" radius on the inside corners, mill the centered 1.25 ± 0.030" wide slot through, reducing the thickness to 0.270 ± 0.010" at the bottom.
6) Clamp the blocks in a vise on the 1.5" thick edge. Mark a 60 ± 1° angle on the sides of the sensor body. Using a thin, sharp hacksaw, cut along this angle to separate the cap from the sensor body. Repeat on the other side. These caps will now only match one side of one sensor.

7) Clamp the sensors on the 2.00” face. Cut the 0.070 ± 0.010” wide bottom grooves that retain the sensing plates. No mill that small and that long can make that cut, so it will be done with a saw or file.
8) Debur all remaining sharp edges on the sensor body.
9) Shear the 316 stainless steel plates to 1.90 ± 0.060” by 0.88 ± 0.060”, and grind all plate edges to a 0.030 ± 0.010” radius.
10) Place the stainless steel sensor plates on top of the sensor bodies. Place the caps on top of the plates. Insert the 1.5” self-tapping screws through the clamps and caps and tighten into the plates. A photo of this sensor is shown in Figure (6.11).

Figure (6.11) Sensor Installed on Coil

6.5 Bench Testing

These sensors were tested using a Tenma 72-690 LCR meter at the Texas A&M Physics Electronics Shop. All measurements were taken at 1 kHz. The overall impedances of the sensor were capacitive and resistive at this frequency, with the current through the devices leading the voltage, so capacitive and resistive components of the impedance were measured by the meter. An explanation of the method the LCR meter uses to determine capacitance, resistance, and inductance is in Section 7 and Figure (7.1). These results are shown in Tables (6.4), (6.5), and (6.6).

Test Conditions: <1 mV DC, 0.5 V AC, 1 kHz					
Unvarnished (Resistive Impedance) Sensor, Tap Water					
Condition	L (mH)	C (pF)	R (kΩ)	Xc (kΩ)	Xtotal (kΩ)
Dry	!	3.8	>20000	42000	42000
Bridged – 1 drop	!	2800 - 7000	1.2 - 1.5	22 - 56	1.46
Bridged – full width	!	24000	0.65	6.6	0.56
Submerged 1 cm	!	28000	0.56	5.6	0.51

Table (6.4) Results From Tenma LCR Meter, Unvarnished Sensor

Varnished (Capacitive) Sensor, Tap Water					
Condition	L (mH)	C (pF)	R (kΩ)	Xc (kΩ)	Xtotal (kΩ)
Dry	!	4.1	20000	38000	13000
Bridged – 1 drop	!	575	220	276	122
Bridged – full width	!	3100	32	51	19.7
Submerged 1 cm	!	5000	14	32	9.7

Table (6.5) Results from Tenma LCR Meter, Varnished Sensor, Tap Water

Varnished (Capacitive) Sensor, RO Water (1 MΩ * cm)					
Condition	L (mH)	C (pF)	R (kΩ)	Xc (kΩ)	Xtotal (kΩ)
Dry	!	3.9	20000	40000	13000
Bridged – 1 drop	!	426	388	373	190
Bridged – full width	!	788	110	202	71.2
Submerged 1 cm	!	1050	52	151	38.7

Table (6.6) Results from Tenma LCR Meter, Varnished Sensor, RO Water

Bench tests and a three week unpowered in-building test showed that the resistive impedance sensor was able to survive three weeks without electrolytic corrosion issues, demonstrating that it was ready for an in-building test. The bench test also showed that the varnish on the capacitive sensor was capable of retaining enough water to keep the sensor shorted out even after none was visible; it had to be dried out with a hair dryer. Therefore, two resistive impedance sensors, one converted from the capacitive sensor, were installed in two SDVAV AHUs featuring cooling coils measuring 4’ x 8’ x 12” with 12 fins/inch.

7. ELECTRONICS

The resistance and capacitance of the coil enthalpy sensor both changed by three orders of magnitude when the electrodes were bridged by water. Electronics were needed to measure this change in impedance and generate a DC output that was < 0.5 V when dry and > 4 V when wet to be used as an input for a digital control system. The sensor needed to operate at 0.25 V AC for corrosion avoidance. A circuit was designed using a square wave oscillator, voltage divider, sensor, filter, and amplifier to power the sensor and generate its outputs. The characteristics of the sensor, measured with a Tenma 72-690 LCR meter, are shown in Table (7.1).

Condition	C (nF) Low Measurement	C (nF) High Measurement	R (KΩ)
Dry	0.0038	0.0038	20000
Bridged – 1 drop	2.8	7.0	1.3
Bridged – Full Width	24	24	0.63
Submerged 1 cm	28	28	0.56
All measurements recorded at 1 kHz using tap water			

Table (7.1) Sensor Characteristics

For a circuit to be designed, the characteristics of the sensor had to be modeled. Measurements taken using the LCR meter suggested using a capacitor and parallel resistor. Agilent [61, p 2-1] described the operating principle of an I-V LCR meter: “The unknown impedance (Zx) can be calculated from measured voltage and current values.

Current is calculated by using the voltage measurement across an accurately known low value resistor (R.).” At 1 kHz, the frequency used by the LCR meter, the sensor was primarily capacitive. Figure (7.1) shows the components and the resulting impedance for a primarily capacitive device, with actual Z_C and Z_L components unknown and only the effective capacitive impedance and total impedance measured.

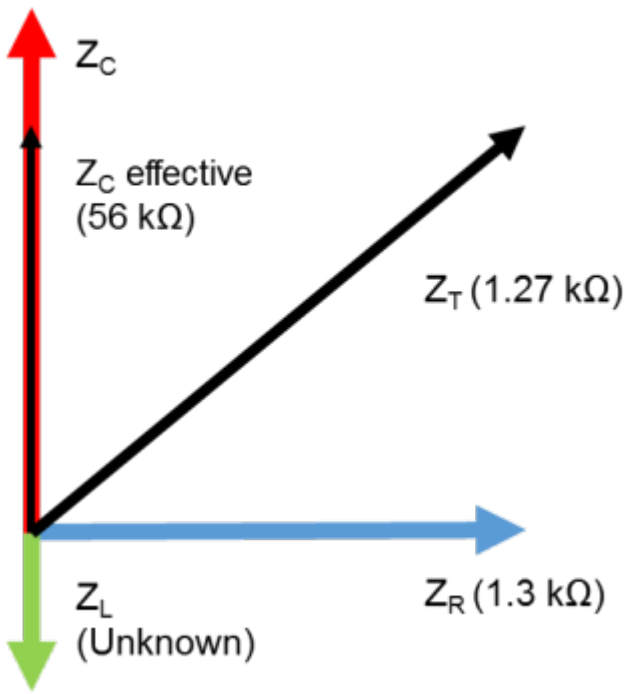

Figure (7.1) Components of Impedance

Since the capacitance increased and the parallel resistance decreased when the sensor was bridged, both components of impedance decreased. A circuit needed to be chosen to give an order of magnitude difference in either current or voltage between dry

and wet states. The current across a resistor is given by Ohm's law, Equation (7.1), and the current across a capacitor is given by Equation (7.2).

$$\mathrm{I} = \frac{V}{R} \qquad \text{Equation (7.1)}$$

$$\mathrm{I} = \mathrm{C}\frac{dV}{dt} \qquad \text{Equation (7.2)}$$

An ideal square wave has an infinite $\frac{dV}{dt}$, and an actual square wave generator will be limited by its maximum current output if it is connected across a capacitor. The voltage across a 2.2 kΩ sensing resistor in series with the sensor, diagrammed in Figure (7.2), for a 131 kHz square wave simulated input, is shown in Figure (7.3). The peak amplitude of the wet output signal, 0.22 V, was 40 times that of the dry output signal, which peaked at 0.005 V. The voltage at V_{out} is given by Equations (7.4) and (7.5).

$$\frac{1}{Z_{sensor}} = \frac{1}{Z_{R,sensor}} + \frac{1}{Z_{C,sensor}} = \frac{1}{R_{sensor}} + \frac{1}{j2\pi f C_{sensor}} \qquad \text{Equation (7.3)}$$

$$V_{in} = V_{out} + V_{sensor} = (i_{total} * Z_2) + (i_{total} * Z_{sensor}) \qquad \text{Equation (7.4)}$$

$$V_{out} = V_{in} * \frac{Z_2}{Z_{sensor} + R_2} \qquad \text{Equation (7.5)}$$

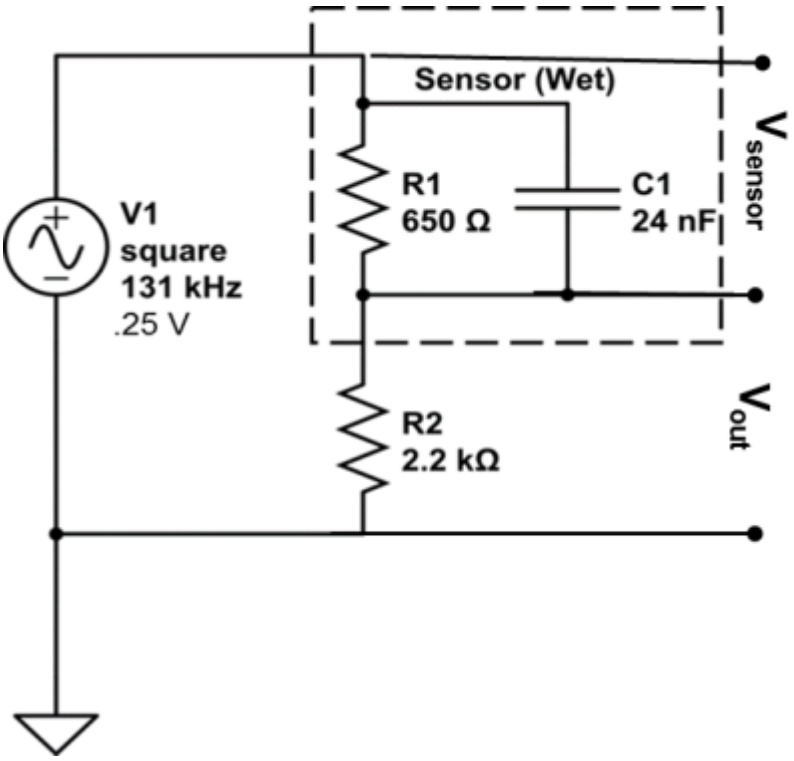

Figure (7.2) Drawing of Square Wave Circuit

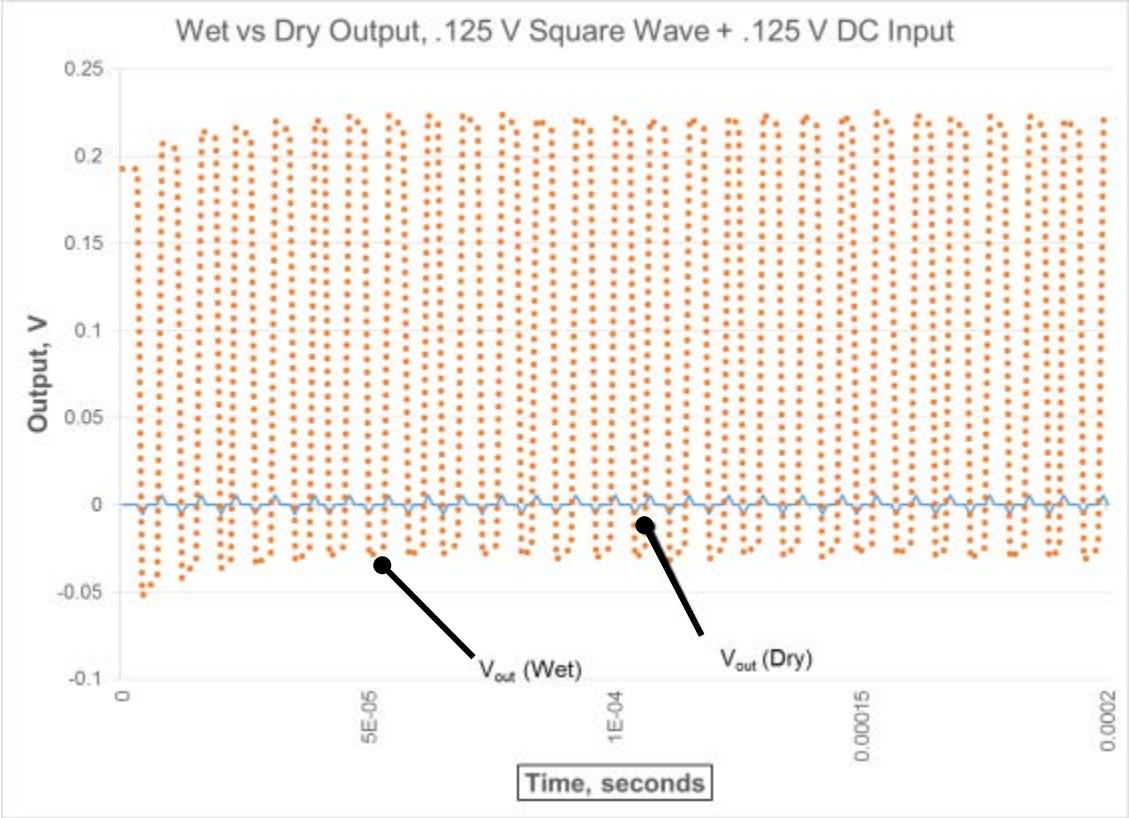

Figure (7.3) Square Wave Outputs

7.1 1 kHz Circuits

Earlier clip-on sensors, seen in Section 5, used a 9 V, 1 kHz square wave AC circuit. This circuit was used to test the clip-on sensors, confirmed that a square wave circuit gave binary outputs, and was the basis for later coil enthalpy sensor circuits. After some experimentation and a brief literature search, an oscillator circuit was prototyped and tested. It used two TI CD4093BE Schmitt triggers, which maintain an output voltage of 5 V while input voltage decreases until it reaches a voltage of 1.6 V

before abruptly switching to a 1.6 V output. This circuit's design was based on Electronics Tutorials' "Astable Multivibrator" circuit [53] and is shown in Figure (7.4).

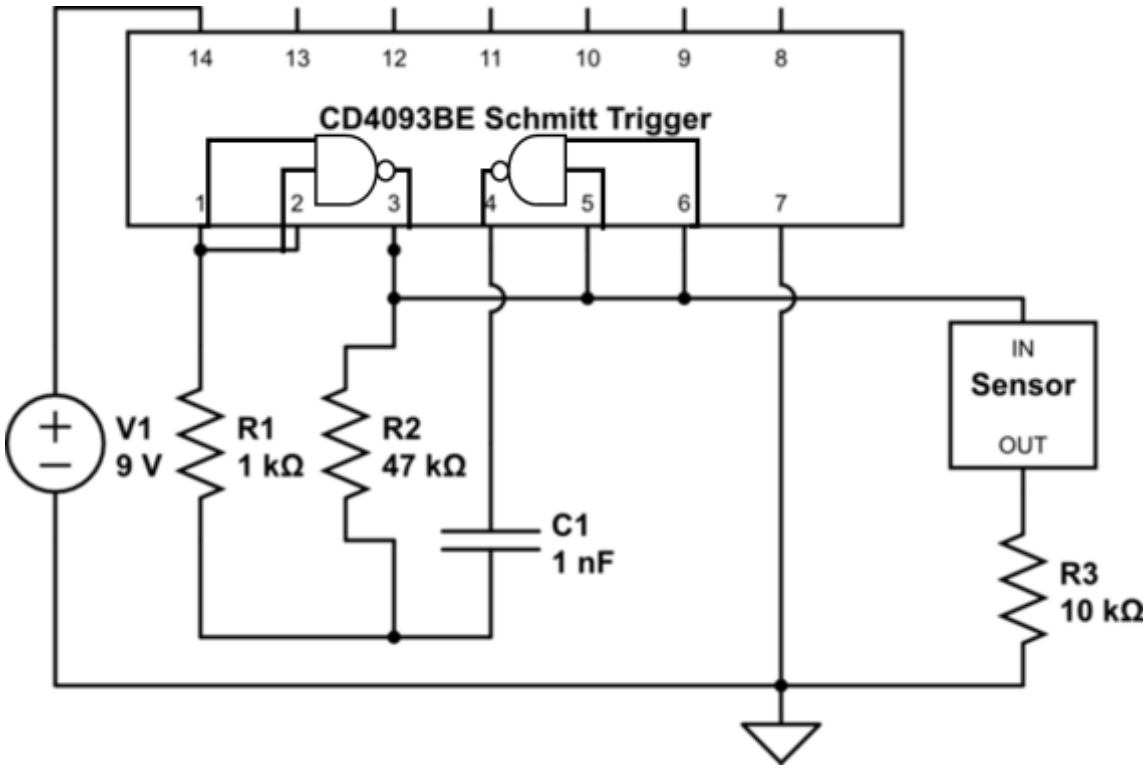

Figure (7.4) Dual Schmitt Trigger Oscillator

This circuit was tested on breadboards and then a PCB was manufactured by Guy Peckitt at PhiTech Laboratories. Stohr [53], provides Equation (7.5) for the oscillation frequency of this type of astable multivibrator.

$$f = \frac{1}{2.2\, R_1 C} \qquad \text{Equation (7.5)}$$

However, testing revealed that the oscillation frequency was dependent on R_2 as well. Each assembly of the oscillator gave a different oscillation frequency, varying up to ± 20% with ± 5% tolerance components. A circuit with a single oscillator capable of powering multiple sensors was drawn up and then a prototype was built by PhiTech. This circuit board is shown in Figure (7.5).

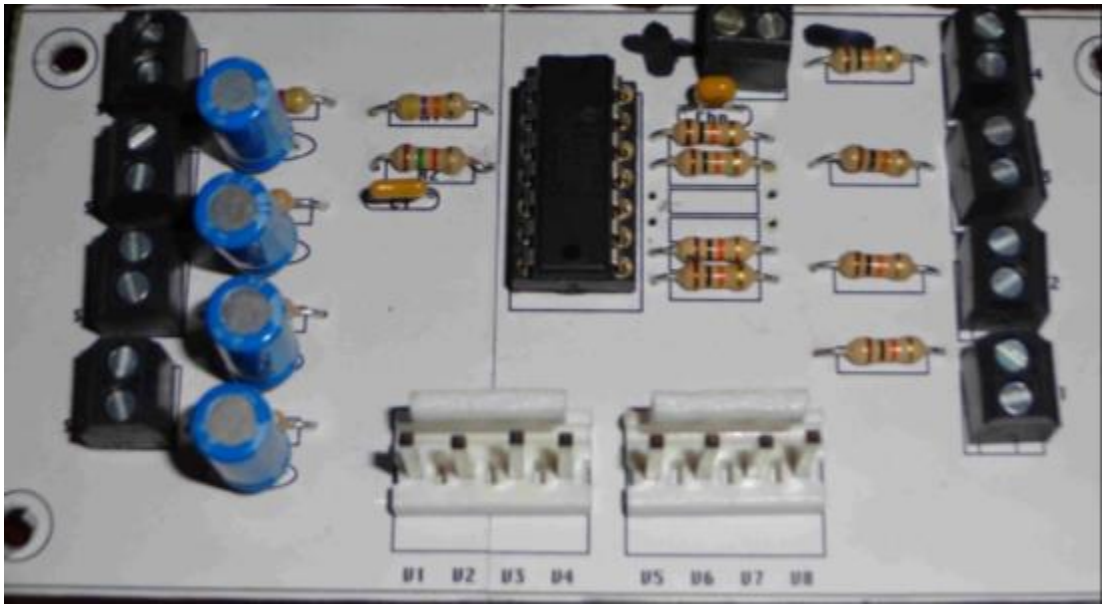

Figure (7.5) PhiTech Multiple Sensor Prototype

The next improvement was to convert the output from square wave AC to DC. A 56 μF capacitor was connected in series with the sensor. When the electrodes of the clip-on sensor were bridged by coil condensate water, this sensor had a resistance of 48 kΩ and a capacitance of 221 pF, giving a time constant for the filter of $\tau = 2.5$ s. This

time constant gave acceptable response, since an acceptable output response time was either 3 or 10 minutes depending on application. The circuit gave a DC output of 9 V when wet and 0 V when dry. The schematic for this circuit is shown in Figure (7.6).

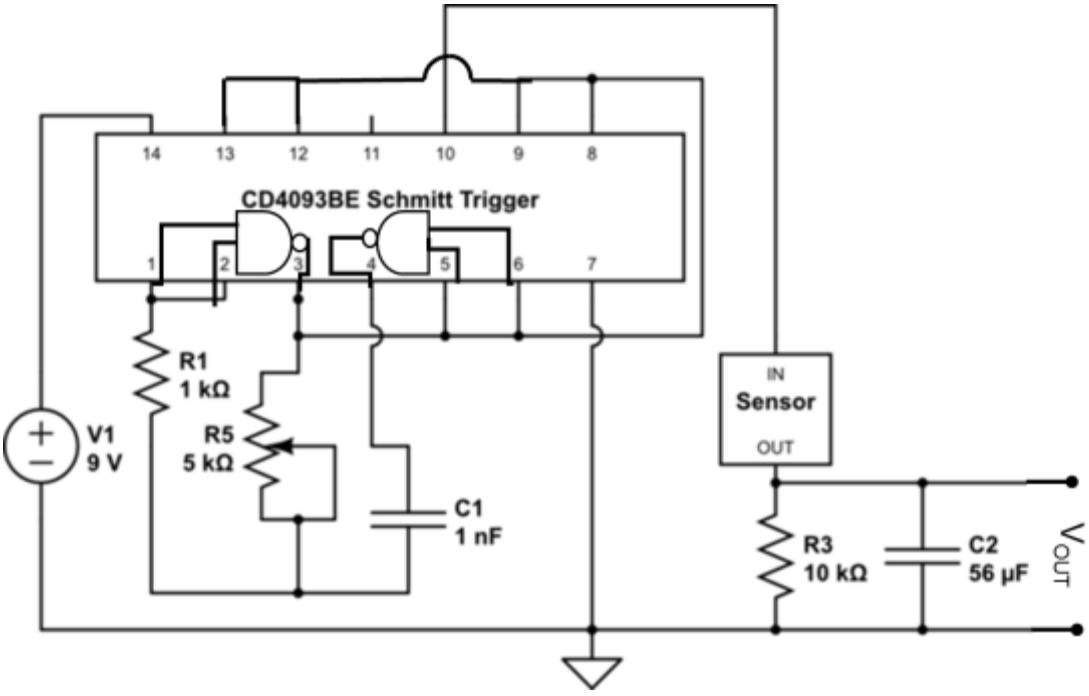

Figure (7.6) Version 12 Circuit

7.2 131 kHz Circuits

After redesigning the sensors in Section 6, the electronics had to be modified. To avoid corrosion, the sensor had to operate at less than 0.25 V, as explained in Section 6.1.1. The new coil enthalpy sensors had larger wet resistances and smaller wet capacitances than the clip on sensors.

The “Version 18” circuit that was used for the final sensor design had five sections: oscillator, divider, sensor, filter, and amplifier. The sensor’s AC impedance dropped by two orders of magnitude when bridged, and this had to be measured at < 0.25 V. The desired output was a digital DC signal, $V_{out} < 0.5$ V dry and $V_{out} > 4$ V wet. The impedance of the coil enthalpy sensor at 131 kHz is shown in Table (7.2). The “Version 18” circuit that resulted from these inputs and desired outputs is shown in the schematic in Figure (7.7).

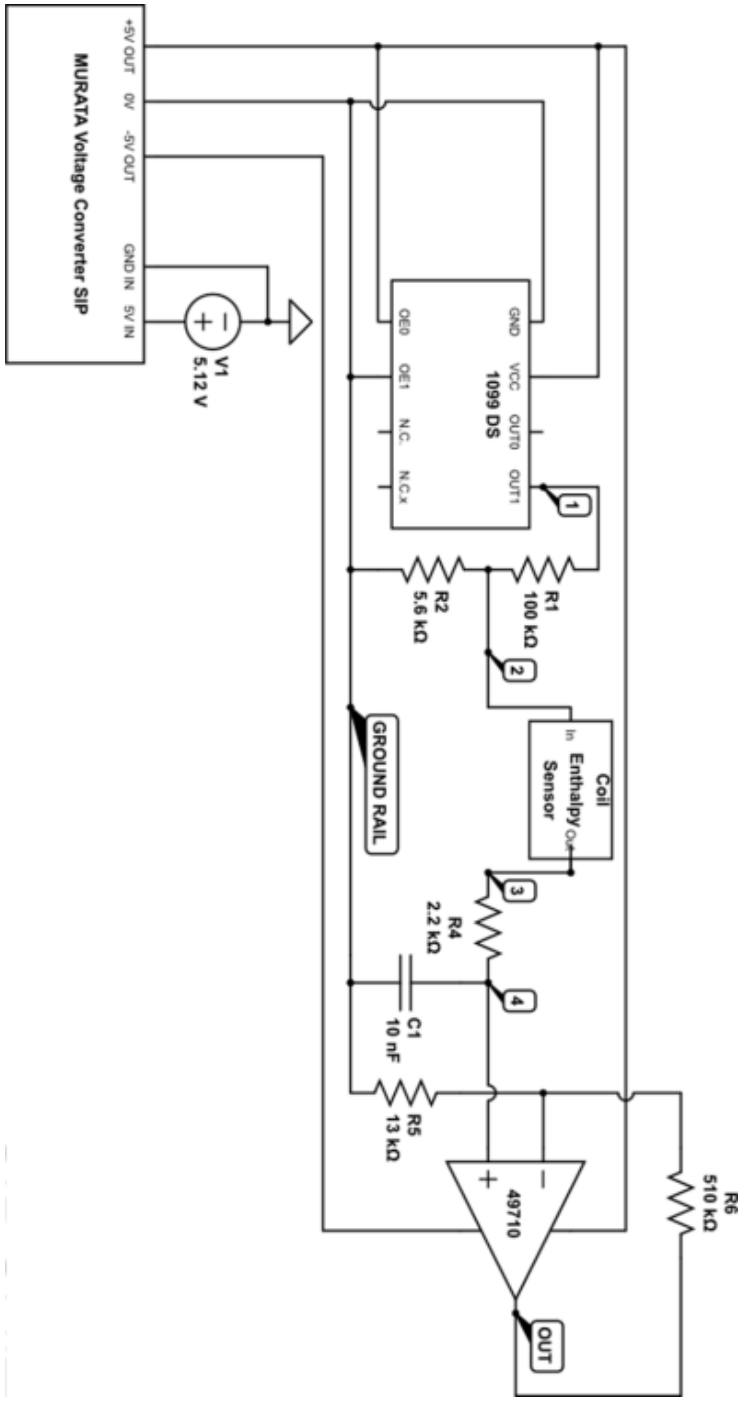

Figure (7.7) Sensor Circuit (Version 18) Schematic

The voltages at each stage of the circuit were calculated to satisfy the sensor input and circuit output requirements. The oscillator stage consisted of a commercial 131 kHz oscillator with an output of a square wave with an amplitude of 2.5 V and a DC level of +2.5 V. The voltage divider reduced this peak-to-trough voltage from 5 V to 0.25 V. The sensor gave an AC output dependent on its state. The filter removed the AC component from the signal, giving only the DC level. Finally, the amplifier boosted this DC level to the high-rail voltage when wet and the low-rail voltage when dry. The input and output for each stage is calculated below. The final schematic and PCB layout are shown in Figures (7.9) and (7.10).

Oscillator: The steady state AC current through a circuit element is given by the equation $i = \frac{V}{Z}$ where Z is the impedance of the circuit element. Since the sensor was supplied with 0.25 VAC it would pass 12 μA when the plates were bridged by one drop of water, when connected to an equal series resistor for measurement. This would require careful encapsulation to avoid noise. Therefore, the new oscillator section would have to operate at a higher frequency than 1 kHz, reducing the reactance.

A commercial 131 kHz oscillator was selected due to its low cost and consistent frequency output. Its output was a square wave with a peak amplitude of 5 V and a trough of 0 V. At 131 kHz, the dry impedance is 310 kΩ, the bridged impedance is 240 Ω, and the submerged impedance is 40Ω.

Sensor: The electrical characteristics of the sensor at 131 kHz are given in Table (7.2), calculated from the resistance and capacitance measurements taken at 1 kHz. Since the sensor is primarily capacitive at this frequency, inductance could not be measured, as shown in Figure (7.1). The wet and dry voltage outputs versus time are shown in Figure (7.3).

Condition	Impedance (Z) at 131 kHz, kΩ
Dry	314
Bridged – 1 drop	0.24
Bridged – Full Width	0.046
Submerged – 1 cm depth	0.040

Table (7.2) Impedance of Coil Enthalpy Sensor (Sensor Only)

Divider: The voltage provided to the sensor must be reduced to 0.25 V to prevent electrolytic corrosion, as discussed in Section 6.1.1. While other solutions are possible, a voltage divider using 100 kΩ and 5.6 kΩ resistances in series dissipated less than 250 μW, which was within the capabilities of the 2.5 W power supply, as shown by Equations (7.6) and (7.7).

$$R_{total} = R_1 + R_2 = 100k\Omega + 5.6k\Omega = 105.6k\Omega \qquad \text{Equation (7.6)}$$

$$P = \frac{V^2}{R_{total}} = \frac{(5\,V)^2}{105.6\,k\Omega} = 2.36 * 10^{-4}\,W \qquad \text{Equation (7.7)}$$

The duty cycle for the oscillator is 50%, so the power dissipated in the 100 kΩ and 5.6 kΩ resistors is 50% of the value when operating: P = $1.18 * 10^{-4}$ W or 118 μW. The peak voltage at the center of the divider is 0.26 V when the impedance of the sensor is 300 kΩ. A diagram of the resistor network is shown in Figure (7.8) with voltages at each stage of the circuit.

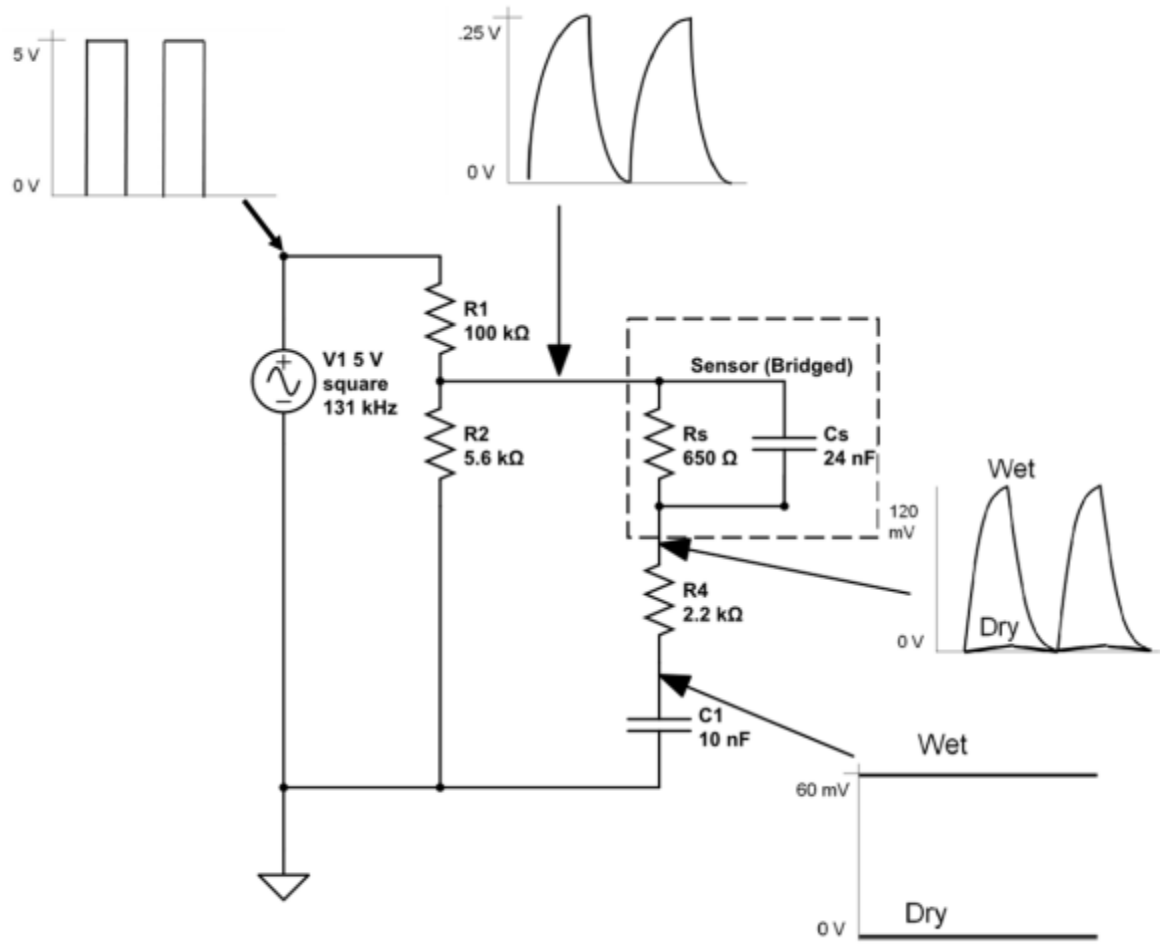

Figure (7.8) Resistor Network Between Oscillator and Ground

Filter: In order to give a DC output, the AC current needs to be eliminated from the circuit. A first-order low-pass filter was used, with a time constant of 22 μs. An assortment of polyester, ceramic, and electrolytic capacitors all gave DC resistances in excess of 40 MΩ, so an ideal resistor and capacitor could be assumed. As the frequency rises, the reactance of the capacitor drops as $X_c = \frac{1}{2\pi f C}$. This causes the

voltage at the center of the divider to fall, as the reactance of the resistor is independent of frequency. Equation (7.8) gave the voltage output from this first-order low-pass filter.

$$V_{out} = V_{in} * \frac{\frac{1}{2\pi f C}}{\frac{1}{2\pi f C} + R} \qquad \text{Equation (7.8)}$$

For this circuit, a 2.2 kΩ resistor and a 10 nF capacitor gave a corner frequency of 3 kHz. At the corner frequency, $V_{out} = 0.7071\, V_{in}$, and higher frequency signals are attenuated at 20 dB/decade beyond the corner frequency. This is shown in Figure (7.9). When the filter receives a signal comprised of a DC level added to a 131 kHz signal, the amplitude of the 131 kHz signal is attenuated by 95%, while the DC level is unchanged. On an oscilloscope, this appears to be a DC signal, ranging from 0 - 2 mV dry to 100 - 120 mV wet.

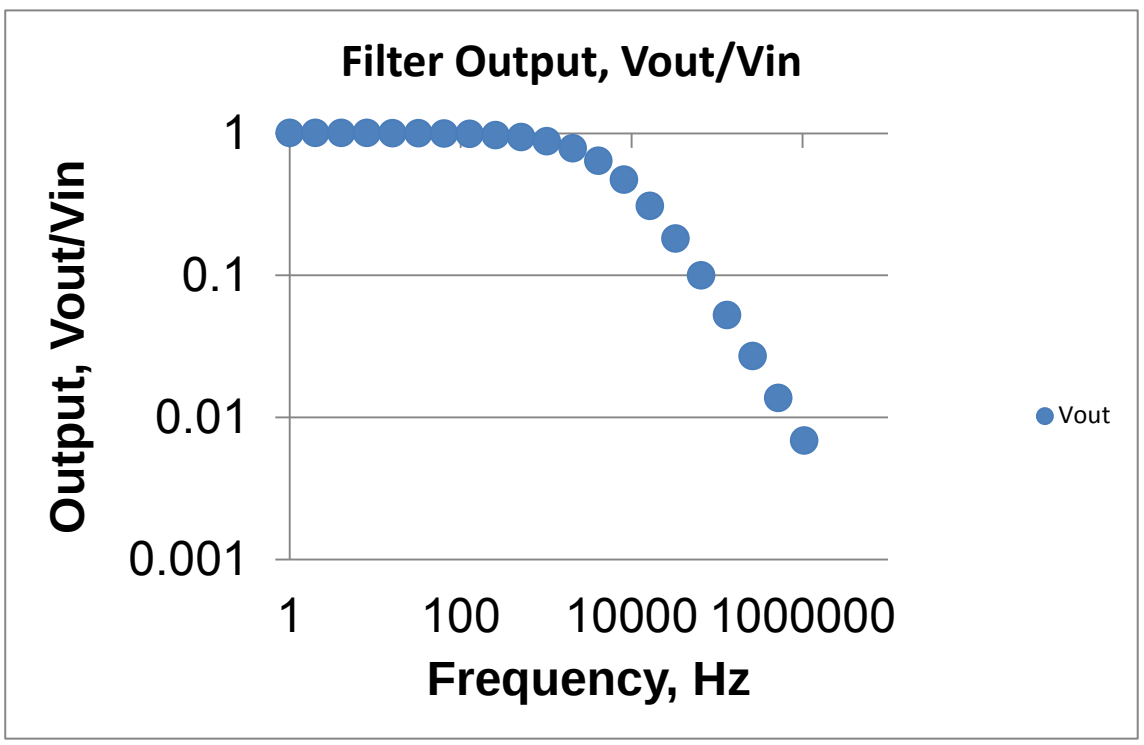

Figure (7.9) Output from First Order Low Pass Filter

Amplifier: With a 100 mV “wet” input signal, the required gain to reach a 5 V “high” output is 50. The operational amplifier was initially designed to be installed before the filter on the output; therefore, it had to operate at 131 kHz, giving a gain bandwidth product of 6.55 MHz. A Dual Inline Package (DIP) was preferred for manual soldering on the printed circuit board, as its pins are 0.100” apart allowing access for the soldering iron. A TI LME49710NA integrated circuit was selected.

In order to take advantage of the 1000 MΩ input impedance [58] of the operational amplifier and reduce the change in voltage output from the filter, the amplifier was connected in a noninverting configuration, as shown in Figure (7.10). The output from this type of amplifier is given by the Equation (7.9) in the linear region between V_{out} = +Vcc and V_{out} = –Vcc. A 510 kΩ R_6 and a 13 kΩ R_5 gave a gain of 39.2.

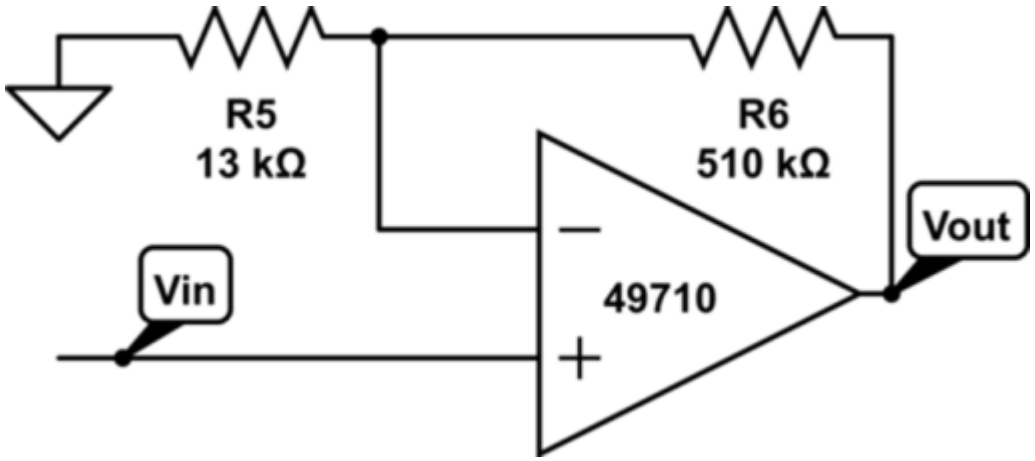

Figure (7.10) Noninverting Amplifier

$$V_{out} = V_{in}\left(1 + \frac{R_6}{R_5}\right) \qquad \text{Equation (7.9)}$$

This circuit was prototyped on a breadboard, and then three PCBs were manufactured. The schematic and PCB layout are shown in Figures (7.11) and (7.12). The outputs when connected to a sensor are shown in the photographs, Figures (7.13), (7.14), and (7.15). Dry output was – 4 V, and wet output was 4.4 V.

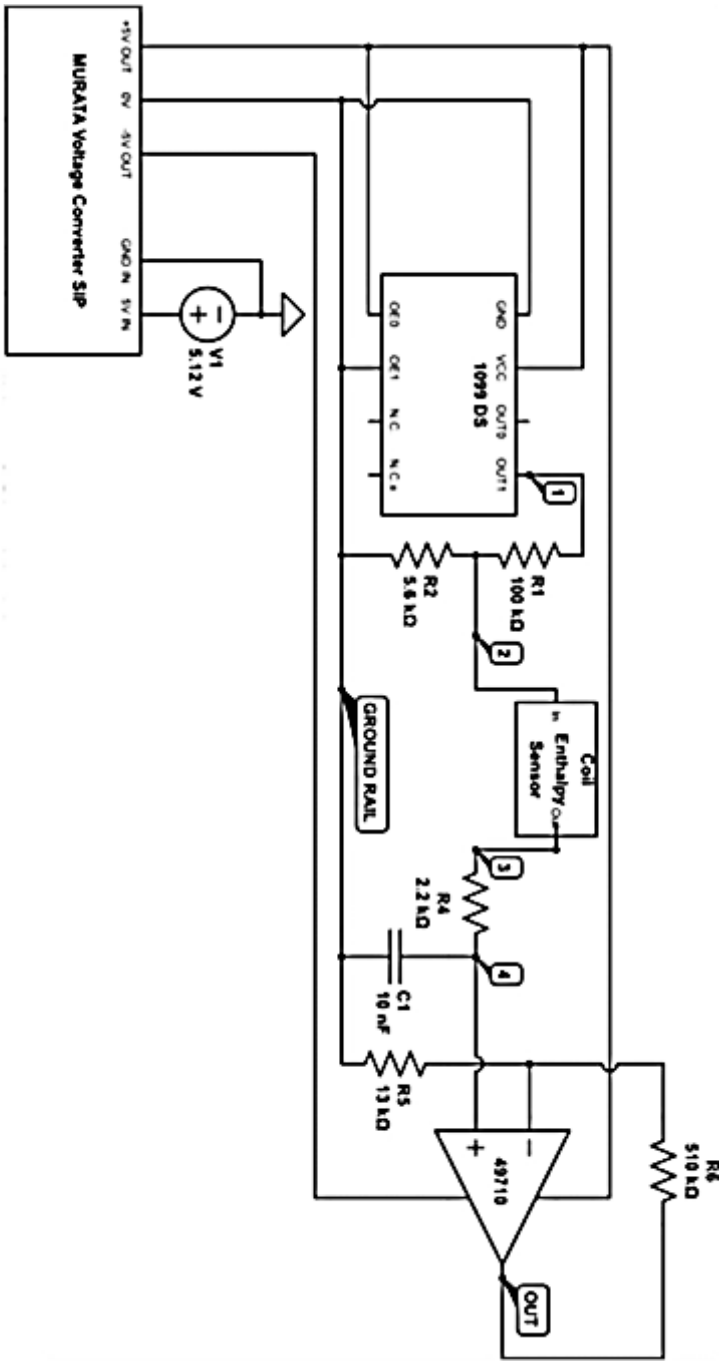

Figure (7.11) Schematic of V18 Circuit

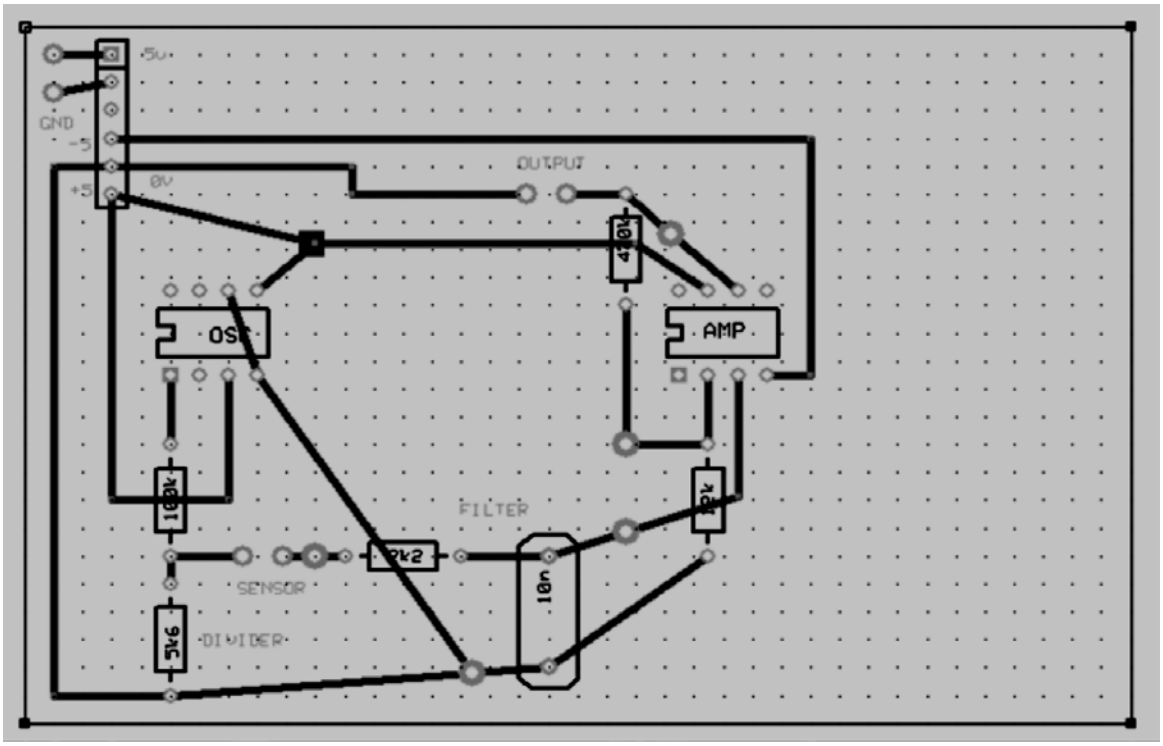

Figure (7.12) PCB Layout of 131kHz Circuit

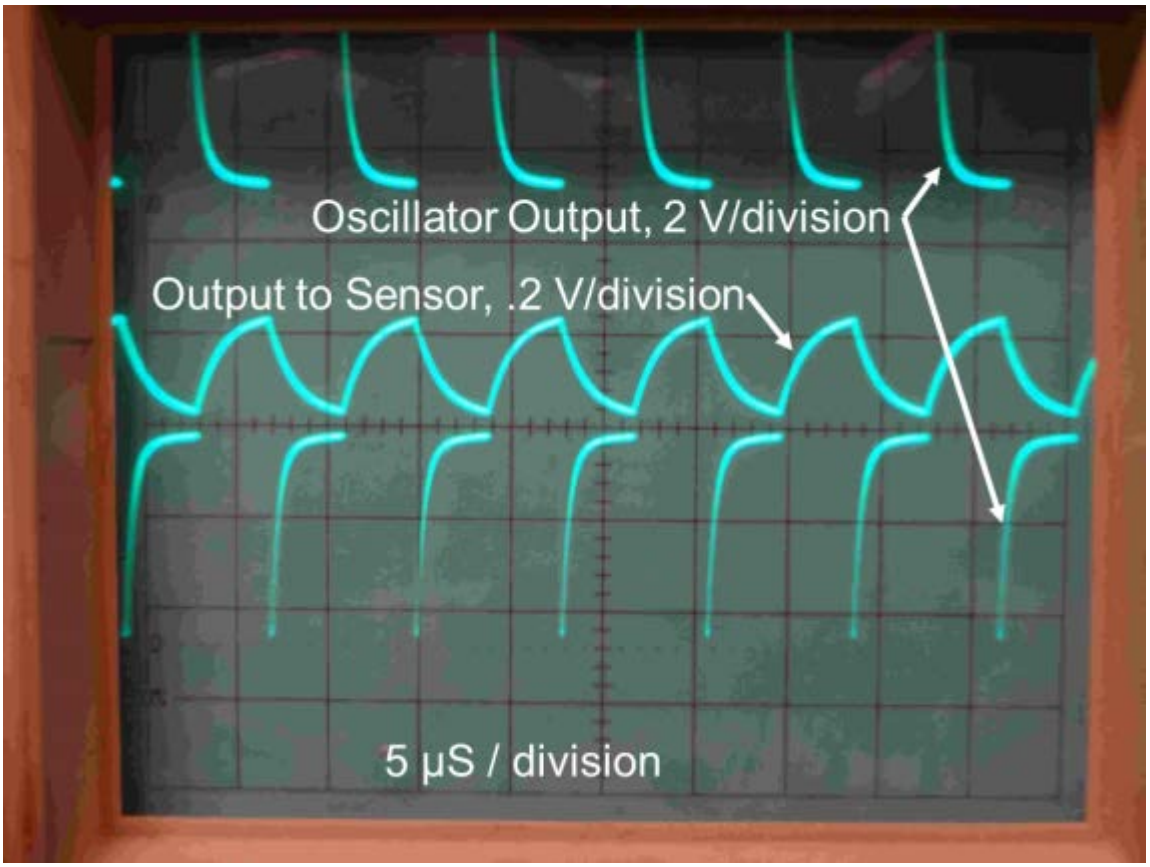

Figure (7.13) Output Provided to Sensor (V_2 in Figure 7.11) and Oscillator Output (V_1)

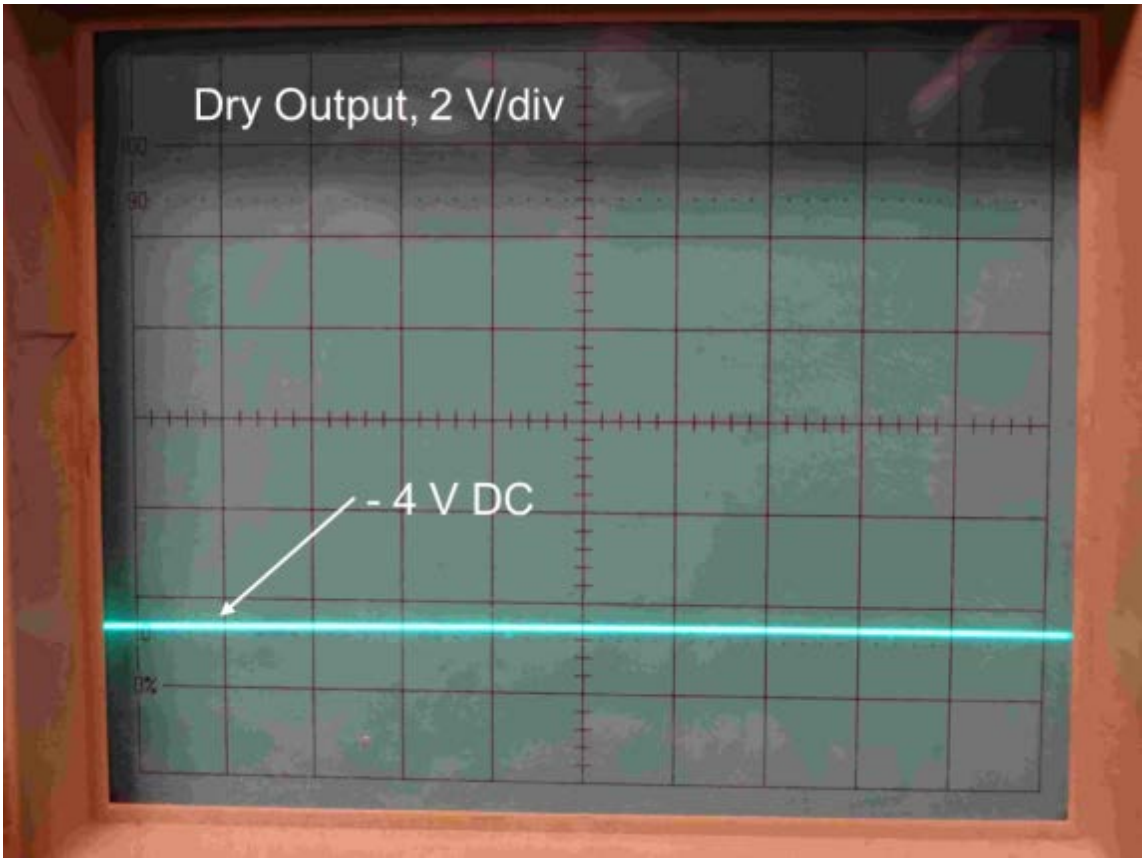

Figure (7.14) Dry Output from Sensor Circuit

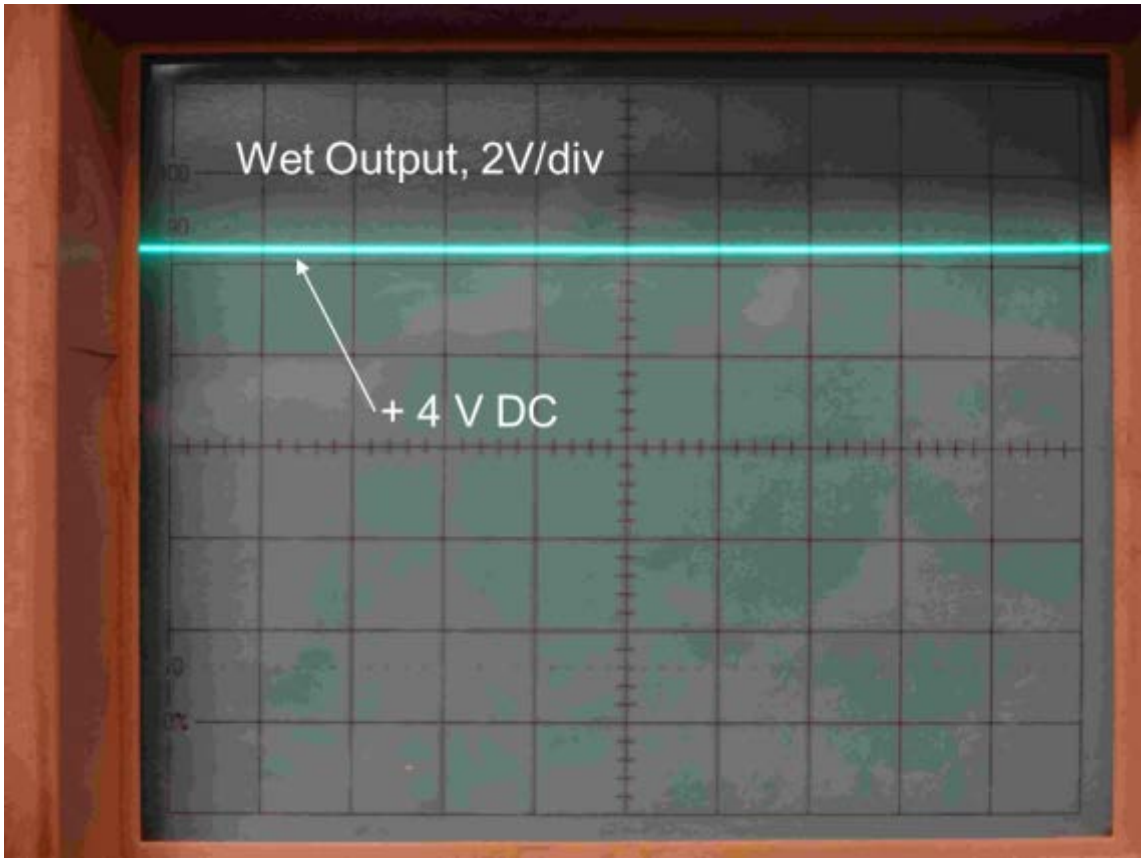

Figure (7.15) Wet Output from Sensor Circuit

8. RESULTS

In-building tests were performed on Coil Enthalpy Limit sensors to test reliability, time response, and durability. Operational testing confirmed that the sensors were able to detect water dripping from the coil into the drain pan when the coil was wet. Timed testing determined that the sensor registered a change from dry to wet between 6 and 45 minutes after the supply air temperature dropped below the mixed air dew point. Durability tests showed that the electrical properties of the sensor were retained after three months in an AHU.

8.1 Operational Testing

Two impedance sensors were installed in Langford AHU A-1, which serves the first floor perimeter zones of an office/classroom building at Texas A&M University. These sensors were initially hung below the drip rail using magnetic clamps, but after observations showed that the sides of the sensor blocked flow from the plates, sheet metal stands were fabricated to hold the sensors underneath the rail in the drip pan. A sensor on its stand is shown in Figure (8.1). Onset Computer HOBO U12-012 data loggers were used to record the supply air temperature, supply air relative humidity, and voltage output from these sensors. The operating sequence for the AHU was left unchanged for this test.

Figure (8.1) Photo of Sensor and Stand

Two sensors were installed in Langford AHU A-1 on May 22, 2013 and their voltage output was monitored by individual HOBO U12-012 loggers. The first sensor was connected in an “inverted” configuration, giving a 1 - 4 V output when dry. The second sensor was connected in the “normal” configuration, giving a 1 - 4 V output when wet. This allowed for testing of reliability and sensor hysteresis. If the sensors gave a positive voltage output simultaneously, then there was a time delay between the coil becoming dry and the sensors registering this change of state.

At the end of this test, both sensors were free from contamination, indicating that the sensors were being kept clean by air and water flow. These results show successful operation of these sensors, with voltage outputs corresponding to dry coil conditions (positive voltages on the “inverted” sensor) after the AHU was shut off at night, and

outputs corresponding to wet operation (positive voltages on the “normal” sensor during the day. Figure (8.2) shows the “inverted” sensor output, Figure (8.3) shows the “normal” sensor output, and Figure (8.4) shows a sensor at the end of testing.

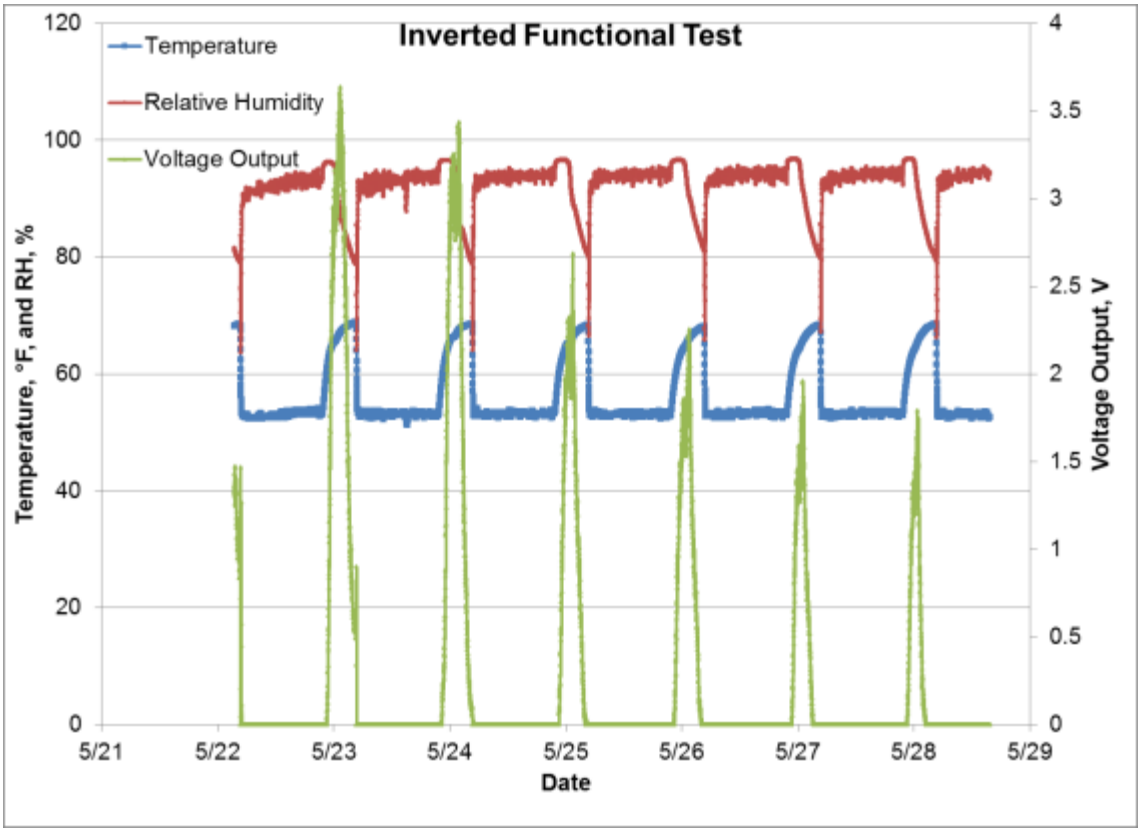

Figure (8.2) Inverted Functional Test – 0 V Output When Wet

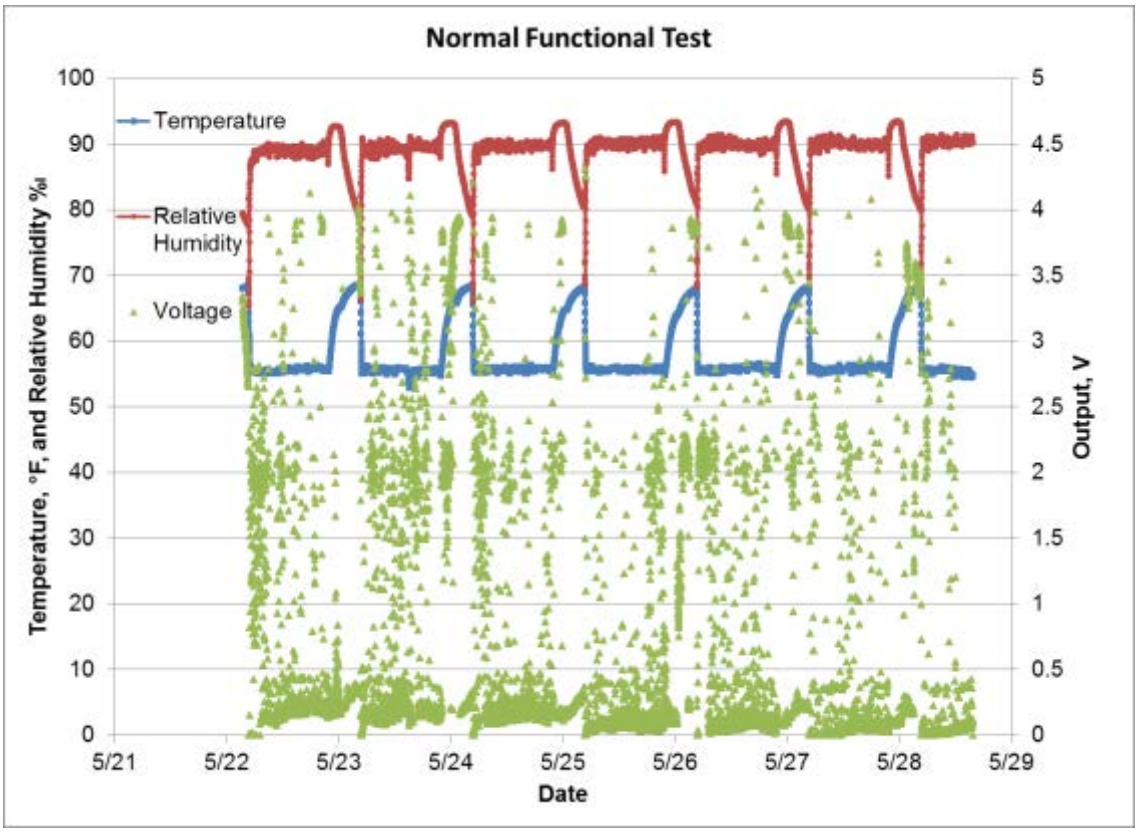

Figure (8.3) Normal Functional Test – 0 V Output When Dry

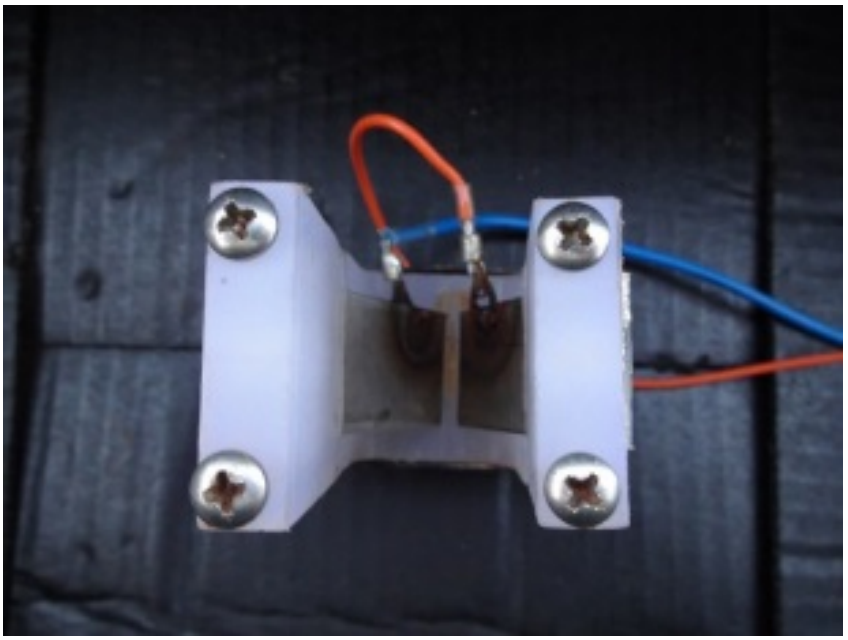

Figure (8.4) Sensor After Test

Since the AHU was shut off between 11 p.m. and 5 a.m. each day, the coil became dry as air passed through it. The observed delay between shutdown and sensor reading varied between one and two hours. Requirement 5 for the sensor in Section 6 was that it respond within 3 minutes for dew point measurement, and within 10 minutes for economizer control, so the observed response was too slow. However, with the AHU's fan shut down, the airflow through the coil was < 10% of the airflow during operation. Timed tests were then performed in order to measure the delay between reaching the dew point and a change in the sensor's state.

8.2 Timed Testing

Two sensors were mounted below the drip rail of the cooling coil in the same locations as used in the reliability tests. The chilled water valve was then manually closed in order to test wet-to-dry sensor response. After the sensors had reached a 0 V output, the chilled water valve was opened in order to measure the delay between the coil reaching the dew point and the sensor returning to >5 V output.

The first test of sensor and coil response was performed at Langford AHU A-1. The chilled water valve was allowed to reopen at 3:50 p.m. By 4:05 p.m., the supply air temperature had reached its set point of 53°F. It took until 4:30 p.m. for water droplets to begin dripping off the rail, and at 4:35 p.m. the sensor returned to a wet state. The 45-minute response time is shown in Figure (8.5). This required an investigation to see if there was a problem with dehumidification in this AHU. The quantity of water condensed in this coil was calculated and then compared against a measurement.

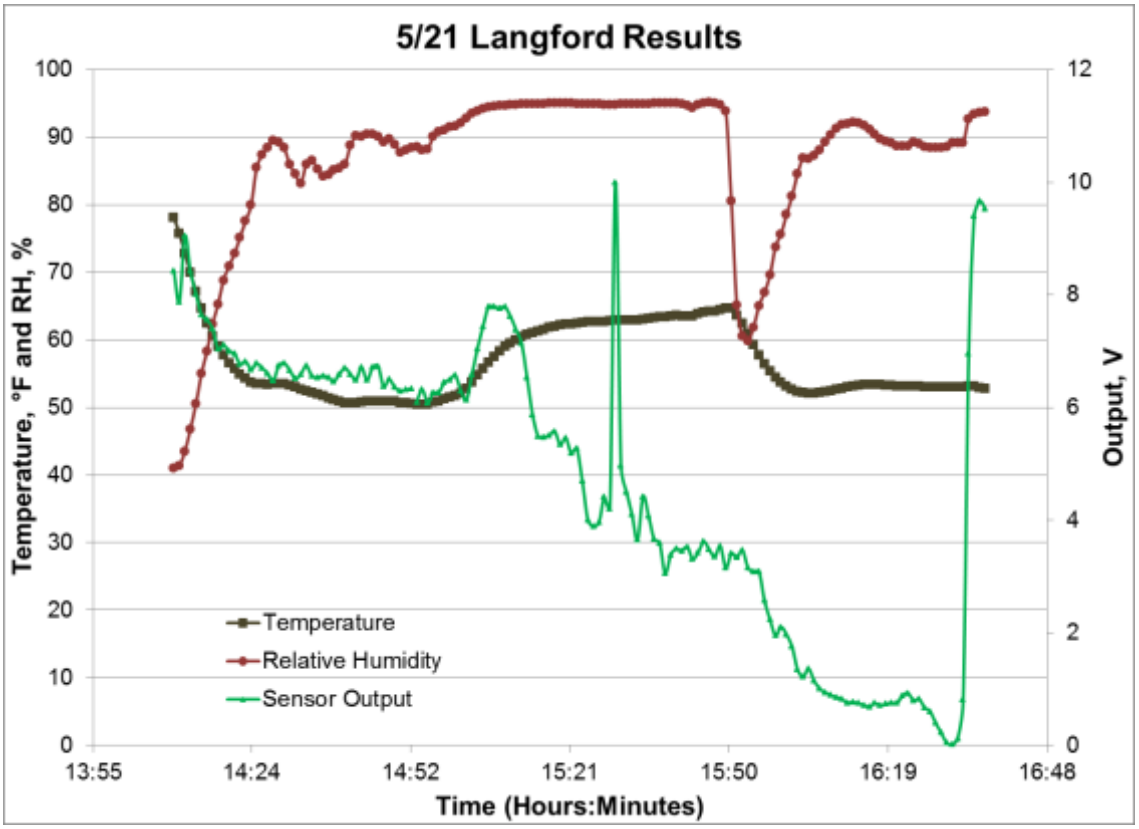

Figure (8.5) Langford A Test Shows Slow Response

Assuming the outside air mass fraction $x_{OA} = 0.2$, and using the recorded local weather, the following temperatures (T), dew points (DP), humidity ratios (w), and densities (ρ) for the return air, outside air, and mixed air were obtained:

$T_{RA} = 80°\text{F} \quad DP_{RA} = 58°\text{F} \quad w_{RA} = 0.009\ \frac{lbw}{lbda}$

$T_{OA} = 92°\text{F} \quad DP_{OA} = 71°\text{F} \quad w_{OA} = 0.0165\ \frac{lbw}{lbda}$

$$T_{MA} = x_{OA}T_{OA} + (1 - x_{OA})T_{RA} = 0.2 * 91°\text{F} + 0.8 * 80°\text{F} = 82.2°\text{F} \qquad \text{Equation (8.1)}$$

$$\rho_{MA} = x_{OA}\rho_{OA} + (1 - x_{OA})\rho_{RA} = 0.2 * \frac{1\ lb}{14.1\ ft^3} + 0.8 * \frac{1\ lb}{13.8\ ft^3} = .072\frac{lb}{ft^3} \qquad \text{Equation (8.2)}$$

This allowed the assumption of constant density throughout the remainder of these calculations, as return air and outside air densities were within ± 2%.

$$w_{MA} = x_{OA} w_{OA} + (1 - x_{OA}) w_{RA} = 0.0105 \frac{lbw}{lbda} \qquad \text{Equation (8.3)}$$

The supply air properties were then calculated. Assuming that the coil is wet, the air leaving the coil will be saturated and at the coil leaving temperature.

$$T_{SA} = 53°\text{F} \;\; DP_{SA} = 53°\text{F} \quad w_{SA} = 0.0085 \frac{lbw}{lbda} \quad \rho_{SA} = \frac{1\ lb}{13.3\ ft^3} \qquad \text{Equation (8.4)}$$

The volumetric and mass airflow were then calculated, based on the assumption that the component of the mean air velocity perpendicular to the coil is constant.

$$\vec{V} = 600 \frac{ft}{min}$$

$$A_{coil} = 30\ ft^2$$

$$\dot{V}_{ma} = \vec{V}\ X\ A_{coil} = 18000 \frac{ft^3}{min} \qquad \text{Equation (8.5)}$$

$$\dot{m}_{MA} = \dot{V}_{ma} \rho_{MA} = 18000 \frac{ft^3}{min} * \frac{1\ lbda}{13.8\ ft^3} = 1300 \frac{lbda}{min} \qquad \text{Equation (8.6)}$$

This then allowed the calculation of the amount of water removed from the mixed air.

$$\dot{m}_{W,MA} = \dot{m}_{MA} w_{MA} = 1300 \frac{lbda}{min} * 0105 \frac{lbw}{lbda} = 13.7 \frac{lbw}{min} \qquad \text{Equation (8.7)}$$

$$\dot{m}_{W,SA} = \dot{m}_{SA} w_{SA} = 1300 \frac{lbda}{min} * 0085 \frac{lbw}{lbda} = 10.95 \frac{lbw}{min} \qquad \text{Equation (8.8)}$$

$$\dot{m}_{removed=} \dot{m}_{W,MA} - \dot{m}_{W,SA} = 2.75 \frac{lbw}{min} \qquad \text{Equation (8.9)}$$

If this water was trapped for 30 minutes within the boundary layer near the cooling coil fins, 82 lbs of water, or 10.2 gallons, was contained there at the end. 30% of the total internal volume of the coil would have been taken up by water in this state. The quantity of water condensed at steady state was then measured. It took 4 minutes 5 seconds to fill a 16 fluid ounce cup. Equation (8.10) shows that the condensate flow rate was less than 10% of the calculated value.

$$\dot{m}_{w,Actual} = \frac{m_{water}}{t} = \frac{1\ lb}{4\ min} = 0.25\ \frac{lb}{min}$$ Equation (8.10)

This discrepancy needed further investigation. Langford AHU-A1 is on Texas A&M's Siemens APOGEE EMCS, and the flow rates and temperatures used for control are available. Since $T_{MA} = T_{RA}$, and the outside air temperature is 10°F hotter, too little outside air is being provided to this AHU to be able to calculate the outside air fraction. As the building was unoccupied during this test, the latent load on the coil was much smaller than assumed. The measured and recorded temperatures and humidities are given below.

$T_{RA} = 73°\text{F}$	$RH_{RA} = 55\%$	$w_{RA} = 0.009\ \frac{lbw}{lbda}$
$T_{OA} = 80°\text{F}$	$DP_{OA} = 70°\text{F}$	$w_{OA} = 0.016\ \frac{lbw}{lbda}$
$T_{MA} = 73°\text{F}$	$\dot{V}_{RA} = 7400\frac{ft^3}{min}$	$\dot{V}_{SA,APOGEE} = 8300\frac{ft^3}{min}$
$T_{SA} = 53°\text{F}$	$DP_{SA} = 53°\text{F}$	$w_{SA} = 0.0085\ \frac{lbw}{lbda}$
OA Damper Position = 10%	RA Damper Position = 10%	
CHWV Position = 44%	HWV Position = 0%	

This allowed calculation of the quantity of water condensed and trapped within the coil.

$$\dot{V}_{SA,actual} = 6200\frac{ft^3}{min}$$

$$\dot{m}_{SA} = \rho_{SA}\dot{V}_{SA,actual} = \frac{1\ lbda}{13.2\ ft^3} * 6200\frac{ft^3}{min} = 469\frac{lbda}{min}$$ Equation (8.11)

$$\dot{m}_{W,MA} = \dot{m}_{MA}w_{MA} = 469\frac{lbda}{min} * 0.009\ \frac{lbw}{lbda} = 4.22\frac{lbw}{min}$$ Equation (8.12)

$$\dot{m}_{W,SA} = \dot{m}_{SA}w_{SA} = 469\frac{lbda}{min} * 0.0085\ \frac{lbw}{lbda} = 3.99\frac{lbw}{min}$$ Equation (8.13)

$$\dot{m}_{removed=}\dot{m}_{W,MA} - \dot{m}_{W,SA} = 0.234\frac{lbw}{min}$$ Equation (8.14)

This result is within ± 7% of the measured value. Over 30 minutes, 7.5 lbs, approximately 1 gallon, of water was trapped in a coil measuring 4' x 8' x 1'. This gave a "trapped water density" of

$$\rho_{trapped} = \frac{m_{trapped}}{V_{coil}} = \frac{7.5\ lbs}{32\ ft^3} = 0.23\ \frac{lb}{ft^3}$$ Equation (8.15)

Since water has a density of $8\ {}^{lbs}/_{ft^3}$, 3% of the total internal volume of the coil was occupied by water when the coil reached its carrying capacity.

Another SDVAV air handler, AHU 1-2 at the Jack E. Brown Building, was selected for further timed testing. Timed tests were performed there showing wet-to-dry delays between 6 and 30 minutes, depending primarily on the difference between the outside air temperature and dew point, and dry-to-wet delays between 45 seconds and 6 minutes. Figure (8.9) shows voltage spikes when the timed tests were performed. The results from the first test, along with calculations of the theoretical carrying capacity of AHU 1-2 at the Jack E. Brown building are as follows.

$$T_{OA} = 87°\text{F} \quad T_{RA} = 74°\text{F} \quad T_{MA} = 78°\text{F} \quad \dot{V}_{OA} = 1800\frac{ft^3}{min}$$

$$DP_{OA} = 73°\text{F} \quad DP_{RA} = 54°\text{F} \quad w_{OA} = 0.0175\ \frac{lbw}{lbda} \quad w_{RA} = 0.009\frac{lbw}{lbda}$$

$$T_{MA} = x_{OA}T_{OA} + (1 - x_{OA})T_{RA}$$ Equation (8.16)

$$T_{MA} = x_{OA}T_{OA} + T_{RA} - x_{OA}T_{RA}$$ Equation (8.17)

$$T_{MA} - T_{RA} = x_{OA}(T_{OA} - T_{RA})$$ Equation (8.18)

$$x_{OA} = \frac{T_{MA} - T_{RA}}{T_{OA} - T_{RA}} = \frac{78°\text{F} - 74°\text{F}}{87°\text{F} - 74°\text{F}} = 0.31$$ Equation (8.19)

$$\dot{V}_{MA} = \frac{\dot{V}_{OA}}{x_{OA}} = 5850\frac{ft^3}{min}$$ Equation (8.20)

$$w_{MA} = x_{OA}w_{OA} + (1 - x_{OA})w_{RA} = 0.0115\frac{lbw}{lbda}$$ Equation (8.21)

Given these coil entering conditions, the expected condensate flow was then calculated using the measured coil leaving conditions using Equations (8.22), (8.23), and (8.24):

$$T_{SA} = 53.5°\text{F} \quad DP_{SA} = 53.5°\text{F} \; w_{SA} = 0.0085 \frac{lbw}{lbda}$$

$$\dot{m}_{w,MA} = \dot{m}_{MA} * w_{MA} = \dot{V}_{MA} * \rho_{MA} * w_{MA} = 5850 \frac{ft^3}{min} * \frac{1\ lbda}{13.6\ ft^3} * 0.0115 \frac{lbw}{lbda} = 4.94 \frac{lbw}{min}$$

Equation (8.22)

$$\dot{m}_{w,SA} = \dot{m}_{SA} * w_{SA} = 430 \frac{lbda}{min} * 0.0085 \frac{lbw}{lbda} = 3.65 \frac{lbw}{lbda}$$ Equation (8.23)

$$\dot{m}_{removed=} \dot{m}_{W,MA} - \dot{m}_{W,SA} = 1.29 \frac{lbw}{min}$$ Equation (8.24)

This was approximately 5 times the quantity of water removed by the coil in Langford AHU A-1. A “cup and stopwatch” method was used and 9 oz. of water was collected in 27 seconds. Using equation (8.10) this gives a flow rate of 1.25 $\frac{lbw}{min}$. Both the Langford A-1 and Jack E. Brown 1-2 calculations were within ±7% of the measured results; therefore, these measurements can be useful for investigation of comfort or control issues.

The volume and fin density of the cooling coil in the Jack E Brown AHU 1-2, 4’ x 8.5’ x 1’ and 12 fins/inch, are within ± 5% of the coil in Langford A-1. The water carrying capacity of the coil should be similar in these two AHUs. Therefore, the response time from the sensor at Jack E. Brown should have been approximately 1/5 of that at Langford. Timed tests agreed with this hypothesis during dry-to-wet transitions when the chilled water valve was suddenly opened as shown in Figure (8.7). Measurement 4 took place when the mixed air dew point was between 55°F and 56°F and the discharge temperature set point was 55° F. This indicated that measurement of the dew point within ±1°F was possible using this method, if 34 minutes is an acceptable time for

measurement. Response time was inversely related to the difference between the dew point and the supply air temperature.

A summary of these timed tests is shown in Table (8.1). The outside air water concentration was determined from the outside air dew point provided by the National Weather Service. Test #1 was run in Langford AHU A-1; it is shown in Figure 8.5. The remaining tests were run in Jack E. Brown AHU 1-2.

Test #	Date and AHU	1	2	3	4	5
Property	Units	5/29 J	5/29 J	6/7 J	7/17 J	7/17 J
OA Temp	°F	87	87	84	80	83
RA Temp	°F	74	75.3	75	76	75
MA Temp	°F	78	78	77	77	77
OA Flow	cfm	1800	1800	1750	1435	1435
x		0.31	0.23	0.23	0.23	0.23
Weather Station Dew Point	°F	72	74	57	73	73
MA Flow	cfm	5850	7800	7609	6250	6250
MA Density	lb/cft	0.075	0.075	0.075	0.075	0.075
MA Mass Flow	lbda/min	438.75	585	571	468	468
MA Water Concentration*	lbw/lbda	0.0115	0.0115	0.0094	0.0110	0.0110
SA Temp	°F	53.5	55.5	55	55	55
SA Water Concentration	lbw/lbda	0.0085	0.0092	0.009	0.009	0.009
MA Water Flow	lbw/min	4.94	6.7	5.4	5.1	5.1
SA Water Flow	lbw/min	3.65	5.4	5.1	4.2	4.2
Water Removal Rate	lbw/min	1.29	1.3	0.2	0.9	0.9
Meas. Water Removal Rate	lbw/min	1.25				
Transition Time	min	5	0.8	23.0	7.0	6.5
Water Capacity	lbs	6.45	1.0	5.0	6.4	5.9

Table (8.1) Summary of Timed Dry-to-Wet Tests

8.3 Run-to-Run Differences In Dew Point and Coil Water Capacity Calculations

8.3.1 Difference Between Measured Dew Point and True Dew Point

The quantity of water condensed from the air by the cooling coil is determined by the mass flow of air through the coil and the change in the humidity ratio of the air as it passes through, as shown in Equation (8.25). The change in humidity ratio across the coil was determined by the difference between the mixed air dew point and the cooling coil leaving temperature. The Magnus-Tetens equation, Equation (8.26), given by Vömel [69], gives the saturation vapor pressure of water P_{sat}, in kPa, in air for a given temperature T, in °C. From this saturation vapor pressure and the barometric pressure (101 kPa at sea level), Equation (8.27) gives the humidity ratio w_{AIR} of the air in $\frac{lb(w)}{lb(da)}$ [70]. Finally, the latent component of enthalpy is calculated from the humidity ratio using the specific heat of vaporization of water, and this is given as Equation (8.28). The relationships between latent enthalpy, humidity ratio, and dew point are shown in Figure (8.6).

$$\dot{m}_{condensate} = \dot{m}_{MA} * (w_{MA} - w_{SA}) \qquad \text{Equation (8.25)}$$

$$P_{water}(kPa) = .61 * e^{\frac{17.3*T}{237.7+T}}, \text{ with T in °C} \qquad \text{Equation (8.26)}$$

$$w_{sat}\frac{lb(w)}{lb(da)} = .622 * \frac{P_{water}}{P_{water}+P_{air}} \qquad \text{Equation (8.27)}$$

$$h_{latent} = 970\ \frac{Btu}{lb} * w_{AIR} \qquad \text{Equation (8.28)}$$

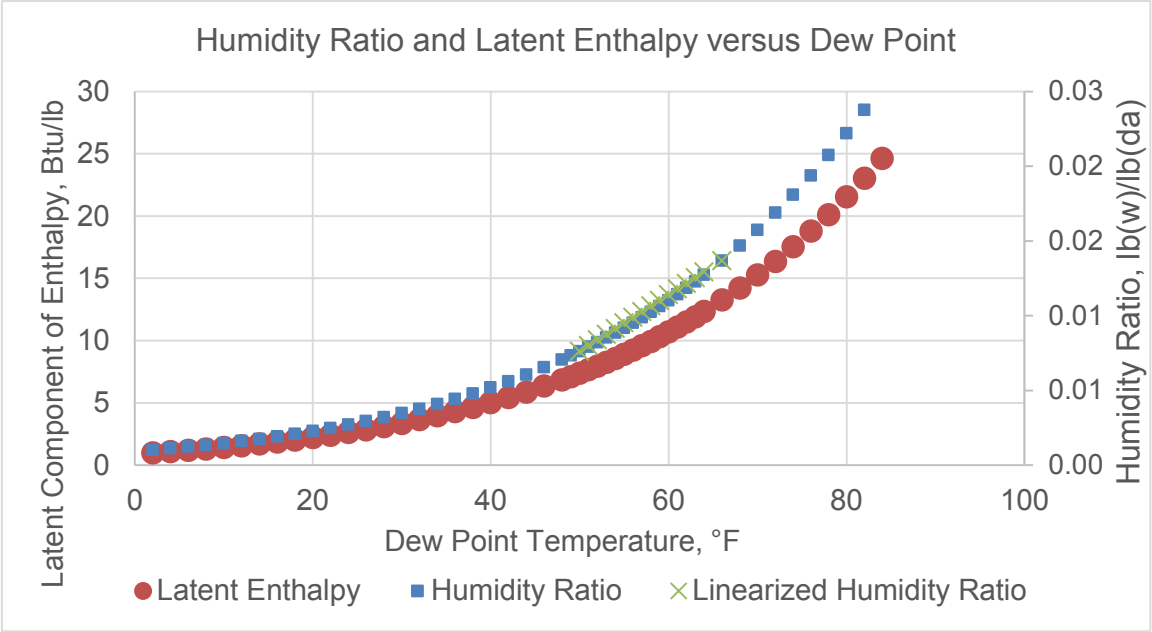

Figure (8.6) Humidity Ratio and Latent Enthalpy vs Dew Point

The saturation humidity ratio can then be linearized in the range between 50°F and 65°F and is shown on the graph. This is done in Equation (8.29) and is shown on Figure (8.6). The mass of water contained in the coil, $m_{trapped}$, calculated in sections 8.3.2 and 8.3.3 is assumed to be constant. If the coil is assumed to reach this lower temperature immediately, the time needed to reach the coil capacity is given by Equation (8.30). If it instead functions as a first-order system with time constant τ = 2 minutes, the time needed is given by Equations (8.31) and (8.32).

$$w_{sat,linearized} = w_{50\,°F} + \frac{w_{66\,°F} - w_{50\,°F}}{16\,°F} * (T_{sat} - 50\,°F) = w_{50\,°F} + \frac{\Delta W}{\Delta T} * \Delta T$$

Equation (8.29)

$$t_{delay} = \frac{m_{trapped}}{\dot{m}_{air} * (w_{Dewpoint} - w_{Sat,CCLT})} = \frac{m_{trapped}}{\dot{m}_{air} * \frac{\Delta w}{\Delta T} * (T_{Dewpoint} - T_{CCL})}$$ Equation (8.30)

$$T_{ccl} = T_{final} + (T_{initial} - T_{final}) * e^{t/\tau}$$ Equation (8.31)

$$t_{delay} = \frac{m_{trapped}}{\int_0^t \dot{m}_{air} * \frac{\Delta w}{\Delta T} * \left(T_{dewpoint} - T_{ccl}\right) dt}$$

$$= \frac{m_{trapped}}{\dot{m}_{air} * \frac{\Delta w}{\Delta T} * \int_0^t \left(T_{dewpoint} - T_{ccl}\right) dt}$$

$$= \frac{m_{trapped}}{\dot{m}_{air} * \frac{\Delta w}{\Delta T} * \int_0^t \left(T_{dewpoint} - (T_{final} + (T_{initial} - T_{final}) * e^{t/\tau})\right) dt} =$$

$$\frac{m_{trapped}}{\dot{m}_{air} * \frac{\Delta w}{\Delta T} * (T_{dewpoint} - \left(T_{final} + (T_{initial} - T_{final}\right) * \tau e^{t/\tau} \Big|_0^t}$$ Equation (8.32)

Figure (8.7) displays the relation between temperature and time for a coil with a constant trapped water capacity of 5 lbs, a constant $\dot{m}_{air}$ of 440 lbs/min, a $T_{dewpoint}$ of 55°F. The cooling coil leaving temperature needs to be 4°F below the mixed-air dew point in order to transition from dry to wet within 10 minutes.

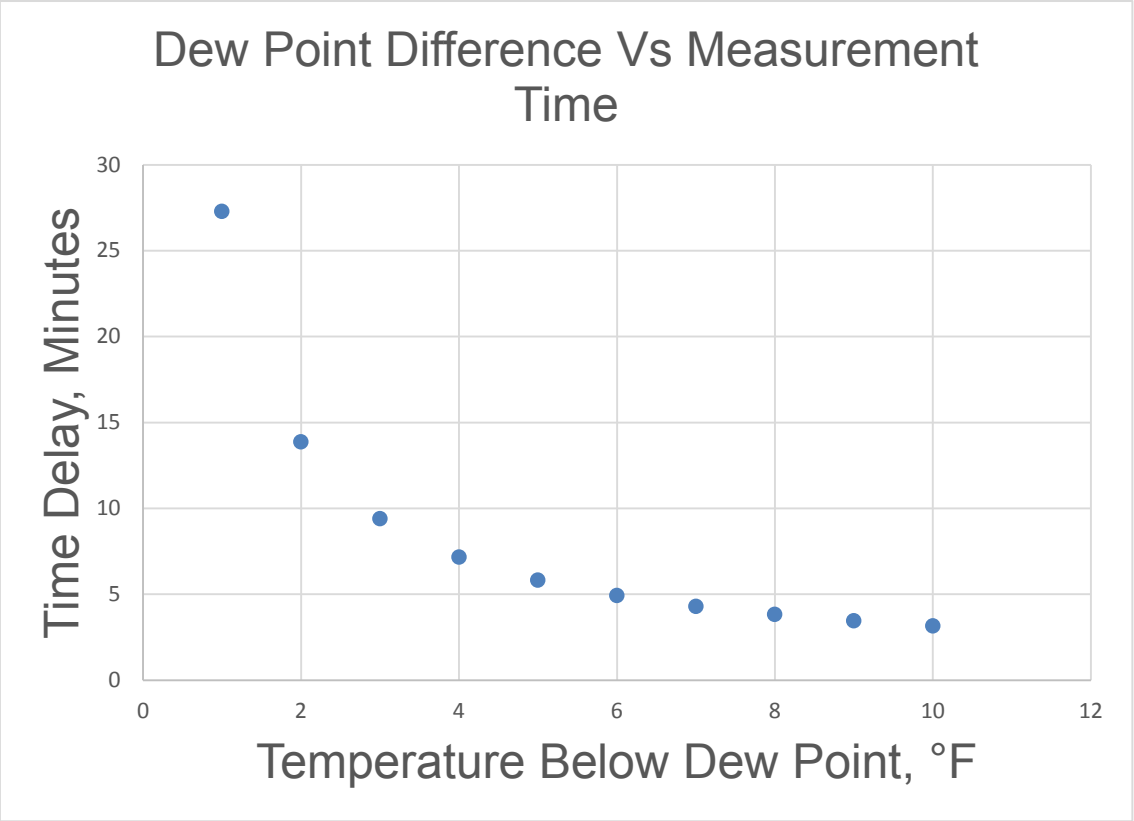

Figure (8.7) Time versus Temperature Difference

8.3.2 Run-to-Run Differences In Coil Water Capacity

Table (8.1) shows the results of five runs to test the dry-to-wet response of a 4'x8'x12" four row cooling coil with 12 fins per inch. The response time of the sensor of electronics was < 1 second from when water bridged the electrodes to the change in output. Therefore, the system response time was driven by the time required for the coil to become saturated. In section 8.2 it was suggested that the maximum mass of water

trapped in the cooling coil was constant. This water capacity was calculated from the water flow rate and the response time.

Five tests were performed at Jack E. Brown Building. The sample size was too small for a normal Gaussian distribution to be calculated. Instead, a Student's t-distribution was assumed, symmetrical about the sample mean. Equations (8.33) through (8.37) are from Beckwith [71, p 70] and were applied to the results. The individual runs are shown in Table (8.2)

Run	Coil Water Mass, lb(m)	Deviation Squared
1	6.5	2.4
2	1	15.7
3	5	0.0
4	6.4	2.1
5	5.9	0.9

Table (8.2) Individual Dry-to-Wet Run Results

The sample mean $\bar{x}$ is given by Equation (8.33). Each individual run's deviation from the mean was then calculated and the sample deviation S_x was calculated by Equation (8.34). A 95% confidence interval was used, and the t-statistic was calculated for n = 5 samples and v = 4 degrees of freedom with α = 0.05. The t-statistic from these was found in table 3.6 of Beckwith [71, p 73] and was then used to calculate the size of the expected interval in water capacities using Equation (8.36). Equation (8.37) is the expression for the quantity of water contained in the coil with 95% confidence.

$$\bar{x} = \sum_{i=1}^{n} \frac{x_i}{n} = \frac{6.5+1+5+6.4+5.9}{5} = 5.0\ lbs\ water \qquad \text{Equation (8.33)}$$

$$S_x = \sqrt{\frac{\sum_{i=1}^{n} x_i^2 - n\bar{x}^2}{n-1}} = \sqrt{\frac{144.02-123}{4}} = 2.3\ lbs\ water$$ Equation (8.34)

$$t_{0.05,4} = 2.132$$ Equation (8.35)

$$t_{a/2,v} * \frac{S_x}{\sqrt{n}} = 2.132 * \frac{2.3\ lbs\ water}{2.231} = 2.85\ lbs\ water$$ Equation (8.36)

$$m_{trapped} = 5.0\ lbs\ \pm 2.85\ lbs\ water$$ Equation (8.37)

Run #2 appeared to be an extreme outlier, having less than 20% of the coil water capacity of any other run. If Equations (8.33-8.37) are recalculated without Run 2, $\bar{x} = 6.0\ lbs$, S_x=1.2 lbs, and $m_{trapped}$ = 6.0 lbs ± 1.84 lbs water. The statistical analysis indicates that the water capacity of a coil is not a constant quantity. Future work may include determining the variables which affect this quantity. These results show that the time to be expected for any given dew point will vary. Times from the tests and the calculated dew point temperature differences are shown in Figure (8.8), along with the calculated dew points from this constant water capacity and error bars in $m_{trapped}$.

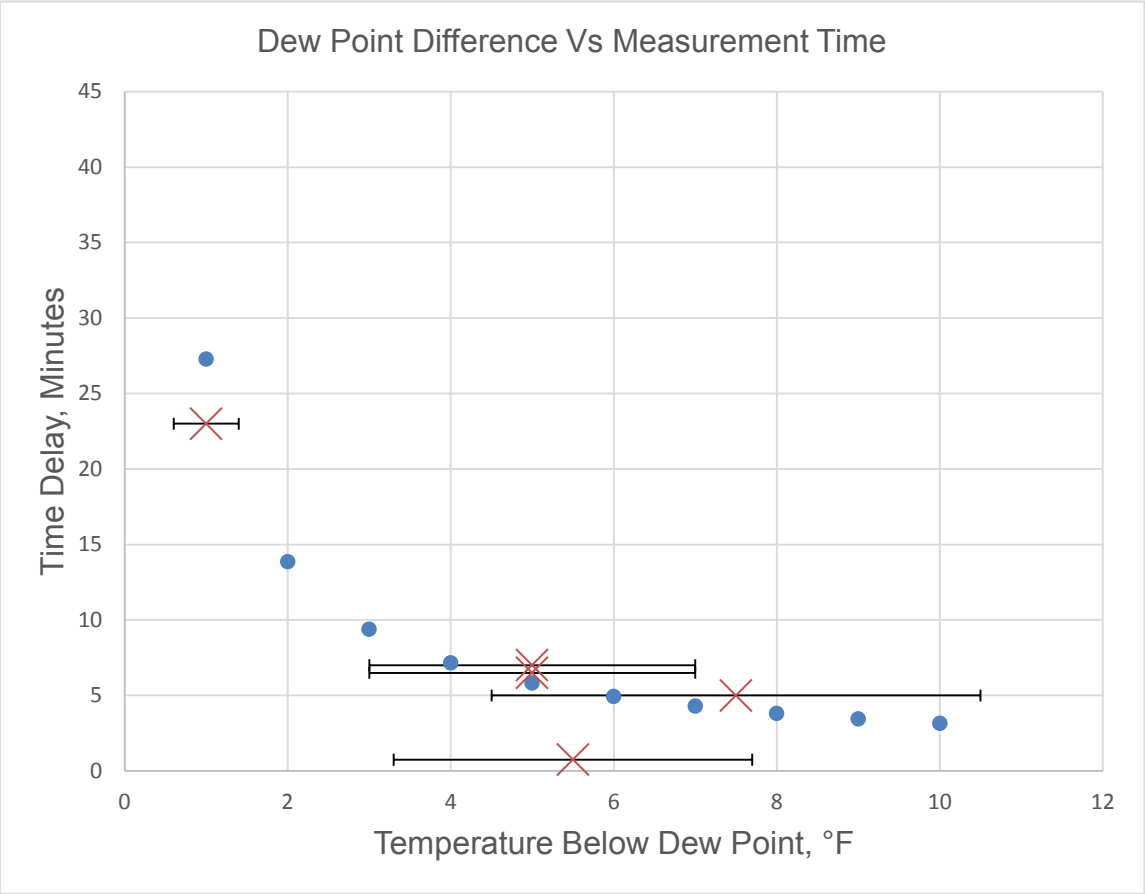

Figure (8.8) Dew Point Difference Versus Coil Transition Time

8.4 GE Telaire Vaporstat 9002 Testing

An IR reflectivity dew point sensor was obtained as a test sample and tested in the mixed air duct of the AHU 1-2 at Jack E. Brown. It was positioned between the OA and RA duct inlets. As the AHU operated continuously, and the return air conditions changed minimally during the test, the main change in the dew point and humidity came from exposure to the varying percentages of OA during the test. Figures (8.9) and (8.10) clearly show the poor mixing at this location. All four sensors (temperature,

HOBO RH, IR dew point, condensation sensor output) alternated between “OA” conditions and “RA” conditions.

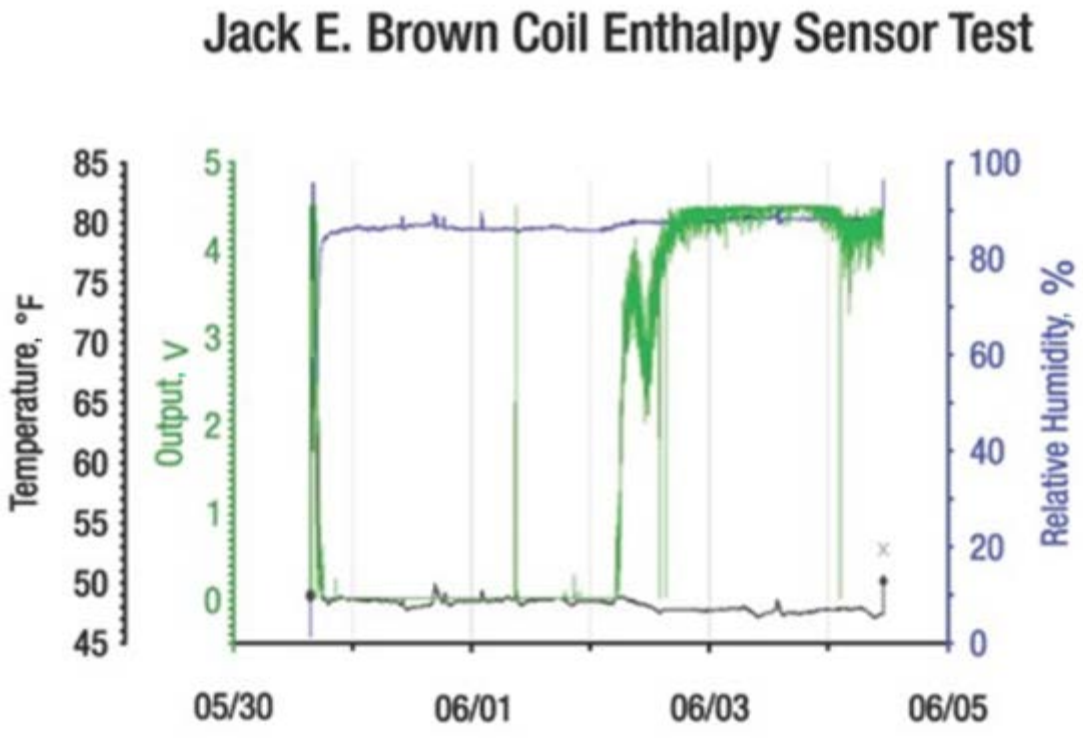

Figure (8.9) Jack E. Brown Test – Poor Location for Mixed Air Testing

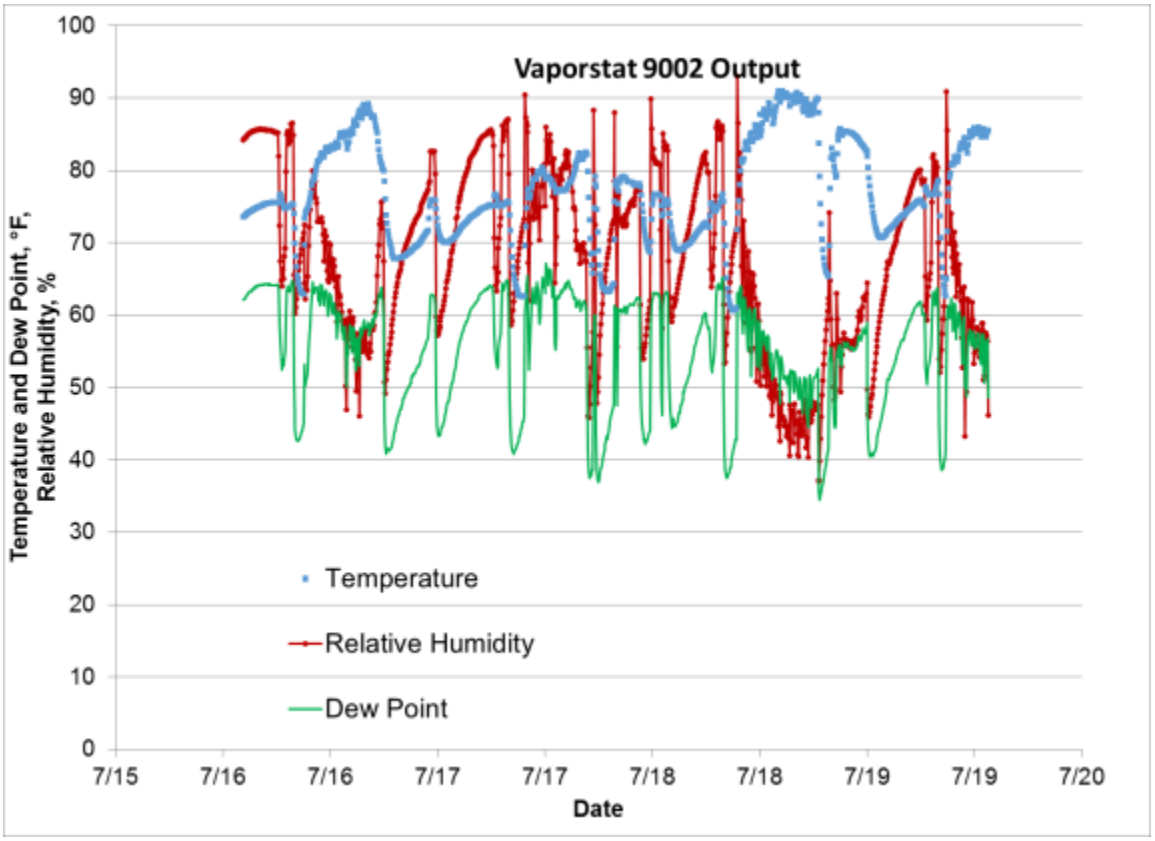

Figure (8.10) GE Telaire Vaporstat 9002 Test

Calibration of the IR-reflectivity dew point sensor was performed by a “single-point” method. The dew point was identical at three separate airport weather stations surrounding the calibration site at the time of calibration. The device was placed outside in a calm location and this dew point was entered. At the end of the test the sensor was found to be in calibration by a similar method. The manufacturer does recommends not using in saturated or condensing environments, but it is suitable for mixed-air dew point measurements.

8.5 Durability Testing

After the timed tests, a Coil Enthalpy sensor was placed in Jack E. Brown AHU 1-2, and left to monitor coil transitions for two months. Temperature and voltage outputs were recorded, and are shown in Figure (8.11). The sensor continued to function throughout the test. Some rust on a stainless steel crimp terminal was noted as the only deterioration, with the sensor plate thickness remaining at .065”. Figure (8.12) shows the sensor after the tests, with a magnet stuck to the rusted terminal.

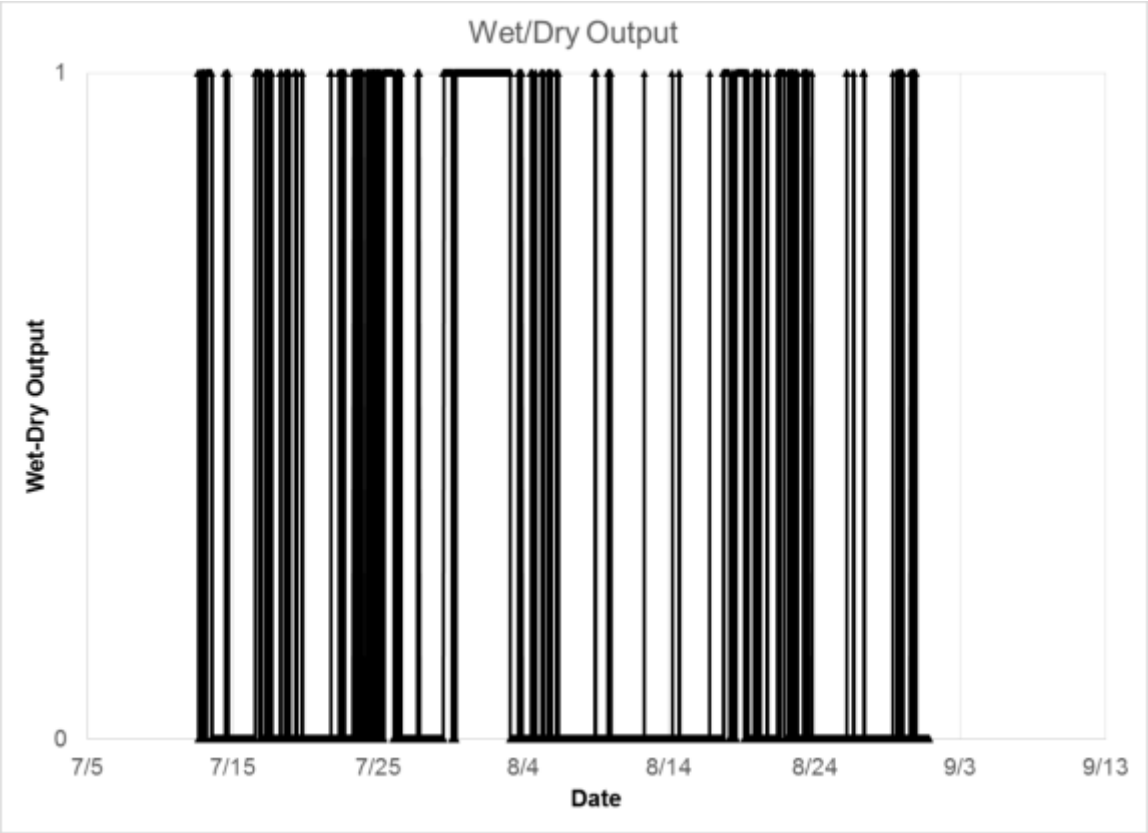

Figure (8.11) Voltage Output From Sensor During Two Months In AHU

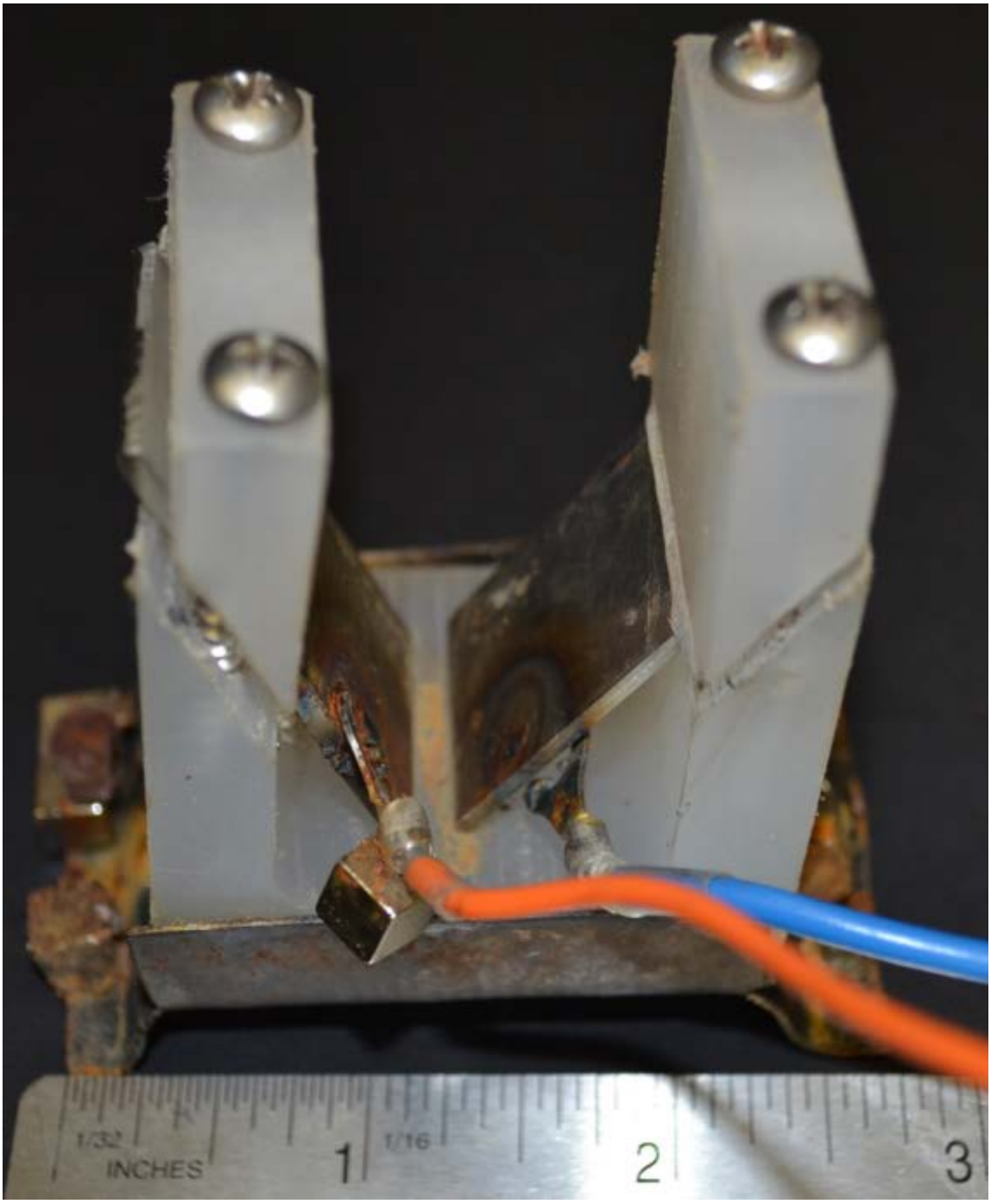

Figure (8.12) Sensor With Magnet and Stand After Test

From the in-building tests, the sensor was found to be able to monitor changes in the coil state for the duration of the test. Timing tests demonstrated that response times depended on the physical size of the coil, airflow, and difference between the mixed air dew point and supply temperature. This meant that the main goal of the project, to determine the state of the coil accurately enough to use it for AHU control, was successfully accomplished.

8.6 Applications

8.6.1 Confirmation of Weather Station Dew Point

If the outside air dew point can be obtained from a weather station, this dew point can be used for control. The Coil Enthalpy Limit sensor can be used to determine whether the weather station is operating or is out of service by bracketing the outside air dew point temperature. Figure (8.13) is a flowchart of the procedure.

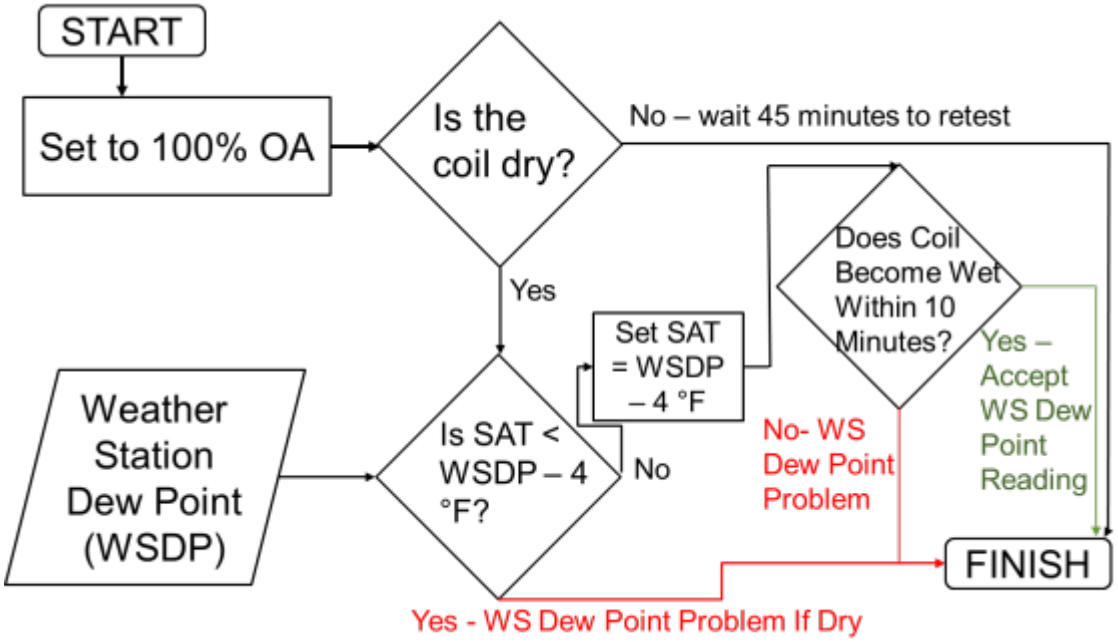

Figure (8.13) Flowchart of OA Weather Station Dew Point Confirmation

This procedure detects two cases where the weather station dew point is erroneous. If the coil is brought 4°F below the weather station dew point and does not transition from dry to wet within 10 minutes, then the weather station is out of operation. If the coil leaving temperature was already more than 4°F below the weather station dew point and the cooling coil was still dry, the weather station dew point reading is too high. In either case, the system will need to operate as if the water content of the air is unknown. If the coil is initially wet, the slow wet-to-dry response of the coil and sensor prevents readings from being taken and the previous “trust the weather station dew point” or “weather station dew point out of range” state remains until the next retest.

8.6.2 Economizer Control – High Limit At SAT

An economizer control using the Coil Enthalpy Limit Sensor reading as a high limit cutoff sets the high limit of economizer operation to an outside air dew point equal to the supply air temperature. If the economizer is operating, and the Coil Enthalpy Sensor indicates that the coil is wet, the economizer is disabled and not restarted until the coil becomes dry. The 30 to 45 minute wet-to-dry response of the coil and sensor prevents rapid cycling between activated and deactivated states. Figure (8.14), a reprint of Figure (3.10), shows the savings or loss of economizer use on a joint-frequency weather bin with the economizer control set to include the 58°F dew point bin, cutting off at 60°F. In combination with a 78°F outside air dry bulb cutoff, this achieves between 97% and 99% of the savings available from a psychrometrically ideal economizer.

Philadelphia savings/cost per year by using economizer rather than 20% OA, by bin

Data are in $\frac{\$}{1000\,ft^2 * year}$

Dew Point Temperature, °F \ Dry Bulb Temperature, °F	28	33	38	43	48	53	58	63	68	73	78	83	88	93	98	103	108
13	14	9.3	5.27	0.7	1.1	0.5	0.3	0.1									
18	17	26	21.2	6.1	2.7	1	0.6	0.2									
23	22	44	25.1	13	4	1.9	1.9	0.3									
28	16	34	26.7	20	10	6.8	1.8	0.4	0.1	-0							
33	5.7	25	24.1	22	11	5	1.6	1	0.3	-0							
38		5.8	32.5	26	19	8	4.1	1.4	0.2	0							
43			19.3	21	19	8.2	4.3	3.1	1.5	0.1	0	0	-0.1				
48				15	25	15	7.9	4.9	3	0.5	-0.3	-0.1	-0.2	-0.1			
53					9.7	21	17	6.8	3.2	1.6	-0.1	-0.8	-0.4	0			
58						10	21	7.5	2.7	0	-2	-3.5	-1.4	-0.2			
63							3.1	2	-3.1	-5.8	-7	-3.9	-2.5	-2.6			
68								-3.3	-19	-15	-17	-13	-10	-4.2	-0.4		
73									-10	-32	-20	-9.1	-2.9	-1	0		
78										-2.6	-1.4	-0.8	0				

Region with economizer active

Region to use minimum OA

Figure (8.14) Economizer Savings using Coil Enthalpy Sensor as Dew Point High Limit

9. CONCLUSIONS

Development of a reliable enthalpy sensor using the state of the chilled water coil was the primary goal of this project. The design of a sensor with a gap between two electrodes to be bridged by coil condensate was described in Section 6, and the successful results of testing that sensor were described in Section 8.

One of the conclusions from the literature survey was that common porous medium capacitive and resistive sensors fail to operate properly when exposed to condensing conditions. The tests performed on commercially available sensors support this conclusion. Cycling chilled mirror sensors last several years between repairs but cost in excess of $1500. Sensors that directly detect and measure water vapor concentration by measuring how much infrared radiation is absorbed by the air passing through the sensor may be able to provide dew point measurements indefinitely. Future work in building humidity measurement includes multiyear testing of commercial IR dew point sensors to determine whether calibration can be maintained over a long unattended interval.

WinAM models and the spreadsheet economizer simulations agreed with the literature that enthalpy economizers are ineffective in climates similar to Houston's, but showed areas where enthalpy control can allow for savings. Approximately 90% of the savings available from the use of an economizer in buildings in Dallas or Philadelphia can be attained with an appropriate dry bulb temperature cutoff. Conservative low-limit controls on the economizer can easily reduce the savings by more than 10%. A reliable dew point or humidity sensor serving as a high-limit cutoff allows the remainder of the savings to be captured.

Future work in economizer control includes using transient building models to consider the effects of night purge modes and supply air temperature resets based on time varying latent loads. Dessicant dehumidification may also require different air control strategies if waste heat can be used for reheat without additional energy inputs.

Reliable wet-or-dry measurements for economizer control can be made without sensor corrosion if the electrodes are made from 316 austenitic stainless steel sheet, the wires are fully encapsulated in crimped and welded terminals, and the potential difference between the electrodes is 0.25 V AC. These sensors can be made on a 3-axis mill out of high-density polypropylene.

One significant limitation of this type of measurement is the slow response time. A typical cooling coil in a 10,000 cfm air handler unit traps almost a gallon of water in the boundary layer near the fins. Condensation of enough water to fill the coil and begin dripping on the sensor took 5 to 10 minutes in a properly operating air handler. Active measurement of the dew point for supply air temperature resets and outside air dew point measurement is impractical.

Measurement of the rate of condensate flow from an AHU can help the diagnosis of comfort complaints. Insufficient outside airflow, insufficient total primary flow, and a partially blocked coil can cause unexpectedly low condensate production, while excessive outside airflow away from economizer-friendly conditions, high return air humidity due to infiltration, a chilled water valve stuck all the way open, or an inoperative economizer can cause excessive condensate flow.

The electronics described in this thesis gave a clear output difference between wet and dry states use commonly available analog components. The circuit consisted of an oscillator to generate the AC signal, a voltage divider to bring the voltage below the half-cell potential needed to oxidize the electrodes, the sensor and its leads, a filter to

convert the AC signal to its DC level, and an amplifier to give a ±5 V output. The cost of the components on the printed circuit board is approximately $10.

Electronically detecting water condensing on the coil by measuring the AC reactance across a gap between conductors can determine whether the dew point is above or below the cooling coil leaving temperature. This was demonstrated early in the development of the sensor and iteratively refined into the final device.

REFERENCES

1. U.S. Energy Information Administration, 2013, "2012 Annual Review of Energy," p 82, accessed on April 18, 2014 from http://www.eia.gov/totalenergy/data/annual/index.cfm
2. TIAX LLC, 2003. "Matching the Sensible Heat Ratio of Air Conditioning Equipment with the SHR," accessed on April 18, 2014 from http://www.airxchange.com/Collateral/Documents/English-US/SHR_Report.pdf
3. Honeywell Sensing and Control, 2007, Honeywell HIH-1000 Data Sheet, accessed on April 18, 2014 from http://sensing.honeywell.com/index.php?ci_id=54699
4. Honeywell Sensing and Control, 2010, Honeywell HIH-5030 Data Sheet, accessed on April 18, 2014 from http://sensing.honeywell.com/honeywell-sensing-hih5030-5031%20series-product-sheet-009050-2-en.pdf?name=HIH-5030-001
5. Measurement Specialties Inc., 2012, Measurement Specialties HS1101LF Data Sheet, accessed on April 18, 2014 from http://www.meas-spec.com/downloads/hs1101lf.pdf
6. Parallax Inc., 2009, Parallax HS1101 Data Sheet, accessed on April 18, 2014 from http://parallax.com/sites/default/files/downloads/27920-Humidity-Sensor-Documention-S1101-v1.0.pdf
7. TDK Inc, 2007, TDK CHS-MSS Data Sheet, accessed on April 18, 2014 from http://www.farnell.com/datasheets/84894.pdf
8. TDK Inc, 2005, TDK CHS-CSC-20 Data Sheet, accessed on April 18, 2014 from http://media.digikey.com/pdf/Data%20Sheets/TDK%20PDFs/CHS-CSC-20%20Specification.pdf

9. Griesel, S., M. Theel, H. Niemand, E. Lanzinger, 2012. “Acceptance Test Procedure for Capacitive Humidity Sensors In Saturated Conditions,” WMO CIMO TECO-2012, Brussels, Belgium, 2012, accessed on April 18, 2014 from http://www.wmo.int/pages/prog/www/IMOP/publications/IOM-109_TECO-2012/Session1/P1_09_Griesel_Acceptance_test_procedure_humidity_sensors.pdf
10. Wilson, J., Fontes, J. 2005. “Sensor Technology Handbook”, Elsevier, Burlington, MA, ISBN 0-7506-7729-5
11. General Electric Measurement and Control, 2006, “GE Sensing Telaire Vaporstat 9002,” accessed on April 18, 2014 from http://www.ge-mcs.com/download/co2-flow/920_332a.pdf
12. ASHRAE Standard 62.1-2010 Committee. 2010. “ASHRAE Standard 62.1 Ventilation for Acceptable Indoor Air Quality” ASHRAE, Atlanta, GA
13. Harriman, L., G. Brundrett, R. Kittler. 2001. “ASHRAE Humidity Control Design Guide For Commercial and Institutional Buildings,” ASHRAE Publications, Atlanta, GA, ISBN 1-883413-98-2
14. Henderson, H.L.1990. “An Experimental Investigation of the Effects of Wet and Dry Coil Conditions on Cyclic Performance in the SEER Procedure,” Florida Solar Energy Center, accessed on April 18, 2014 from http://docs.lib.purdue.edu/cgi/viewcontent.cgi?article=1082&context=iracc
15. Rose, W.B. 2005. “Water in Buildings: An Architect’s Guide To Moisture and Mold,” Wiley, Hoboken, NJ, ISBN 0471468509
16. Schell, M. 2004. “Measuring the Right Thing For Humidity Control – It’s the Dew Point, Stupid,” AirTest Technology, accessed on April 18, 2014 from https://www.airtest.com/support/reference/dpstupid.pdf

17. Shah, D., J. Krueger, R. Strand, 1993. U.S. Patent 5346129, “Indoor Climate Controller System Adjusting Both Dry Bulb Temperature and Wet-Bulb Or Dew Point Temperature In The Enclosure”, accessed on April 18, 2014 from http://www.google.com.ar/patents/US5346129
18. Taylor, S., C. H. Cheng. 2010. “Economizer High Limit Controls and Why Enthalpy Economizers Don’t Work,” accessed on April 18, 2014 from http://www.taylor-engineering.com/downloads/articles/ASHRAE%20Journal%20-%20Economizer%20High%20Limit%20Devices%20and%20Why%20Enthalpy%20Economizers%20Don't%20Work%20-%20Taylor%20&%20Cheng.pdf
19. Wang, G., L. Song. 2012. “Air handling unit supply air temperature optimal control during economizer cycles,” University of Miami/University of Oklahoma, Elsevier “Energy and Buildings” June 2012, accessed on April 18, 2014 from http://www.sciencedirect.com/science/article/pii/S0378778812001016
20. Feng, Jingjuang., M. Liu., X. Pang. 2005. “Economizer Control Using Mixed Air Enthalpy,” accessed on April 18, 2014 from http://digitalcommons.unl.edu/cgi/viewcontent.cgi?article=1024&context=archengfacpub&sei-redir=1&referer=http%3A%2F%2Fscholar.google.com%2Fscholar%3Fhl%3Den%26q%3Deconomizer%2Bcondensation%2BHVAC%26btnG%3DSearch%26as_sdt%3D0%252C44%26as_ylo%3D%26as_vis%3D0#search=%22economizer%20condensation%20HVAC%22
21. All-Weather Inc., “Model 5190-E Temperature-Humidity Probe,” 2010, accessed on April 18, 2014 from http://www.allweatherinc.com/reference/sensors/5190-e-001.pdf

22. Sealed Unit Parts Company, no copyright date given, “DTVH Temperature Humidity Logger With Display,”, accessed on April 18, 2014 from http://www.supco.com/images/pdfs/Manuals-Instructions/DVTH%20Manualpdf.pdf
23. Mumma, S., 2001. “Designing Dedicated Outdoor Air Systems,” ASHRAE Journal 2001, accessed on April 18, 2014 from http://doas-radiant.psu.edu/Journal1.pdf
24. Shank, K. M., S. Mumma, 2001. “Selecting the Supply Air Conditions for a Dedicated Outdoor Air System Working in Parallel with Distributed Sensible Cooling Terminal Equipment,” ASHRAE Transactions 2001, V107, p 562.
25. Roveti, D., 2001. “Choosing A Humidity Sensor, A Review Of Three Technologies,” Sensors Magazine, accessed on April 18, 2014 from http://www.sensorsmag.com/sensors/humidity-moisture/choosing-a-humidity-sensor-a-review-three-technologies-840
26. Consense Corp, “Consensor”, no copyright date given, accessed on April 18 2014 from www.consense.com.
27. Kang, Uksong., K.D.Wise. April 2000. “A High-Speed Capacitive Humidity Sensor With On-Chip Thermal Reset,” IEEE Transactions, accessed on April 18, 2014 from http://www.umel.feec.vutbr.cz/~hubalek/skola/vyuka/zima%202005%5Csenzor%20vlhkosti%5Ccapacit_humidit_sens.pdf
28. Vaisala, Inc., 2010, “Choice of outdoor humidity sensors critical to economical free cooling system,” accessed on April 18, 2014 from http://www.vaisala.com/Vaisala%20Documents/Application%20notes/Outdoor-Humidity-App%20Note-B210967EN-A-lores.pdf
29. Chen, Z., C. Lu, 2005. “Humidity Sensors, A Review of Materials and Mechanisms,” University of Kentucky, American Scientific Publishers Sensor Letters Vol 3, 274-295

30. Stokes, W., 2006. “Discharge Humidity Sensor Saturated.” Accessed on April 18, 2014 from http://www.eng-tips.com/viewthread.cfm?qid=166897
31. Francisco, C. C., 1963, U.S. Patent 3195344. Accessed on April 18, 2014 from http://www.google.com/patents/US3195344
32. Able Instruments and Controls, 2006. “Humidity Sensors for Industrial Applications,” accessed on April 18, 2014 from http://www.iceweb.com.au/Analyzer/humidity_sensors.html,
33. Heinonen, M. 1999. “Investigation of the Dew-Point Temperature Scale Maintained at the MIKES,” Measurement Science Technology Vol 10 36, accessed on April 18, 2014 from http://iopscience.iop.org/0957-0233/10/1/010/pdf/0957-0233_10_1_010.pdf
34. Cooper, F.G., 1996, U.S. Patent 5507175. “Cycling Chilled Mirror Hygrometer Including a Sapphire Optical Mirror” Accessed on April 18, 2014 from http://www.google.com/patents/US5507175
35. EdgeTech Moisture and Humidity, no copyright date given. “DewTrak II Model DT-PL-W-AT/W-RD,” Accessed on April 18, 2014 from http://www.edgetechinstruments.com/moisture-humidity/gallery/item/dewtrak-ii-chilled-mirror-transmitter
36. GE General Eastern, 2011. “Optisonde Chilled Mirror Hygrometer,” accessed on April 18, 2014 from http://store.ge-mcs.com/products/23780/ge-general-eastern-optisonde-chilled-mirror-hygrometer
37. GE General Eastern, 2011. “Optisonde Chilled Mirror Hygrometer,” accessed on April 18, 2014 from http://www.ge-mcs.com/download/moisture-humidity/920-423B-LR.pdf

38. Ueno, K., J. Straube, 2008. ”Laboratory Calibration and Field Results of Wood Resistance Humidity Sensors,” accessed on April 18, 2014 from http://c.ymcdn.com/sites/www.nibs.org/resource/resmgr/BEST/BEST1_004.pdf
39. Nguyen Thi Thu Ha, et al., 2000. “Study and performance of humidity sensor based on the mechanical-optoelectronic principle for the measurement and control of humidity in storehouses,” Elsevier Sensors and Actuators B, Chemical, Volume 66 Issues 1-3, accessed on April 18, 2014 from http://www.sciencedirect.com/science/article/pii/S0925400500003609
40. Liu, Xingbin., et al. 1998. “A theoretical model for a capacitance tool and its application to production logging,” Daqing Production Well Logging Institute, Daqing City, PRC, Elsevier Flow Measurement and Instrumentation Volume 9 Issue 4, accessed on April 18, 2014 from http://www.sciencedirect.com/science/article/pii/S0955598698000211
41. Davis, D.R., J. E. Hughes. 1970. “A New Approach To Recording The Wetting Parameter By The Use Of Electrical Resistance Sensors,” The Plant Disease Reporter, Volume 54 Issue 6, p474-9.
42. Blad, B.l., J. R. Steadman, A.Weiss. 1978. “Canopy Structure and Irrigation Influence White Mold Disease and Microclimate of Dry Edible Beans,” accessed on April 18, 2014 from http://www.apsnet.org/publications/phytopathology/backissues/Documents/1978Articles/Phyto68n10_1431.pdf
43. Seyfried, M.S., M.D. Murdock. 2001. “Response of a New Soil Water Sensor to Variable Soil, Water Content, and Temperature,” Soil Science Society of America Journal, accessed on April 18, 2014 from https://www.soils.org/publications/sssaj/abstracts/65/1/28

44. Hanek, G., M.Truebe, M. Kestler, 2001. “Using Time-Domain Reflectrometry (TDR) and Radio Frequency (RF) Devices to Monitor Seasonal Variation in Forest Road Subgrade and Base Materials,” US Forest Service 2001, accessed on April 18, 2014 from http://www.fs.fed.us/t-d/pubs/html/00771805/00771805.html
45. Iwashita,T., H. Katayanagi. 2011. “Needle-type in situ water content sensor with polyethersulfone polymer membrane,” Keio University, Kanagawa, Japan, Elsevier “Sensors and Actuators B: Chemical,” Volume 154 Issue 1, accessed on April 18, 2014 from http://www.sciencedirect.com/science/article/pii/S0925400509008843
46. Malazian, A. et al. 2011. “Evaluation of MPS-1 soil water potential sensor,” University of California Davis/Decagon Devices, Elsevier Journal of Hydrology, Volume 402 Issues 1-2, accessed on April 18, 2014 from http://www.sciencedirect.com/science/article/pii/S0022169411001661
47. Mealy, R., G. Bowman. No copyright date given. “Lab Regent Water Concerns” Wisconsin Department of Natural Resources, accessed on April 18, 2014 from http://dnr.wi.gov/regulations/labcert/documents/training/ReagentH2O.pdf
48. Lenntech B.V. No copyright date given. “Water Conductivity,” accessed on April 18, 2014 from http://www.lenntech.com/applications/ultrapure/conductivity/water-conductivity.htm
49. Roby, D. New Mexico Department of the Environment, 2007. “Reagent Water,” accessed on April 18, 2014 from http://www.nmrwa.org/sites/nmrwa.org/files/WWLabStudyGuide.pdf
50. Rame-Hart Instrument Co, 2013. “Contact Angle,” accessed on April 18, 2014 from http://www.ramehart.com/contactangle.htm

51. Sumner, A. L., et al. 2004. "The nature of water on surfaces of laboratory systems and implications for heterogenous chemistry in the trophosphere," Phys. Chem, Chem. Phys, accessed on April 18, 2014 from http://132.68.226.240/english/pdf/Professors/Yael_Dubowski/1.pdf
52. Onset Computer Corp., 2008. "HOBO U12-012 Data Logger," accessed on April 18, 2014 from http://wpc.306e.edgecastcdn.net/80306E/onsetcomp_com/files/manual_pdfs/7661_C_MAN_U12_012.pdf
53. Storr, W., 1999. "Electronics Tutorials, Waveform Generators," accessed on April 18, 2014 from http://www.electronics-tutorials.ws/waveforms/generators.html
54. Fairchild Semiconductor, 1983. "MM74HC14 Schmitt Trigger," accessed on April 18, 2014 from http://www.fairchildsemi.com/ds/MM/MM74HC14.pdf
55. Maxim Semiconductor, 2007. "Low Frequency Dual EconOscillator," accessed on April 18, 2014 from http://datasheets.maximintegrated.com/en/ds/DS1099.pdf
56. Shrader, R. 1975. "Electronic Communication," 3rd Edition, McGraw-Hill, New York, ISBN 9780070571389
57. Sinclair, I., J. Dunton. 2007. "Practical Electronics Handbook," 6th edition, Newnes, Oxford, UK, ISBN 978-0750680714
58. Texas Instruments, 2013 "LME49710 High-Performance, High-Fidelity Operational Amplifier," accessed April 18, 2014 from http://www.ti.com/lit/ds/snas376c/snas376c.pdf
59. Lee, W.Y., J.M. House, N-H. Kyong. 2004. "Subsystem level fault diagnosis of a building's air handling unit using general regression neural networks," Elseveir Applied Energy, Volume 77, Issue 2, accessed on April 18, 2014 from http://www.sciencedirect.com/science/article/pii/S0306261903001077

60. Zhou, J., G. Wei, W.D. Turner, D.E. Claridge, 2008. "Airside Economizer - Comparing Different Control Strategies and Common Misconceptions," ESL-IC-08-10-54, accessed on April 18, 2014 from http://repository.tamu.edu/bitstream/handle/1969.1/90822/ESL-IC-08-10-54.pdf?sequence=1
61. Agilent Technologies, 2013. "Agilent Impedance Measurement Handbook, 4th Edition," accessed on April 18, 2014 from http://literature.agilent.com/litweb/pdf/5950-3000.pdf
62. Lomas, C. G, 2011. "Fundamentals of Hot Wire Anemometry," Cambridge University Press, Cambridge, UK, ISBN 0521283183
63. Mei, Y., Z.J. Zhou, H.L. Luo, "Electrical resistivity of rf-sputtered iron oxide thin films," Journal of Applied Physics, 1987, Volume 61, p 4388-4389, accessed on April 18, 2014 from http://scitation.aip.org/getpdf/servlet/GetPDFServlet?filetype=pdf&id=JAPIAU000061000008004388000001&idtype=cvips&doi=10.1063/1.338431&prog=normal
64. Accuratus Corporation, 2013. "Aluminum Oxide, Al_2O_3 Ceramic Properties," accessed on April 18, 2014 from http://accuratus.com/alumox.html
65. McCafferty, E. 2010. "Introduction to Corrosion Science," Springer Science and Business Media, New York, NY, ISBN 978-1-4419-0455-3
66. Popov, Branko, 2007. "Basics of Corrosion Measurements," accessed on April 18, 2014 from http://www.che.sc.edu/faculty/popov/drbnp/ECHE789b/Corrosion%20Measurements.pdf

67. Boulangé-Petermann, L., J. C. Joud, B. Baroux. 2008. “Wettability Parameters Controlling the Surface Cleanability of Stainless Steel,” Contact Angle, Wettability, and Adhesion, Volume 5, p139-151

68. Halladay, D., 1974. “Fundamentals of Physics,” Wiley Publishing, New York, ISBN 0471344311

69. The Engineering Toolbox, 2014. “Humidity Ratio of Air,” accessed on April 18, 2014 from http://www.engineeringtoolbox.com/humidity-ratio-air-d_686.html

70. Vömel, Holger, 2011. “Saturation Vapor Pressure Formulations,” accessed on April 18, 2014 from http://cires.colorado.edu/~voemel/vp.html

71. Beckwith, T., R.D. Marangoni, J.H. Lienhard. 1993. “Mechanical Measurements, Fifth Edition,” Addison-Wesley, Reading, MA, ISBN 0-201-56947-7